

Wrinkling analysis and design of Offshore Flexible Floating Solar Structures

Master Thesis

Sam de Bode

Master Thesis
Marine Technology



Wrinkling analysis and design of Offshore Flexible Floating Solar Structures

Master Thesis

by

Sam de Bode

to obtain the degree of Master of Science

at the Delft University of Technology,

to be defended publicly on Tuesday August 17th, 2021 at 15:00 PM.

Student number: 4953509
Project duration: November 15, 2020 – August 17, 2020
Thesis committee: Dr. ir. J. H. Den Besten, TU Delft 3mE, supervisor
Ir. H. M. Verhelst, TU Delft 3mE, supervisor
Dr. ir. M. A. Bessa, TU Delft 3mE

This study is confidential and cannot be made public until August 17, 2021.

Preface

This thesis on wrinkling analysis and design of Offshore Flexible Floating Solar Structures has been written for the completion of the Master of Science degree in Marine Technology at the Delft University of Technology. The research was performed under the supervision of Ir. H.M. Verhelst and Dr. Ir. J.H. den Besten.

This study could not have been done without the generous support which I received. Hugo, you inspired me to dive into the world of wrinkling, and you encouraged me to use my practical background to convert conceptual methods to hands on solutions. Furthermore, thank you for always taking the time to answer my questions and pointing me in the right directions to improve the level of my work. Also, your curious attitude motivated me to think outside of the box and combine insights of different research fields.

Henk, thank you for your valuable feedback, and always making time to discuss my research. Your critical attitude and work ethic is an inspiration for many.

Furthermore, I want to thank Miguel Bessa, for being part of my graduation and reviewing my thesis. I am grateful for having had the opportunity to work with you all and am looking forward to my endeavors ahead.

*Sam de Bode
Terschelling, August 2021*

Contents

Abstract	vii
1 Introduction	1
1.1 Background and Motivation	1
1.1.1 Offshore Floating Solar Platforms	1
1.1.2 Flexible Floating Structures	2
1.1.3 Wrinkling of Flexible Floating Solar Structures	3
1.2 Thesis Goal	4
1.3 Outline	5
2 Literature Review	7
2.1 Loading conditions.	7
2.1.1 Wrinkling phenomena	7
2.1.2 Numerical Aspects	10
2.1.3 Conclusion	11
2.2 Wrinkling Resistant Structural Design	12
2.2.1 Gossamer Structures	12
2.2.2 Geometry Optimization	12
2.2.3 Permeability	13
2.3 Auxetic Materials	13
2.4 Mooring of Flexible Bodies Offshore	15
2.5 Concluding Remarks.	16
3 Methodology	17
3.1 Numerical Modelling.	17
3.1.1 Wrinkling Modelling	18
3.1.2 Material Models	19
3.1.3 Element Selection	19
3.1.4 Load Definition	19
3.1.5 Hydrostatic Pressure Effect Wrinkling.	19
3.2 Conclusion	20
4 Base Design	23
4.1 Global Dimensions.	23
4.2 Thickness	24
4.2.1 Installation	24
4.2.2 Material Selection	26
4.2.3 Hydrostatics.	27
4.3 Conclusion	28
5 Numerical Wrinkling Analysis	29
5.1 Benchmark Cases	29
5.2 Wrinkling Analysis Approach	30
5.2.1 Principal Stress Analysis	30
5.2.2 Post-Buckling Analysis	31

5.3	Results Principal Stress and Post-Buckling	32
5.4	Numerical Parameter Sensitivities	34
5.4.1	Modes	35
5.4.2	Stabilization.	36
5.4.3	Grid size	36
5.4.4	Sensitivities Wrinkles and Amplitudes	37
5.4.5	Sensitivities Conclusion	37
5.5	Conclusion	39
6	Wrinkling of Offshore Flexible Floating Solar Structures	41
6.1	Wrinkling affecting parameters	41
6.1.1	Hydrostatic Stiffness	42
6.1.2	Embedded Solar Panels	44
6.2	Wrinkling resistant design	47
6.2.1	Shear Compliant Zone	47
6.2.2	Auxetic Solar Panel Orientations	49
6.3	Conclusions.	51
7	Conclusions	53
8	Future Work	57
8.1	Wrinkling Modelling Method	57
8.2	Wrinkling Modelling of OFFSSs and Ocean Dynamics	58
8.3	Wrinkling Resistant Design	58
8.4	Structural Design with Solar Panels.	59
8.5	Mooring.	59
A	Auxetic Structure Design	61
A.1	Auxetic Solar Panels Design	61
A.2	Auxetic behaviour	61
B	Elastic Foundation Contact Type	65
B.1	Working Principles	65
B.2	Wrinkling Results.	66
B.3	Conclusion	66
C	OFFSS Permeability Variations	69
C.1	Grid of Holes Over the Whole Platform	69
C.1.1	Conclusion	69
C.2	Elliptical Hole Shear Compliant Zone.	72
C.2.1	Conclusion	72

Abstract

Solar energy is considered to be one of the most promising energy alternatives among many renewable energy sources. On the pathway towards achieving climate goals, dramatic scale up of clean technologies is required, however the installation of solar energy has the burden of intense land requirement. Therefore, the onset of floating solar technology can be the turning point to give incentive for more substantial deployment of solar energy, avoiding land occupancy concerns. Besides the potential of installing bodies on water, floating solar brings the benefit of an efficiency increase superior to 10 percent in relation to land based solar, depending on the solar panel technology and environmental conditions. This efficiency increase can be attributed to the natural cooling effect of the seawater, located below the solar platform.

For global scale up of these technologies, moving to offshore locations is inevitable. Loads of current, wind and waves induce high loading in ocean environments. Flexible solar platforms have the advantage that they can yield with wave motion, rather than withstand its impact, hence allowing structures and mooring to be subjected to significantly less force. Flexible solar platforms are designed with very low bending stiffness to be able to move along with wind and waves. Flexible structures have a tendency to buckle in presence of local compressive stresses, and develop out of plane displacements called wrinkling. For flexible floating solar structures there is a demand for a higher understanding of this behaviour and how to reduce it, as this is assumed to be a potential limit state.

In literature, the elementary load conditions uni-axial tension, bi-axial tension, compression and shear have shown to induce wrinkling. When wrinkling occurs on a global structural level, large out of plane deformations are leading to risk of failure and uncertainty about structural integrity. In several Aerospace structures, wrinkling reduction design solutions are established, such as geometry optimization and addition of permeability. Furthermore, auxetic materials, i.e. structures with a negative Poisson's ratio, have the potential of reducing wrinkling behaviour by removing compressive stresses in the structure, upon deformation.

The wrinkling behaviour of Offshore Flexible Floating Solar Structures (OFFSSs) is affected by hydrostatic stiffness of the water below the platform. This effect can be modelled using an elastic foundation. When applying an elastic foundation with bonded contact to an solar platform, only the load case shear results in significant wrinkling.

Rigid solar panels reduce the number of wrinkles on a solar platform in shear as well as the amplitudes, while for flexible solar panels only the amplitudes are slightly reduced. Consequently, based exclusively on wrinkling behaviour, rigid solar panels seem more favourable for OFFSS application than flexible solar panels. Two wrinkling reduction methods are proposed for wrinkling reduction in OFFSSs: shear compliant zones, and auxetic solar structures. Results of simulations of platforms in shear showed that shear compliant zones have to potential to reduce wrinkling by minimising compressive stresses throughout the whole platform. Auxetic solar structures have shown to remove compressive stresses from the middle of the platform, hence reducing global wrinkling.

This research offers a scientific contribution to the field of wrinkling analysis and design of OFFSSs, by providing conclusions on wrinkling behaviour of flexible platforms with embedded rigid (solar) structures, the effect of hydrostatic stiffness on wrinkling and by analysis of wrinkling reduction methods for these structures.

Introduction

1.1 Background and Motivation

In this thesis, wrinkling reduction in Offshore Flexible Floating Solar Structures (OFFSSs) will be studied. Three key-concepts are identified for this topic which will be addressed in the following introduction: *Offshore floating solar platforms*, *Flexible floating structures* and *Wrinkling in flexible structures*.

1.1.1 Offshore Floating Solar Platforms

Solar energy is considered to be one of the most promising energy alternatives among many renewable energy sources [29]. According to the World Energy Outlook, released by the International Energy Agency [1], solar photovoltaics (PV) is one of the more mature renewable technologies which is consistently cheaper than new coal- or gas-fired power plants in most countries.

On the pathway towards achieving climate goals, dramatic scale-up of clean technologies is required [1] however, the installation of solar PV has the burden of intense land requirement which will always be a premium commodity [75]. Therefore, the onset of floating photovoltaic (FPV) technology can be a turning point to give incentive for more substantial deployment of PV technology, avoiding land occupancy concerns. Globally, FPV has the potential to unlock a terrawatt-scale power generation opportunity [48].

In recent years, FPVs have gained substantial traction not only for their immense potential of the installation on bodies of water, but also for bringing some co-benefits such as higher efficiency compared to PV systems [49], due to natural cooling of the panels by seawater. In literature [49], an efficiency increase superior to 10 percent is anticipated in relation to land-based solar PV, depending on the PV technology and environmental conditions [14]. This is caused by the linear relation between solar PV operating temperature and electrical efficiency [21], the increased heat reduces the output voltage of the solar panel, while the current only increases slightly, hence decreasing total power output [14, 3]. In an experiment by Do Sacramento et al. [20], where they compared the power output of two solar PV modules, of which one was floating in a water basin and the other one was ground-mounted, an average efficiency increase of 12.5% the floating module was observed. In Figure 1.1 below the current \times Voltage curves for one time instance during the test are shown. In another experiment in Japan [66], where an FPV production system was analyzed against a similar ground-mounted system in the vicinity, they observed an efficiency gain of 7.4%-17% for the FPV platform, due to the cooling effect.

Recently, FPV deployment has emerged, typically in regions where the costs of available land are high,

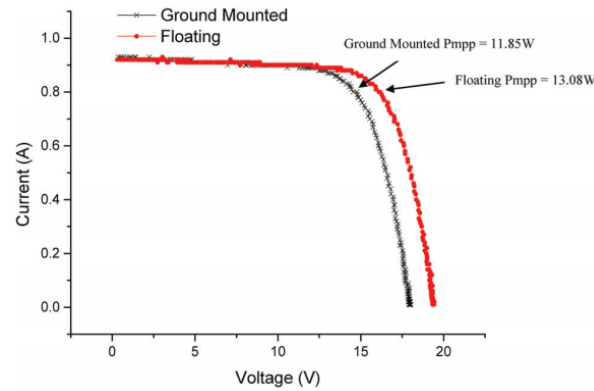


Figure 1.1: Solar module $I \times V$ diagram at one time instance [20]. It can be observed that the floating module operates at higher voltage, thereby achieving higher efficiency

but where water bodies are in abundance. Examples thereof are Japan, South Korea, Singapore and China, but it is seen in other parts of the world as well [48]. Experience from inland floating solar projects could open up possibilities to scale up and move to nearshore or even offshore conditions. For the global development of large scale FPV, moving to offshore locations becomes inevitable. However, technology is not there yet [48, 66].



Figure 1.2: FPV platform near Chiba, South Korea



Figure 1.3: Huainan FPV farm in China

Nonetheless, few examples in test phase can yet be found offshore [63, 22], where loads of current, wind and waves make deployment of FPV platforms much more challenging. While most FPV examples are found in still water and sheltered areas, the structures are typically not designed to withstand ocean dynamics. For this reason, flexible floating platforms have substantial potential for marine applications [84].

Flexible solar platforms have the advantage that they can yield with wave motion, rather than withstand its force, and hence, allowing moorings to be subjected to significantly less loading force, which is a large issue in the reliability of offshore structures [84]. The most recent concepts of these floating solar structures, designed for offshore applications are also flexible [55, 63].

1.1.2 Flexible Floating Structures

Existing floating PV technology uses stiff connections such as ears and pins to connect the floaters. In marine locations, these connections will be facing heavy loads, compromising the reliability of the system [66].

For large scale offshore applications, conventional FPV structures will therefore not suffice [84, 66].

Flexible structures have high potential for FPV platforms, since they can deform to the on-coming wavefronts. This allows minimal magnitudes of the loading on the structures and its mooring lines. Examples of flexible floating structures can be found in aquaculture [46], floating docks [58], flexible life rafts [98] and wave energy converters [65]. These structures are designed as a continuum, by usage of flexible materials and couplings. This ensures that even in rough conditions of the sea, the structure will not fail. Examples of floating fish farm, floating dock, flexible life raft and flexible wave energy converters are depicted in Figures 1.4, 1.5, 1.6 and 1.7 respectively.



Figure 1.4: Flexible floating fish farm, deforming with oncoming wave fronts [46]



Figure 1.5: Floating dock in breaking waves [58]

1.1.3 Wrinkling of Flexible Floating Solar Structures

Flexible solar platforms are designed to have very low bending stiffness to be able to move along with wind and waves. This makes them one of a kind in the maritime offshore industry, general engineering rules do not apply to these structures. Since the structures are flexible, deformations are much larger, and wrinkling is assumed to be a potential limit state.

Several cases of damage to inland FPV structures are observed [64, 54], for instance during the failure of the Yamakura Dam FPV project [54], after a typhoon hit the platform. The mooring system failed, and the platform deformed. This led to short circuits in the electrical systems, which caused a fire on the FPV. Here, the risk of severe damages to FPV during a collapse is underlined. This motivates the requirement for a higher understanding of the limit states of a FPV structure, of which wrinkling is suspected to be one.

Even though numerous works have been performed on the wrinkling behavior of membranes, engineering methods for wrinkling avoidance in large flexible structures are yet to be determined. From



Figure 1.6: Flexible life raft deployed next to a ship in heavy sea conditions[98]



Figure 1.7: Flexible Wave Energy Converter Prototype by SBM Offshore, being tested in a pool [65]

literature, we know that wrinkling occurs when there is local compressive stress in a flexible (i.e. low bending stiffness) structure. Key factors that therefore play a role in wrinkling behavior of these large flexible solar structures are: *Load conditions*, *Boundary conditions* and *Wrinkling resistant design*. Since no converged solution has been established in literature for these items [66], more research on these topics is required.

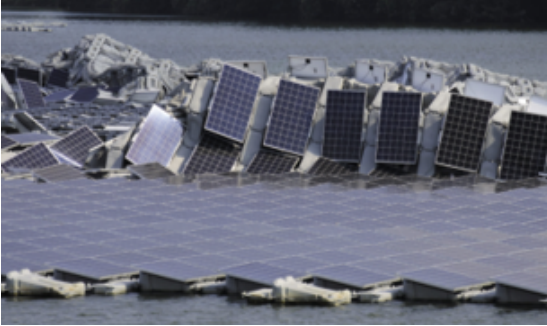


Figure 1.8: Collapse of Yamakura Dam FPV [54]



Figure 1.9: Fire on Yamakura Dam FPV [54]

In the thesis, the previously stated topics will be researched in the context of wrinkling reduction of OFFSSs. *Load conditions* are the loads caused by currents or mooring loads which are assumed to adhere to the concept, and which are effected by the boundary conditions. Dynamic loads such as wind and waves are not considered in this research. The loads are of influence on potential wrinkling behavior, *Boundary conditions* entails the geometry, solar panel type and mooring configuration that are expected for the platforms. After a more thorough understanding on these concepts is obtained, *Wrinkling resistant structural design* is left to be explored in analyzing the reduction of wrinkling behavior in OFFSSs.

1.2 Thesis Goal

The relevance of wrinkling reduction for offshore FPV has been demonstrated in the previous section. OFFSSs have not been analysed previously in the context of wrinkling. As wrinkling is assumed a potential limit state for these structures, a more thorough understanding of this behavior is required, and design methods for reducing this behavior should be investigated. The goal of this thesis is to extend current research on flexible floating offshore solar platforms, by studying the wrinkling behavior of offshore flexible platforms with embedded solar panels, and exploring methods to reduce this potential hazardous behavior.

The main research question which is posed, based on the previous motivation is:

What is the wrinkling behavior of Offshore Flexible Floating Solar Structures, and how can it be modelled and reduced?

The result to this inquiry is to be obtained through answering the following sub-questions:

1. a) *What load conditions adhere to wrinkling in offshore flexible floating solar structures?*
To model the wrinkling behavior of OFFSSs, it is essential to know what load conditions can occur which induce wrinkling. The load conditions adhering to wrinkling in OFFSSs will be based on cases from literature.
1. b) *How can a base design for offshore flexible floating solar structures be developed, taking into account location and installation?*
Since no converged solution on the design of OFFSSs has been established in literature, some assumptions have to be made before the model can be created. Therefore, a study is required

to obtain a base design of OFFSSS, taking into account size and installation, on which wrinkling analyses will be performed.

1. c) *What is the influence of numerical tools on wrinkling results of offshore flexible floating solar structures?*

Wrinkling analyses require numerical tools (see chapter 5), which may influence the result. It should be investigated, what numerical tools are required to conduct research in wrinkling behavior, and what the sensitivity of the numerical results is to these parameters. The sensitivities are important for interpreting or establishing the credibility of the findings.

1. d) *What is the wrinkling behavior of Offshore Flexible Floating Solar Structures?*

When the numerical model has been established, and sensitivities of numerical tools are studied, it is time to investigate the wrinkling behavior of OFFSSs. The outcome of this inquiry will function as a reference for comparison with results using wrinkling reduction methods.

1. e) *How can wrinkling resistant design methods be utilized to reduce wrinkling in Offshore Flexible Floating Solar Structures?*

After the wrinkling behavior of OFFSSs is known, wrinkling reduction methods are applied to investigate their potential for reducing wrinkling in OFFSSs. Wrinkling reduction methods obtained from literature are investigated in the wrinkling reduction analyses.

1. f) *How can the properties of auxetic materials be incorporated in Offshore Flexible Floating Solar Structures to create wrinkling resistance?*

Auxetic materials exhibit characteristics that could potentially reduce wrinkling, which will be discussed in the forthcoming chapter 2. Their potential for wrinkling reduction in OFFSSs is inspected.

1.3 Outline

The structure of this thesis is as follows. An introduction to offshore flexible floating solar platforms has been provided in the previous chapter. After this, relevant literature will be substantiated in Chapter 2. Fundamentals of wrinkling, geometric adaptations for wrinkling reduction and mooring of flexible bodies offshore are discussed. Concluding remarks will yield after this study, where the gap in literature is identified which is to be filled upon completion of this research. Thereafter, Chapter 3 will describe the methodology for the thesis and Chapter 4 explores design considerations and assumptions for the base design which will be utilized for wrinkling analyses. Subsequently, Chapter 5 will go into numerical tools for wrinkling analyses and will establish their sensitivities. In Chapter 6, the results of the wrinkling analyses are presented and discussed. In Chapter 7 the conclusions of the research are provided, and lastly in Chapter 8 recommendations for future work are given.

2

Literature Review

In this chapter relevant literature to the topic is outlined. The following topics can be distinguished in literature in relation to wrinkling of flexible offshore FPV platforms: *Wrinkling fundamentals*, *Wrinkling Resistant Structural Design*, *Auxetic materials* and *Mooring of flexible bodies offshore*. A comprehensive study on these fields is presented.

In section 2.1 of this chapter, the following research sub-question will be answered:

1. a) *What load conditions adhere to wrinkling in offshore flexible floating solar structures?*

2.1 Loading conditions

In this section, wrinkling phenomena are discussed based on four elementary load cases. Furthermore, numerical aspects of wrinkling are described. Afterwards, a conclusion will follow.

2.1.1 Wrinkling phenomena

An issue that might occur with these flexible structures, is wrinkling. Elastic sheets develop wrinkles in the presence of local compressive stresses [80]. The analysis of membrane wrinkling has a long history which started with the works of Wagner 1929 [86]. They studied the formation of localized buckling in thin metal structures used in the aircraft industry and identified the wrinkling phenomenon.

Wrinkling can be caused as a result of different elementary loading conditions. The following load conditions have shown to induce wrinkling in thin sheets, as identified in literature: *uni-axial tension*, *uni-axial compression*, *bi-axial tension* and *shear*. See figure 2.1 for a schematic overview of these situations. Throughout the current section, examples of these load conditions from literature are discussed. An overview of the literature sources per load condition is concisely presented in table 2.1.

Table 2.1: Wrinkling Literature Review

Load condition	Literature
(a) - Uni-axial tension	[16, 15, 33, 80, 47, 27, 69, 87]
(b) - Uni-axial compression on an elastic substrate	[15, 71, 74]
(c) - Bi-axial tension	[93, 12]
(d) - Shear	[94, 80]

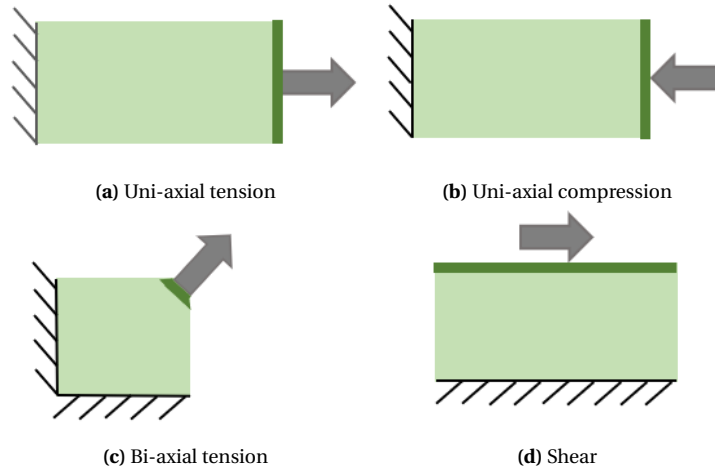


Figure 2.1: Load conditions on a thin rectangular membrane. The diagonally striped boundaries indicate a mooring system holding the platform on the edge. The load is applied over the bold regions.

Uni-axial tension This research was noticed and further extended by Cerda 2002 [16] for an elastic sheet under uni-axial tension. In this pioneering work, Cerda deduced that the clamped boundaries prevent the membrane from lateral contraction in its proximity, which sets up a state of shear near the boundaries. This causes the transverse stresses to be compressive locally, further away from the edges. The wrinkled geometry was determined by minimizing the total energy in the material, consisting of bending energy and strain energy. Hence they concluded, that wrinkles arise when the energy due to in-plane forces, is in balance with the bending energy in the sheet. Figure 2.2 shows the wrinkles on a thin sheet under uni-axial strain. Taking into account the physical mechanism of this behaviour, scaling laws were derived for the amplitude (A) and wavelength (λ) of the wrinkles for a thin rectangular sheet in uni-axial tension.

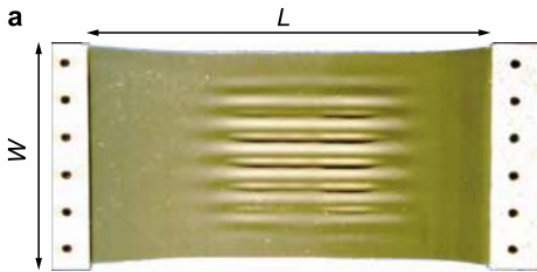


Figure 2.2: Wrinkles in a highly stretched thin sheet (a) [16]

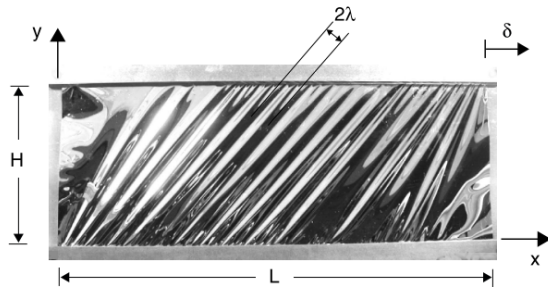


Figure 2.3: Wrinkles in a sheared membrane (d) [94]

More recent research has shown that wrinkling is an inherently unstable phenomenon and for stable emerged wrinkling, wrinkling amplitudes first increase, reach a maximum and then decreases and return to zero again [33]. Accurate prediction models of wrinkling patterns in thin elastic sheets are created [80] which were expanded to highly stretched sheets [47, 27, 87, 69]. Panaitescu et al. [69] demonstrated this phenomenon through experiments and then compared the results to the non-linear Neo-Hookean, Saint Venant-Kirchhoff and Mooney-Rivlin hyperelastic models. Numerical results from the Mooney-Rivlin model showed the best agreement with the experimental data for the growth and decay of wrinkles in the hyperelastic regime. A novel numerical resolution framework was developed by Fu et al. [27], which precisely predicts the wrinkling response for both compressible and incompressible materials. They concluded that, for incompressible materials, different constitutive laws mainly affect

restabilization points and wrinkling amplitudes quantitatively. Restabilization is the disappearance of wrinkles upon excess stretching [27]. For compressible materials, the Poisson's ratio plays a large role in the wrinkling restabilization and response. The smaller the Poisson's ratio is, the less likely it is to develop wrinkles.

Shear Wrinkling of thin sheets can also be provoked by shear loads, a detailed study of this condition was adduced by Wong and Pellegrino [94]. Here a numerical simulation technique was presented for nonlinear wrinkling which provided results that were validated by experiments. Figure 2.3 shows a photograph of a sheared membrane. In their analysis, Wong and Pellegrino found that, for a rectangular membrane in shear, the wrinkled pattern varies abruptly when the load magnitude is changed. Moreover, in this study an assumption on the relation between the compressive principal stress σ_2 , the Young's Modulus E , Poisson's ratio ν , thickness t and wrinkle half-wavelength λ was confirmed. This resulted in the following analytical expression [94] for the average principal compressive stress in a uniformly wrinkled membrane, which enables unprecedented simplification of complex wrinkling behaviour analyses on sheared membranes.

$$\sigma_2 = -\frac{\pi^2 E t^2}{12(1-\nu^2)\lambda^2} \quad (2.1)$$

Bi-axial tension Wrinkling in a square sheet under bi-axial tension was studied by Wong, Pellegrino, and Park [93]. Two wrinkling regimes were pinpointed for square membranes under bi-axial tension. The first regime occurs for symmetric and moderately asymmetric loading and is characterized by small, radial corner wrinkles. The second regime arises for strong asymmetric loading and is marked by a single, large diagonal wrinkle, plus small radial corner wrinkles.

Compression on an elastic substrate Another very fundamental contribution was deployed by Cerda and Mahadevan in 2003 [16]. In this inquiry, the effect of an elastic substrate on the wrinkling behaviour of a thin film was added to the prior understanding of wrinkling physics. They deduced a theory for wrinkling, using the physics of bending and stretching, valid for a multitude of origins. They found that the expression for stretching energy is analogous to the form of the energy in an elastic foundation supporting a thin sheet. Hence they concluded that the balance between the foundation stiffness and the bending energies leads to the selection of wrinkles. This theory was first tested on the tangible case of wrinkles on the skin of a shrivelled apple, see Figure 2.4. Here, the wrinkles arise due to the compression induced by the drying of the flesh, which is an elastic substrate. From an estimated elasticity of the apple flesh and skin, the wrinkle wavelength λ could be calculated, which was qualitatively consistent with observations.

The research on wrinkling on elastic substrates was later on extended by the localization of folds [71]. Incorporating the nonlinear response of a thin membrane on an elastic solid or fluid. If this membrane is compressed even further after the initial wrinkling response, the wrinkles disappear except for a few select locations that exhibit folds. More accurately, folds appear whenever a membrane is compressed beyond a third of its initial wrinkle wavelength [71], which involves highly localized curvature. In Figure 2.5 the transition of wrinkles into a fold of a thin sheet on an elastic substrate is depicted. The physical mechanism behind the formation of folds on an elastic foundation is the energy balance between bending energy in the membrane and the potential energy of the displaced fluid. The shape of the film is thus obtained by minimization of the total energy, expressed in the following equation [71], whereby U_B and U_K are the bending and potential energy respectively.

$$U = U_B + U_K \quad (2.2)$$

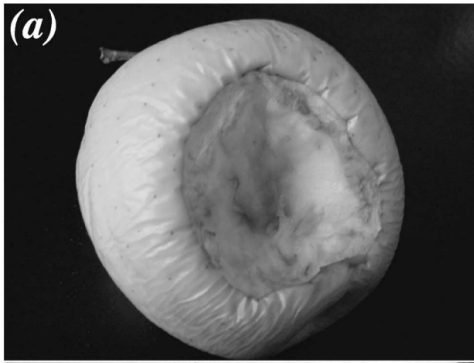


Figure 2.4: Wrinkles on the skin of a dried apple (b) [15]

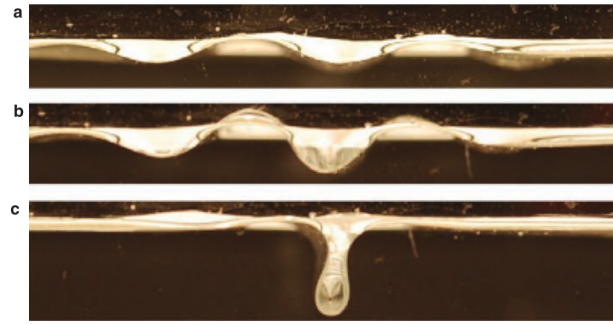


Figure 2.5: Experimental representation of the physical transition of a wrinkled membrane on an elastic substrate into a localized fold. (b) [71]

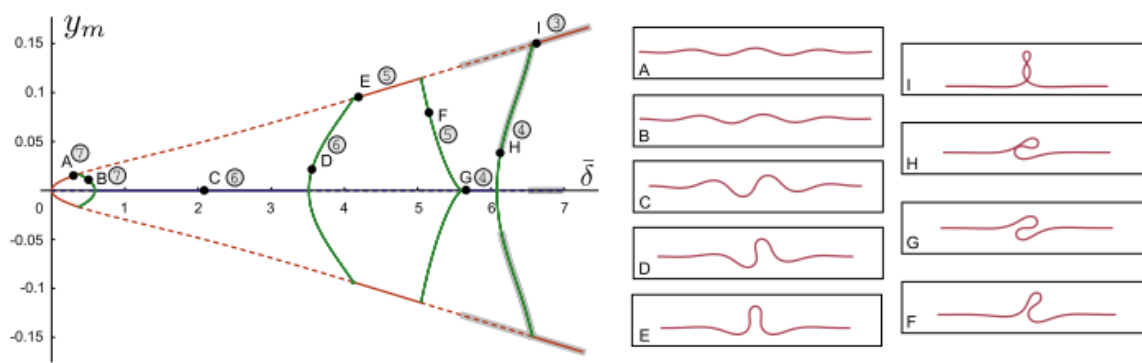


Figure 2.6: The mathematical route to localization of folds for thin sheets on an elastic substrate (b) [74]. On the vertical axis of the graph, the vertical deflection in the middle of the sheet is indicated by y_m , on the horizontal axis the displacement δ are marked. The post-buckling equilibrium shapes are displayed on the right side of the chart, which is also depicted with a label in the graph. The label number of each shape corresponds to the number of points in the membrane where the rotation is zero. As this number decreases with displacement, the initial wrinkled shape transforms into a localized fold.

The understanding of the folding mechanism of thin sheets on a liquid bath was deepened by mathematicians Rivetti and Neukirch [74], who performed a numerical study of the general case of a slender beam resting on an elastic foundation, where the intensity of the liquid foundation and the confinement were both varied. They derived that, if the confinement of the beam is increased an alternation of symmetric and anti-symmetric shapes emerges, connected by non-symmetric transitions. By post-buckling analysis, they carefully reconstructed the theoretical route of the initial sinusoidal wrinkled pattern to localization of a well-defined fold. They identified that the root cause of the localization mechanism is that, the ending configuration of every connection branch is characterized by the internal moment vanishing at the ends of the beam.

2.1.2 Numerical Aspects

The prevailing method found in literature for modelling wrinkling behaviour, is non-linear post-buckling analysis [12, 33, 80, 27, 69]. However, in this method, geometrical imperfections need to be applied to the structure to allow wrinkling [12]. These user defined bifurcations appeared to have a large influence on the wrinkling response [41], which makes it a less applicable method for analysis on a multitude of geometries and load cases since these perturbations can be hard to obtain [41].

Another method, proposed in literature is the use of principle stress criteria [53]. The principal stress criteria for identifying wrinkling onset are given by Luo et al. The principle stress criterion was used

in several topology optimisation studies to design wrinkle-free membrane structures [53, 45, 96], discussed in forthcoming Section 2.2. From these studies, it is known, that the second principal stress field can be used to analyse the wrinkling behaviour of a structure. Additionally, the computational costs of this approach are far less than when modelling the 3D deformed pattern to analyse wrinkling. A concise explanation of the influence of these principle stresses on the wrinkling result is presented by Lavaerts. It was found that when negative principle stresses are present in a membrane, wrinkling *can* occur [41]. In this research, global wrinkling will be minimised for a multitude of load cases, and the exact post-buckling shape is not required, therefore the inspection of the onset of wrinkling is sufficient and less computationally extensive. This would be more relevant when investigating the fluid-structure behaviour of the wrinkled platform.

In the work of Panaitescu et al. [69] it appeared, that the Mooney-Rivlin model predicts the birth and decay of wrinkles in a thin flexible sheet under tension up to 50 per cent, more accurately than both the Saint Venant-Kirchhoff (SVK) model and the Neo-Hookean model. Fu et al. [27] described the evolution of wrinkles for a slender thin flexible sheet under tension, for several material models such as Neo-Hookean, Mooney-Rivlin and the Gent model. They discussed that both the Neo-Hookean and Mooney-Rivlin are more accurate at predicting the birth and death of tension wrinkles, and the results were similar. The Gent model is more adequate for specific cases where severe strain-stress phenomena are involved such as in biological tissue [27].

In the work of Kim et al. [39] an extensive comparison is made between the general hyperelastic models Neo-Hookean, Mooney-Rivlin and Ogden's model. It was concluded that Ogden's 3rd order model was the most accurate for large deformations, in a variety of load conditions, for chloroprene rubber. Similarly, Marckmann and Verron studied different hyperelastic models for rubber-like materials. Based on a comparison with two experimental data sets, they created a ranking of 20 different hyperelastic models. Ogden's model was ranked at 4th due to its efficiency for several loading conditions such as uniaxial tension, equibiaxial tension, pure shear and biaxial tension. The downside which is mentioned for using this model is that multiple material parameters are required to successfully run the model [56]. Furthermore, the derivation of these parameters is not physically motivated and therefore necessitate a large experimental database to be fitted [56]. In addition, for moderate strains, i.e. up to 250%, the Mooney-Rivlin is the most computationally time-efficient [56].

There are compressible and incompressible hyperelastic material models [56, 85, 8]. When $\nu = \frac{1}{2}$ the bulk to shear modulus $\frac{B}{G}$ is infinite, a material is described as *incompressible* [59]. Experimentally, all materials are compressible as they have a finite bulk modulus, and while flexible materials approach $\nu \rightarrow \frac{1}{2}$, it never actually equals $\nu = \frac{1}{2}$ [59]. As rubber-like materials are nearly incompressible [34], they are often assumed incompressible for the sake of simplicity [85, 56, 39].

2.1.3 Conclusion

Elastic sheets are susceptible to wrinkling. Wrinkling can occur in thin sheets under various load conditions: *uni-axial tension*, *uni-axial compression on an elastic substrate*, *bi-axial tension* and *shear*. Wrinkling can be modelled using nonlinear hyperelastic material models, either compressible or incompressible depending on the material type. In most applications, wrinkling in a structure can significantly degrade the structural performance [76]. When wrinkling occurs on a global structural level, large out of plane deformations are leading to the risk of failure and uncertainty about structural integrity.

2.2 Wrinkling Resistant Structural Design

In literature, several concepts are established for the reduction of wrinkling behaviour in thin elastic sheets. Concepts originated especially from the field of aerospace, where applications of these structures can be found in *Gossamer structures*.

2.2.1 Gossamer Structures

Wrinkling reduction in membranes has been widely researched for the development and improvement of Gossamer structures. The term Gossamer structure refers to the general category of space ultra-low-mass structures, such as inflatables or many forms of expandable structures. Some examples of Gossamer structures are solar sails, space telescopes [11] and sun shields. Gossamer structures are extensively described in the book of Chmielewski [17]. In Gossamer structures, wrinkles in the membrane can significantly degrade the structural performance of the material. For example, wrinkles in a solar sail may reduce thrust. The prevailing approach to prevent this has been to maintain a wrinkle free condition by using a catenary cable along the membrane edges [76], and thus inducing bi-axial prestress in the membrane. However, the high rigidity of these cables is required to be able to apply sufficient tension. Which comes with a weight penalty.

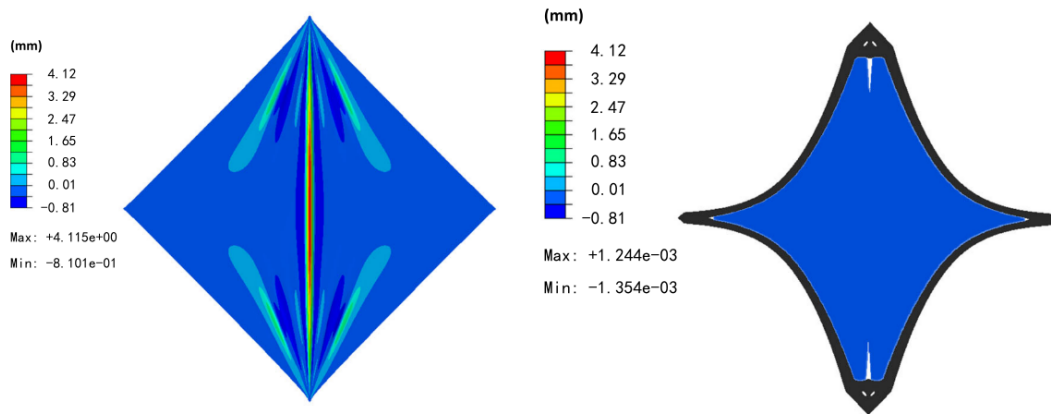


Figure 2.7: On the left: wrinkled square membrane, on the right: optimized design with cable suspension around circumference which shows no wrinkles (c) [53]

A web-cable girded design was proposed by [76, 77] to suppress wrinkles in a membrane. They found that using a web cable, wrinkles in a membrane under rhombic displacement can be suppressed by applying tension to all four corners of a square membrane, which is also the most mass efficient solution. In an effort of Luo et al. [53] optimized the geometry and structure of a square bi-axially loaded membrane, to avoid wrinkling. In this study, topology optimization was used to create the optimal membrane geometry for minimal wrinkling. The comparison of wrinkling behaviour for membranes with and without cable suspension around the circumference of the membrane was also included. It was concluded that cable-suspended designs were more structurally efficient compared to membrane-only designs to avoid wrinkling. This design is illustrated using the wrinkling analysis of Luo et al. in Figure 2.7.

2.2.2 Geometry Optimization

Another strategy for the wrinkle-free design of membrane structures is geometry optimization. Using the principal stress criterion for wrinkled state [53], topology optimization is used to design geometries specifically avoiding wrinkling. Luo et al. [53] showed the possibilities of this technique, creating

wrinkle-free designs for square and rectangular membranes.

$$\left\{ \begin{array}{ll} \text{if } \sigma_1 > 0, \sigma_2 > 0; & \text{Taut state} \\ \text{if } \sigma_1 > 0, \sigma_2 \leq 0; & \text{Wrinkled state} \\ \text{if } \sigma_1 \leq 0, \sigma_2 \leq 0; & \text{Slack state} \end{array} \right. \quad (2.3)$$

Luo et al. [52] also used topology optimization to find optimal wrinkle-free configurations for gossamer structures, including a cable suspension. Xing et al. [96] analysed the principal stress criterion for different fixture designs, using topology optimisation to find the best geometry of the clamps. In research related to Gossamer structures [11], it was proved that for square and triangular membranes, trimming the edges into gentle circular arcs can drastically reduce the extent of corner wrinkles.

2.2.3 Permeability

In shape optimization of several membrane geometries under tension, [53], it already became clear that holes in the geometry can lead to a reduction of wrinkling behaviour. This was further examined and confirmed for different membrane geometries and membranes with a stiffer region [45]. In all previous works on shape optimization and permeability induced wrinkling reduction, topology led to the desired wrinkle-free result. The physical principles behind the influence of permeability on wrinkling behaviour, however, was not well understood. For this reason, most recently these physics have been further examined in a master thesis by Lavaerts [41]. Furthermore, a similar solution can result in

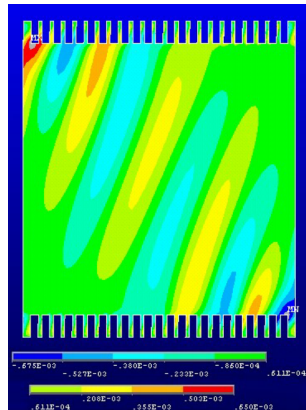


Figure 2.8: Wrinkle pattern for shear displacement predicted for a membrane shear compliant borders by Leifer et al. [42]

wrinkle reduction in shear tensioned membranes, namely by the use of shear compliant borders [42, 43], see Figure 2.8. Shear compliant borders are edges with many small incisions in them, designed to reduce the propagation of shear through the material.

2.3 Auxetic Materials

Conventional materials undergo lateral compression when longitudinal tension is applied. The behaviour of the material under deformation is governed by one of the fundamental mechanical properties of materials—the Poisson's ratio (ν). Consequently, most materials have a positive ν [25]. This may result in local compressive stresses in a structure as a result of tension forces, and for structures with very low bending stiffness, wrinkling can occur.

In some other materials called *auxetic materials*, using permeability or hinges, the opposite can be achieved, namely a negative Poisson's effect. Auxetic materials are of interest in this research because they have been shown to reduce global wrinkling in some cases [10]; therefore an in-depth literature

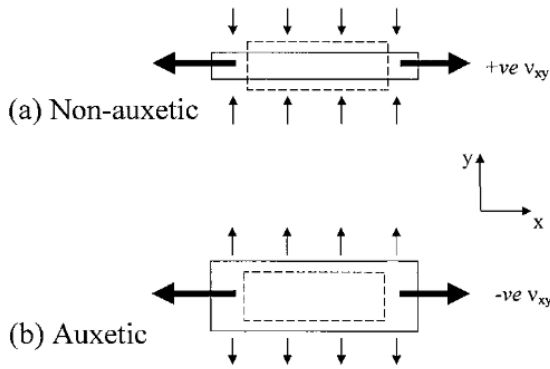


Figure 2.9: Conventional material behavior versus auxetic behavior [25]

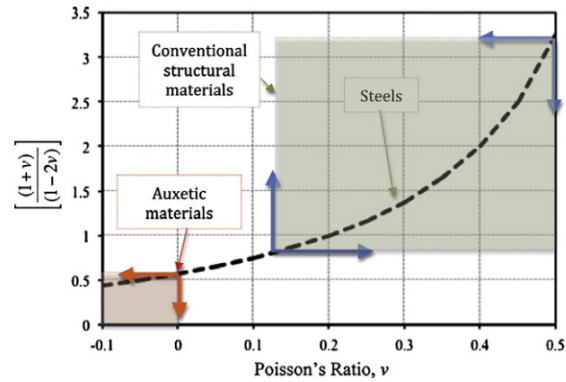


Figure 2.10: Graphical description of the relation between the Poisson's ratio and the value of $\frac{(1+v)}{(1-2v)}$ for conventional structural materials [72]

analysis on them is performed. By definition, auxetic materials are metamaterials which exhibit a Poisson's ratio of zero or below [25]. Materials with a negative Poisson's ratio, undergo lateral expansion, when stretched longitudinally. This is illustrated in Figure 2.9.

Auxetic materials are of interest because of the novel behaviour they exhibit under deformation, and also because many material properties can be enhanced as a result of a negative, or even semi-negative ν [25], depicted in Figure 2.10. This is illustrated in the work of Evans and Alderson [25]. An example of those material properties is indentation resistance, which is useful in the design of bulletproof clothing. When an object impacts the auxetic material, material flows into the vicinity of the impact as a result of lateral contraction accompanying the longitudinal compression. Hence the material densifies at the impacted location, which leads to increased indentation resistance. Evans and Alderson described another application where the potential of auxetic materials seems evident, namely blood vessel prostheses. When a pulse of blood flows through a non-auxetic material, the material may deform and become thinner, leading to the risk of rupture. If an auxetic material is applied, the material will become thicker upon deformation, hence not inducing any risk of rupture in this location.

In recent studies, several types of auxetic materials have been investigated, either using folds [26], perforations [78, 61, 10] or hinge-like structures [40, 73, 28, 31]. In another study, isogeometric shape optimization was used to design a material with a minimal Poisson's ratio and minimized stress concentrations in the hinges [89]. It also proved to be possible, to design an isotropic auxetic material, which has a petal shape. In the contributions of Sigmund, Assidi and Ganghoffer [79, 6] it appeared that materials can be tailored to a structure endowed with the desired constitutive properties.

In the context of wrinkling reduction, the potential of auxetic materials was already highlighted by the work of Bonfanti and Bhaskar [10]. They compared the wrinkling behaviour of two similar shaped membranes, of which one is auxetic and one is non-auxetic. It showed that the non-auxetic membrane had a global wrinkling response, whereas the auxetic membrane showed a local wrinkling response, near the clamped edges. Using diamond shaped holes, with different orientations, they architected a microstructure with an apparent negative Poisson's ratio. They applied tensile stress in a displacement controlled mode. The film that possessed a positive Poisson's ratio developed wrinkles at the centre upon stretching while remaining taut near the clamped edges, analogous to the behaviour described by Cerda [16]. On the contrary, the film which exhibited a negative Poisson's ratio formed localized wrinkles near the clamped edges upon stretching, while maintaining taut at the centre. This stabilization is a result of the auxetic material properties. In figure 2.11 the two deformed strips are portrayed.

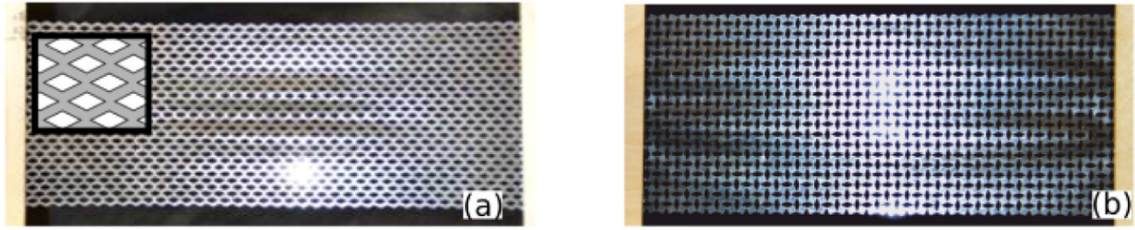
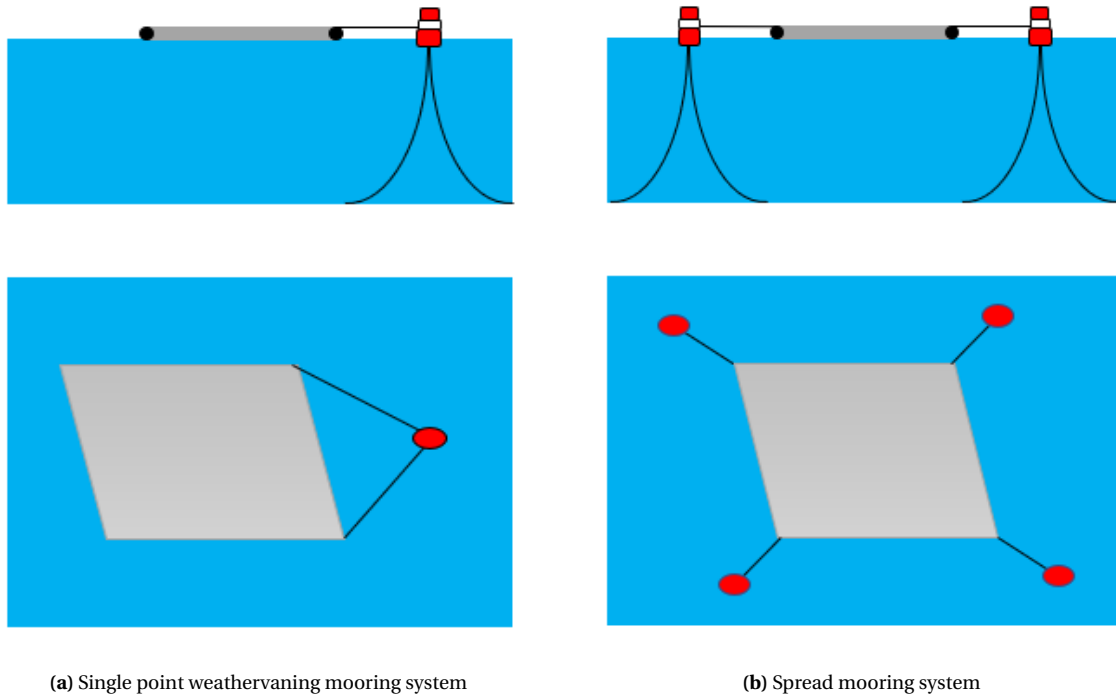


Figure 2.11: (a) structured film with a positive apparent Poisson's ratio shows wrinkles at the center, (b) perforated film with an apparent negative Poisson's ratio is stabilized at the center [10]

2.4 Mooring of Flexible Bodies Offshore

A mooring system holds the floating solar platform in a suitable position according to water depth and direction and sometimes helps to maintain the shape of the structure [46]. For the design of mooring systems for OFFSSs, no converged solution is observed in literature.

Trapani and Millar [84] expected that offshore flexible floating solar mooring arrangements will be similar to those of wave energy converters (WEC) or fish farm cages. Two types of mooring configurations are identified for WECs [32]: *spread moorings* (SM), using catenary cables, which are common for semi-submersible platforms; and *single point moorings* (SPM), which enable the structure to weather-vane into the incident waves. Since OFFSS mooring design is yet to be developed, these systems will be looked into further in this research. The mooring configurations discussed previously are illustrated in Figure 2.12a and 2.12b respectively.



(a) Single point weathervaning mooring system

(b) Spread mooring system

Figure 2.12: Mooring configurations schematically illustrated. Side view and bird eye view.

It is noticed, that in existing WEC technology, a spread catenary mooring system is rarely used, due to its deficient performance in shallow water [97]. Hence, the single point mooring system is advised by Xu, Wang, and Soares [97] to be applied to large dimension WECs owing to the ability to minimise environmental loads, due to their freedom of rotation. In a study of Li et al. [44] an optimized single

point mooring configuration for an offshore fish farm is demonstrated. In a similar review on mooring design for WECs from Luca Martinelli and Cortellazzo [51] a different mooring configuration was discussed, which likewise exhibits the weathervaning effect.

In the effort of Liu et al. [50] an analytic approach for the prediction of mooring loads on flexible floating structures is presented. Additionally, they concluded that mooring force increases in proportion to wave height for each structure and has a larger inclination for a thicker one, which again secures the potential thin flexible structures for offshore floating solar. A thin film flexible floating PV array prototype has been realised by Trapani and Millar [84], involving an SPM system inspired by WEC technology. Yet, this prototype was only analysed in sheltered, still water conditions. In the work of Pociavsek et al. [71], it was concluded that thin sheets on elastic solids or fluids will develop folds under compression. Folds are characterized by highly localized curvatures. For floating solar FPV, this is predicted to be a potential failure mode, and therefore it is to be avoided. Considering the latter, mooring systems for flexible floating bodies should be configured so that compression is averted in the structure.

In conclusion, literature lacks a thorough understanding of the most effective mooring system for OFFSSs, taking into account wrinkling reduction. However, the SPM design and the SM are expected for OFFSS applications. The mooring system should be designed such that compressive loads in the structure are avoided.

2.5 Concluding Remarks

In the previous chapter, literature is described concerning wrinkling fundamentals, a state-of-the-art on design for wrinkling resistant structural design, auxetic materials and mooring systems for OFFSSs.

- OFFSSs are susceptible to **wrinkling**. Wrinkling can be provoked by elementary **loading conditions uni-axial tension, compression on an elastic substrate, bi-axial tension and shear**. The phenomenon wrinkling arises when in-plane forces are in balance with the bending resistance in the sheet. For OFFSSs, this induces structural risks, as wrinkling is assumed a potential limit state.
- **Wrinkling resistant structural design** for OFFSSs has not been done before, although in Gossamer structure design different solutions are established. Geometry optimization by topology optimization tools has been shown to reduce wrinkling in thin sheets under various loading conditions. Moreover, adding permeability to thin structures has been shown to minimize wrinkling.
- **Auxetic materials** are of interest because of the novel behaviour they exhibit under deformation, namely a Poisson's ratio of 0 or smaller. Material properties can be enhanced due to this behaviour. The auxetic behaviour can have a positive effect on the minimisation of global tension wrinkles. A negative Poisson's ratio is not desired when the auxetic material is clamped, as the auxetic behaviour can *cause* wrinkling. Auxetic materials with a Poisson's ratio of zero does not induce this risk and are therefore of interest.
- **Mooring systems for OFFSSs** are relevant for global wrinkling analysis in OFFSSs, as they transfer the load which holding the structure in its place, to the structure. Hence, they are influencing the load condition and thus the potential wrinkling response. Specific mooring systems for OFFSSs have not been developed yet, but two types of mooring systems are expected in literature: *single point mooring systems* and *catenary mooring systems*. A general design of both mooring systems will be examined further in the thesis.

3

Methodology

In this chapter, the methodology is described, which entails the concrete steps that will be taken to answer both research questions based on the literature gaps, identified in chapter 2.

3.1 Numerical Modelling

The type of modelling that will be adopted in this research is numerical modelling. Literature has shown, that numerical models are sufficiently capable of predicting the nonlinear wrinkling behaviour [94, 93, 69, 27, 48]. Numerical modelling is required for the investigation of the wrinkling behaviour of OFFSSs, as the structures are typically very large and full-scale experiments would therefore be too expensive. Furthermore, experimental inquiries at model scale are also not favourable, as scaling of the wrinkling behaviour structures is not trivial [16, 71]. Numerical modelling has additional benefits: simulating different load conditions can be achieved by tuning parameters and it can provide insights that would be hard to obtain in experiments, such as stress distribution over a very small length scale such as thickness. The commercial FEM software ANSYS [4] will be used for analysis. ANSYS is selected as it offers a wide range of features such as element types, material models and meshing options. In other approaches for computational structural analysis such as Isogeometric Analysis (IGA), these features are not yet publicly available [2].

Firstly, a base case will be designed to get an image of what the platform could look like (see Figure 4.1). The base design will be based on practical considerations, such as the location of the platform, the required amount of buoyancy and installation aspects, all discussed in forthcoming chapter 4. The base case will not be used for wrinkling simulations, as this is numerically not feasible due to memory limitations, which will be discussed more thoroughly in Chapter 6. Therefore, three load cases which expected to capture similar deformation behaviour as the base case are created for further analysis, which can be seen in 5.2. Secondly, platforms are created with the base case material and thickness, but with the aspect ratios and boundary conditions the same as the cases from literature. Then, an investigation is done to find the range of platform sizes that are computationally feasible to analyze. After that, the wrinkling behaviour of the platforms is analysed

Solar panels will be integrated in the base case geometry, by adding multiple solar panel shaped very stiff zones (finite) to the surface of the platform. The solar panels will be modelled with a finite stiffness so that solar panels with of lower stiffness (e.g. flexible solar panels) can be implemented as well. This ensures broad applicability of the model. Schematics of the models with solar panels can be viewed in Chapter 6.

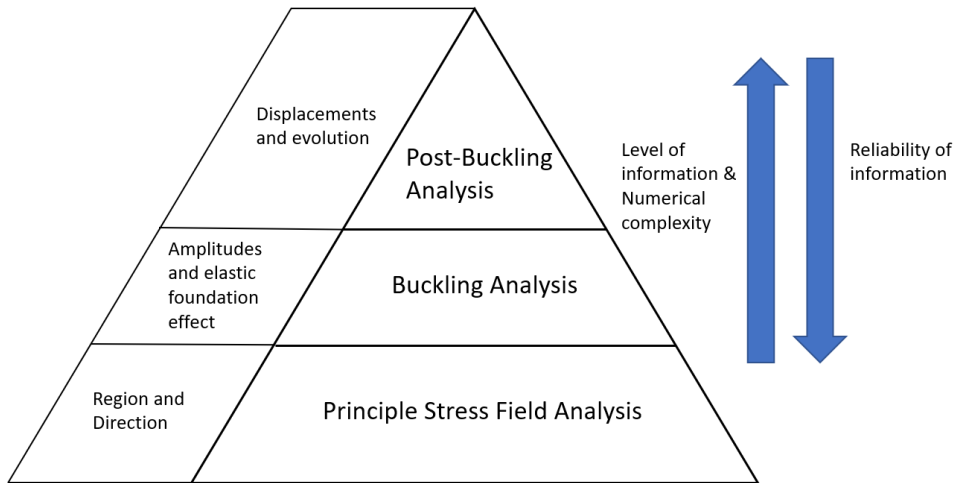


Figure 3.1: Wrinkling Analyses methods Pyramid diagram

3.1.1 Wrinkling Modelling

The wrinkling modelling methodology is illustrated in Figure 3.1. In chapter 2, methods concerning wrinkling modelling are described. It is observed from literature, that nonlinear post-buckling analysis is very sensitive to user-defined bifurcations [93, 80, 27, 69]. An alternative approach is presented, namely the principal stress field approach [94, 95, 41]. In this approach, the principal stress field is studied to investigate the wrinkling onset. For this analysis type, only in-plane simulations are required. This is computationally much less intensive than post-buckling simulations. However, OFFSSs will be deployed in water which has proven to highly influence the wrinkling response of thin sheets to in-plane loading [71, 62, 74]. Therefore, the substrate will also be considered in the thesis. For analyzing wrinkling response on an elastic substrate, the principal stress field is not sufficient, as the wrinkled geometry is formed by the energy balance between the bending energy of the structure and the potential energy of the elastic substrate [15], hence out of plane deformations should be considered when evaluating the wrinkling onset stage. Yet, as further discussed in upcoming Chapter 5, the numerical costs of analyzing nonlinear post-buckling behaviour of the wrinkled membrane including the elastic support are large, since this requires a high mesh refinement. Consequently, for analyzing the wrinkling onset and direction, principal stress analysis is acceptable, but for evaluation of the wrinkling amplitude sizes and wavelengths, one should consider calculating the buckling modes and performing full post-buckling computations.

The benefits of each method are outlined in the pyramid chart in Figure 3.1. principal stress field analysis gives only the region and direction of potential wrinkles. By analyzing buckling modes, an indication is also obtained of the wrinkling profile (i.e. number of wrinkles and wavelengths). Furthermore, since principal stress field analysis is 2D by definition, it can not include the effect of the elastic foundation. The most computationally intensive method is full post-buckling analysis; here the wrinkling evolution and displacements can be gathered. However, achieving a converged result often requires the use of non-physical numerical tricks, such as artificial damping, hence compromising the reliability of the result. In this thesis, the lower part of the pyramid, principal stress field analysis will be used for the bulk of the investigation, due to its lower numerical complexity and higher reliability. The upper two sections will be used to gather more information about the wrinkled shape and elastic foundation effect, in case the presence of wrinkles has already been concluded from principal stress analysis.

3.1.2 Material Models

While flexible materials can be considered as linearly elastic for small strains, when analyzing large strain effects, large strain theory should be considered [85]. Furthermore, general materials display elastic behaviour turning to their original state when a load is applied in a linear regime [39]. Yet, when flexible materials are deformed, they are characterized by hyperelastic tendencies, acting elastically in the range of large strain thus showing a nonlinear relation between load and strain [39]. Accordingly, modelling thin flexible structures involves hyperelastic material models for load cases where strains are large [8]. In section 2.1.2 an extensive description of different nonlinear material models is given. It appeared that while the Ogden material model is very accurate, it requires quite some specific material parameters, which are often hard to obtain. The Mooney-Rivlin model requires three fewer parameters, which have a physical meaning and can be obtained based on material properties. The Neo-hookean material model requires one less material constant, making it easy to implement, but is less accurate for very large strains compared to Mooney-Rivlin. Furthermore, rubber-like materials are nearly incompressible, and for the sake of simplicity, they are often assumed to be incompressible. Since investigation will exhibit a general case of a flexible material under several loads, and focuses on the global wrinkling response, where the elastic substrate is implemented in the analysis, relatively small strains are assumed. For shear, this is especially the case [95], and a Saint Venant-Kirchhoff hyperelastic material model will be utilized. For axial tension and bi-axial tension, wrinkling is expected at higher strain rates [27], and the Neo-Hookean model will be used. If the analyses require materials with a lower Poisson's ratio, a compressible material model should be employed.

3.1.3 Element Selection

FEA will be used for the nonlinear wrinkling calculations. In this section, the used element type will be discussed. In previous literature [27, 47, 12, 80, 94, 93, 69, 33], shell type elements have been used to model the 3D geometry of wrinkled membranes, as they include bending stiffness [4]. Since the principal stress fields will be used to analyze wrinkling behaviour in load cases, instead of the 3D wrinkled geometry, only a 2D element is required. Therefore, the PLANE182 element will be used for the principal stress analyses for the investigation of wrinkling onset. This element is defined by four nodes, with two degrees of freedom at each node: translations in the nodal x- and y-directions. It can model plane stress and plane strain, which will be utilized for the principal stress analysis. Furthermore, incompressibility is safeguarded in the PLANE182 element [8]. For analyzing the wrinkle wavelengths and amplitude sizes, in combination with the elastic foundation, 3D post-buckling is compulsory. For the 3D inquiry, the quadratic shell element (8 nodes) SHELL281 will be used. This element considers out of plane deformations, and is well-suited for linear, large rotation, and/or large strain nonlinear applications [8]. The quadratic element is chosen over a linear element in this case because it can capture bending and it is more capable of capturing complex geometries, such as the wrinkled OFFSS.

3.1.4 Load Definition

The loads which will be applied to simulate a current, are axial tension, bi-axial tension and shear. These load cases are defined in Chapter 5, and illustrated in Table 5.2.

3.1.5 Hydrostatic Pressure Effect Wrinkling

As mentioned in literature [71, 62, 74], the fluid layer below a thin membrane influences the wrinkling behaviour. The stiffness of this elastic substrate penalizes long wrinkle wavelengths. Therefore, when analyzing the exact wrinkled geometry upon deformation, this effect should be considered.

In numerical analysis, several options are at hand for modelling the interaction between the structural deformation of the platform and the water below. For modelling the interaction between flow dynam-

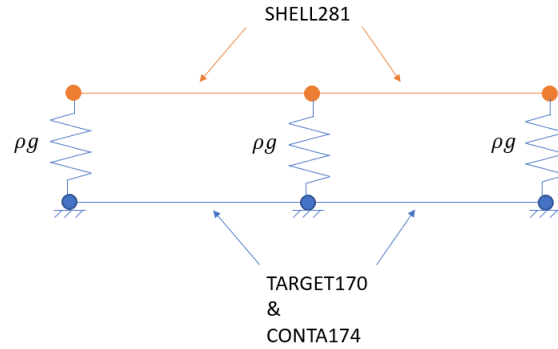


Figure 3.2: Schematic of the elastic foundation element model. The elements TARGET170 and CONTA174 are at the same location. The springs indicate the hydrostatic stiffness.

ics and deformation behaviour, fluid-structure interaction analysis could be applied. This method couples the structural and fluid mechanics to simulate the interaction between these elements. For this type of modelling, the flow field dynamics need to be solved, after which the structural deformations can be computed, which can be numerically challenging due to moving meshes and geometric nonlinearities [81].

Another option for modelling the interaction with the water below the platform, without incorporating the fluid dynamics, is to model the fluid as a static elastic foundation. Elastic foundations are widely used for the analysis of soil-structure interaction, aero-thermo-elastic forces on aeroplane wings and mechanisms in the human body [99]. Both linear and nonlinear elastic foundation models exist, the selection should be based on the expected deformation and load size, as these might induce geometric nonlinearities [99]. Furthermore, some models take into account the effect of shear or friction [99].

In this investigation, the water will be modelled as a linear elastic foundation [30], as wrinkling behaviour will be modelled in a (quasi-)static manner, and the exact fluid dynamics are still unknown (based on platform location, environmental conditions, water depth and so on). The elastic support applies stiffness on each node, normal and tangential to the modelled surface. The value of this stiffness is equal to the hydrodynamic pressure, $P = \rho g \cdot \left[\frac{\text{kg}}{\text{m}^2 \cdot \text{s}} \right]$. This way, the out of plane deformations are penalized and the wrinkles will change shape and location [71].

The elastic support consists of a layer of CONTA174 elements which are connected with bonded contact to the membrane elements, on the same location. On top of the CONTA174 elements, there is a layer of TARGET170 elements, which are fully constrained. Between the target elements and the contact elements, normal and tangential stiffness is applied. The tangential stiffness is set to a value near zero, and the normal stiffness is equal to the hydrodynamic pressure of seawater. A schematic of this situation is provided in Figure 3.2. In this elastic foundation, either bonded contact or unilateral contact can be applied. In Appendix B, these two methods are explained and a comparison is provided between results with elastic foundation wrinkling with bonded contact and with unilateral contact. The differences are addressed and it is concluded that even though the bonded contact presumably overestimates surface tension effects, the deformation is more realistic compared to the unilateral contact considering gravity effects.

3.2 Conclusion

In light of the sections above, the following conclusions can be drawn with regards to the methodology employed during this research.

- The research questions will be answered by analysing a numerical model, created in **ANSYS FEM software**. Numerical modelling is preferred as OFFSS are large structures and scaling of wrinkling behaviour is not trivial. Commercial ANSYS FEM Software is selected because this software is mature and allows analysis of complex structures.
- From literature, it is known that the onset of wrinkling and its location can be well predicted using **principal stress field analysis**. For the analysis of the wrinkled geometry, affected by the hydrostatic pressure, **post-buckling analysis** is required. However, post-buckling analysis is much more computationally intensive, may be influenced by tuning parameters. Consequently, principal stress analysis will be used to analyse whether wrinkling will occur; and if the results indicate this, post-buckling will be used to inspect the deformed geometry.
- Relatively small strains are assumed during the wrinkling analyses for the load case shear [95], therefore, in that case, the **Saint Venant-Kirchhoff material model** will be used. For the cases axial and bi-axial tension, wrinkling occurs at higher strains [27] and therefore the Neo-Hookean model will be utilized, as it is computationally time-efficient and requires few additional parameters.
- The 2D element **PLANE182** will be used for principal stress field analysis, 3D element **SHELL281** will be used for 3D post-buckling analysis.
- The hydrostatic support will be modelled using an **elastic foundation**, comprising of two additional layers of elements that induce a out-of-plane stiffness on the platform.

4

Base Design

This chapter outlines the formulation of a base case that will function as the starting point for the wrinkling analyses. It will focus on sub-question 1.b):

1. b) *How can a base design for offshore flexible floating solar structures be developed, taking into account location and installation?*

Firstly, the global dimensions of the design are estimated, based on practical considerations. Then the influence of thickness on size is examined, given installation requirements. After this, a material type is selected and the implications of required buoyancy on the design are argued.

4.1 Global Dimensions

In this study, the base for the OFFSS design will be existing offshore wind farms. Several benefits are foreseen for locating OFFSS between offshore wind turbines. First of all, it is a relatively sheltered area from shipping, so the OFFSS will not conflict with shipping routes. Secondly, wind farms provide an infrastructure for mooring the OFFSSs, as well as a power infrastructure in the form of an electrical grid [82]. An example set-up of an OFFSS in an offshore wind farm is illustrated in Figure 4.1.

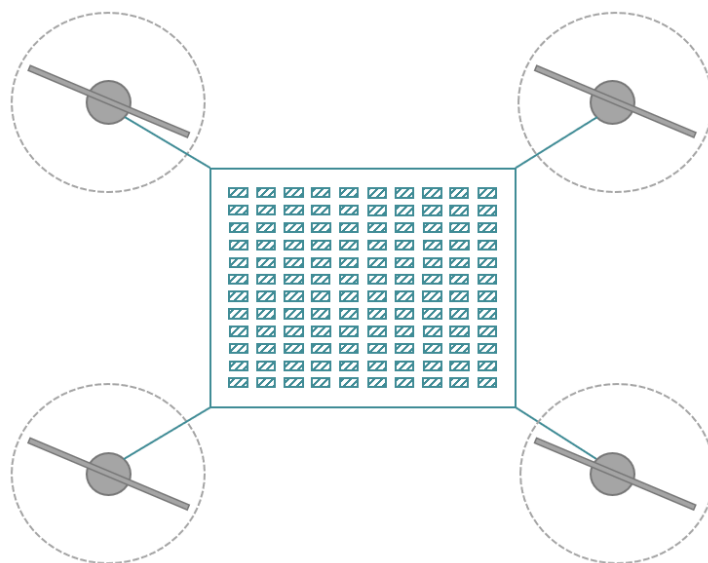


Figure 4.1: Sketch of an OFFSS between four offshore wind turbines. The dimensions are not at scale.

As a starting point for deriving global dimensions of the design, current offshore wind parks in front of the Dutch coast are analysed. The Borssele 3 & 4 site consists of 9.5 MW turbines, with a rotor diameter of 164 meters [9]. The typical distance between two offshore wind turbines is 5 to 8 diameter lengths [13]. Therefore, a distance of 1000 meters between turbines is estimated as a common distance between offshore wind turbines. Furthermore, the grid of offshore wind parks generally consists of squares and/or rectangles. Therefore a rectangular shape will be assumed, to use the available space efficiently. A range of aspect ratios will be studied. Next to that, it is assumed that the length of the solar platform is 80 per cent of the length between turbines, to leave sufficient space for mooring. If 80 per cent of the length between wind turbines is covered by solar platform, the dimensions would be $L \times B = 800 \times 800$ meters.

4.2 Thickness

Working in an offshore environment is generally regarded as a high-risk operation, due to the harsh weather conditions. Therefore, minimising offshore time can reduce risks as well as costs of the operation. Accordingly, to increase the feasibility of OFFSS technology, the structure should be easy to install, by making it lightweight and compact. This will allow for efficient and fast transport and installation operations. Furthermore, based on a selected platform material, the influence between thickness and buoyancy can be determined. These aspects are discussed in the following sections.

4.2.1 Installation

To make the structure compact, inspiration can be drawn from pipe laying vessels, which use reels to transport very long pipes. The same can be done for OFFSSs to make the structure compact; by coiling the platform up around a reel. For minimising the weight of the structure, as well as reel dimensions, the platform thickness should be kept at a minimum. In the following calculation, rough reel dimensions are estimated based on assumed thicknesses. The calculation is based on a simplified cross-section of a membrane coiled around a reel. This situation is illustrated in Figure 4.2, whereby the main parameters used in the calculation are indicated as well. The relation between the platform

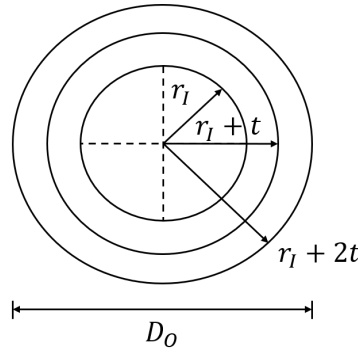


Figure 4.2: Reel with Windings Sideview Sketch

length, the reel inner diameter and platform thickness is roughly as follows

$$L = \sum_{k=0,1,2,\dots,n} (2\pi (r_I + k \cdot t)) \quad (4.1)$$

Whereby L is platform length, r_I is the reel inner diameter, k equals the number of windings and t is the platform thickness. Making use of the triangular number $T_k = \frac{k(k+1)}{2}$ [90], the formula can be rewritten without the summation mark.

$$L = 2\pi \left((k+1)r_I + \frac{k(k+1)}{2}t \right) \quad (4.2)$$

Rewriting the previous expression, using the abc-formula, the number of windings on the reel can be calculated.

$$k = \frac{-\frac{t}{2} - r_I + \sqrt{\left(\frac{t}{2} - r_I\right)^2 + \frac{tL}{\pi}}}{t} \quad (4.3)$$

The outer diameter of the reel can be determined by the following formula.

$$D_O = 2(r_I + k \cdot t) \quad (4.4)$$

In the Figure 4.3, the relation between platform thickness, and reel outer diameter is illustrated for reel inside diameters: 5, 10, 15 meters.

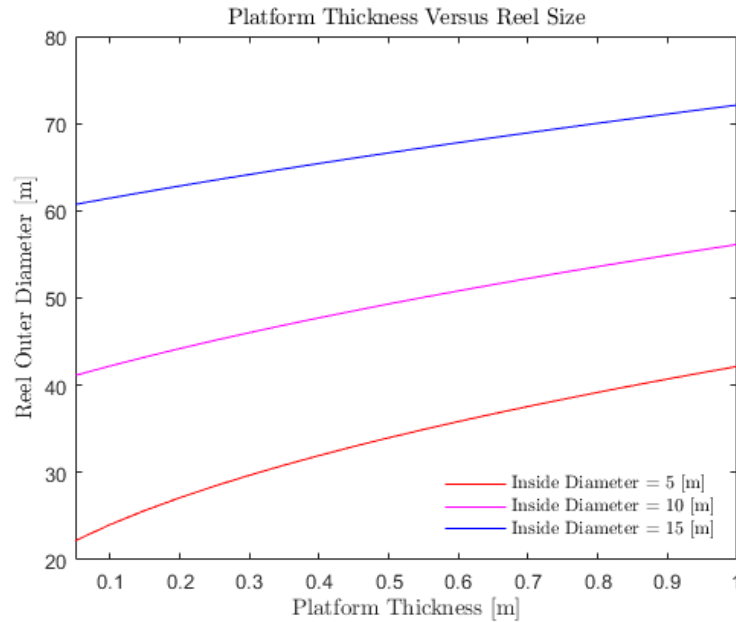


Figure 4.3: Platform Thickness versus Reel Diameter

To determine the minimum thickness, inspiration is drawn from pipe laying reel dimensions. In Figure 4.5, a pipe laying vessel is shown with two reels on board. In Figure 4.6, a reel under construction in a shipyard can be seen. Both reels have an outer diameter of approximately 30 meters, as indicated in the figures. The inner diameter of the illustrated reels seems to differ but is assumed to be between 15 and 25 meters. Due to the high flexibility of the solar platform, it is expected that a smaller inner diameter should suffice for coiling the platform itself. However, the panels are stiff, and a larger inner diameter reduces the risk of the panels cracking when being coiled around the reel.

Furthermore, the thickness of a typical conventional solar panel is around 0.05 meters [23]. It is assumed that having the panels embedded with additional membrane material below the panels reduces the risk of damage to the solar panels. This will allow higher bending angles for the platform, i.e. a smaller inner diameter. Since it is not clear what the maximum bending radius of solar panels embedded in membrane material is, for the sake of this research, the highest inner diameter of 15 meters is assumed to be the most feasible.

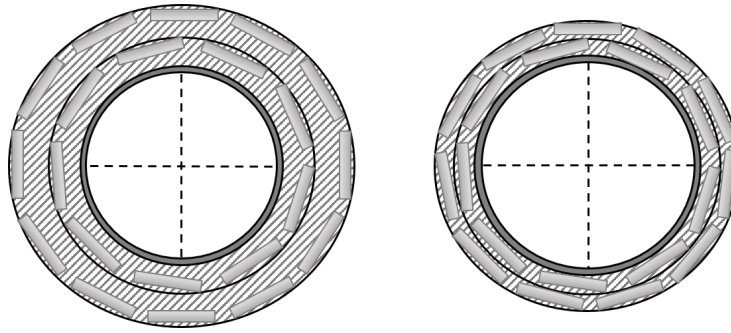


Figure 4.4: Cross-section of Reel with Solar Platform. On the left: Solar platform with additional membrane material below the panels. On the right: solar platform without additional membrane material below panels

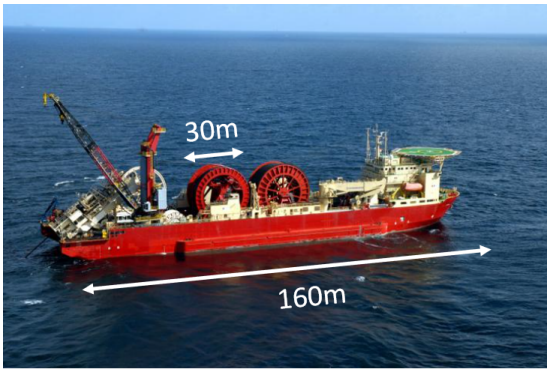


Figure 4.5: Pipe laying Vessel with Reels[24]

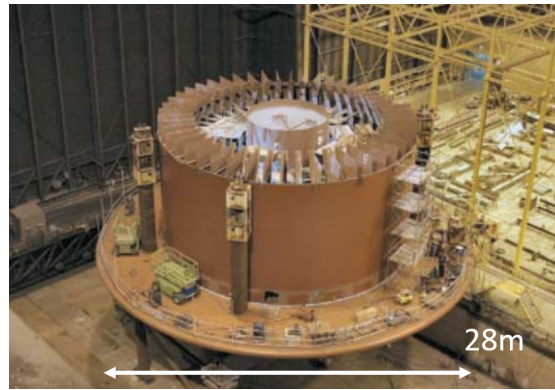


Figure 4.6: Pipe lay Reel Construction[35]

See Figure 4.4 for a schematic illustration of this. Therefore a thickness of 0.05 meters between the panels and the water will be taken, which yields a total platform thickness of 0.1 meters. This results in an outer diameter of 60 to 65 meters when rolled up. This is larger than the size of a offshore pipe laying reel. Further research is recommended into the maximum bending radius of the solar panels embedded in the membrane, to investigate the possibility of using a smaller inner radius. Another option could be to coil smaller lengths of platform around the reel.

4.2.2 Material Selection

For the material selection of OFFSS, three flexible and weather resistant (water and UV) materials are considered: Ethylenevinyl-acetaat (EVA), Neoprene and Polyurethane. The materials and their properties and applications are discussed below. In Table 4.1, the mechanical properties of the materials are stated, which are used to select the most suitable material for OFFSS application.

1. EVA is the copolymer of ethylene and vinyl acetate, with a weight rate of vinyl acetate typically varying from 10 to 40%, and the remainder being ethylene [91]. EVA materials are "rubber-like" in softness and flexibility. Furthermore, it has the characteristics of being hardwearing, weather resistant and buoyant [67]. Applications of EVA can be found in flip-flop soles, garden kneelers and foam flutter boards.
2. Neoprene is a synthetic rubber which is produced by the polymerization of Chloroprene [92]. Foamed neoprene is a popular material for making protective clothing for aquatic activities, such as fishing waders and wetsuits, as it provides excellent insulation against cold and the material is buoyant [92].
3. Polyurethane foam is an open celled polymer material, which is lightweight and water resistant [7]. This material is used for a variety of products, including washing sponges, bedding and isolation

Table 4.1: Material Mechanical Properties

Material Type	Density [$\frac{kg}{m^3}$]	Youngs Modulus [MPa]	Tensile strength [MPa]	Reference
EVA	280	15	20	[67, 70]
Neoprene	1230	5	20	[5, 19]
Polyurethane Foam	70	20	1	[7]

material.

As discussed above, all three materials are water resistant and flexible. Therefore the selection of the most suitable material for OFFSSs is based on the comparison of their mechanical properties. As can be seen in Table 4.1, the density of Polyurethane is the lowest, and Neoprene is the heaviest material. EVA is also relatively lightweight compared to Neoprene. Since the membrane should remain afloat whilst carrying solar panels and their electrical infrastructure, it is essential for the material to provide sufficient buoyancy. Therefore both EVA and Polyurethane are more favourable, based on their lower densities compared to Neoprene. As the Youngs Moduli of these two materials are in the same range, their flexibility characteristics are assumed similar. Comparing the tensile strengths of the two materials, it can be seen that EVA can withstand higher tensile stresses than Polyurethane foam. As OFFSSs are expected to carry high tensile loads due to the mooring and environmental loads, this is assumed to be an important parameter for the material. Therefore, EVA is expected to be the most appropriate material for OFFSSs.

4.2.3 Hydrostatics

The hydrostatics of the platform are investigated, by studying the relation between the platform thickness and draft.

Table 4.2: Parameters for Hydrostatics Calculation

Parameter	Size	Unit	Reference
m_{PV}	20	kg	[23]
A_{PV}	1.60×1.00	m	[23]
A_{OSP}	800.00×800.00	m	See section 4.1
ρ_{EVA}	280	$\frac{kg}{m^3}$	See table 4.1
ρ_{sw}	1025	$\frac{kg}{m^3}$	
$PV_{coverage}$	80%	-	
n_{panels}	320.000	-	

The parameters used for the following hydrostatics calculation can be found in Table, 4.2. The number of panels is estimated by assuming 80 percent of the platform area is covered by panels.

Then the total mass of the structure is computed by

$$m_{tot} = n_{PV} \cdot m_{PV} + A_{OSP} \cdot \rho_{EVA} \cdot t \quad (4.5)$$

Which results in the draft of the platform using the following relation

$$T = \frac{m_{tot}}{\rho_{sw} \cdot A_{OSP}} \quad (4.6)$$

The free board per thickness can be calculated by

$$F = T - t \quad (4.7)$$

If the free board is positive, the structure has sufficient buoyancy to float.

$$T - t > 0 \quad (4.8)$$

This is the case for all thicknesses larger than 0.05m. This thickness minimum is called t_0 .

$$t_0 = 0.05 \quad (4.9)$$

This means that, due to the low density of the material EVA, buoyancy forms no constraint for the selection of a platform thickness. All thicknesses above t_0 are feasible from a hydrostatics perspective. Therefore the thickness will be based on minimal reel size and platform weight, as well as solar panel protection considerations during transport; a thickness of 0.1 meters will be selected for the base design.

4.3 Conclusion

The conclusion to the posed sub-question 1.b is given, by establishing the main parameters for the base case design to evaluate the wrinkling behaviour of an OFFSS. The main parameters are selected for the base design which will be required for upcoming wrinkling analyses. These are summarized below in Table 4.3.

- Offshore wind farms are used as a starting point for the location of OFFSSs. Based on this, the global dimensions are $L \times B = 800 \times 800$ meters.
- For the thickness of the platform, the aspects of installation; material type and hydrostatics are considered. The platform will be **transported coiled on reels**, to enhance transport and installation efficiency. The **material type EVA** is chosen, for its buoyancy and weather resistance properties. Due to the low density of the material, **buoyancy forms no constraint** on the selection of a thickness. Based on minimal reel size and platform weight as well as solar panel protection considerations during transport; a **thickness of 0.1 meters** will be selected for the base design.

Table 4.3: Base Design Main Parameters

Parameter	Size or type	Unit
Global dimensions	800 × 800	m
Platform thickness	0.1	m
Material type	EVA	-
ρ_{EVA}	280	$\frac{kg}{m^3}$
E_{EVA}	15	MPa
ν_{EVA}	0.31	-

5

Numerical Wrinkling Analysis

As mentioned in chapter 2, wrinkling of thin sheets is a highly unstable phenomenon, due to large deformations and nonlinear effects. This makes numerical analysis challenging. In this chapter the numerical tools used for the wrinkling analyses will be described, using three benchmark cases for demonstration purposes. Firstly, the benchmark cases are discussed briefly, and their boundary conditions are explained. Then, wrinkling results obtained by principal stress analysis, buckling and post-buckling analysis are established. The differences are examined. Thereafter, the sensitivities of the parameters applied modes as bifurcation, stabilization and grid size are investigated. This will result in a conclusion to research sub-question 1.c:

1. c) *What is the influence of numerical tools on wrinkling results of offshore flexible floating solar structures?*

5.1 Benchmark Cases

Recall the numerical methods for wrinkling analysis from chapter 3: principal stress analysis and post-buckling analysis. Three basic wrinkling load cases, inspired by cases from literature [95, 27], are used to benchmark the numerical tools, required for wrinkling analysis. The cases that are investigated with regards to their wrinkling response are uni-axial tension, bi-axial tension, and shear, as these are assumed to be close to load cases that could physically occur when the OFFSS is located in between offshore wind turbines. The schematic figures in the first column of table 5.2 represent the analysed load cases and the boundary conditions are indicated. The geometry dimensions of the three benchmark cases are provided in table 5.1, based on cases from literature from Wong and Pellegrino, Fu et al. [95, 27].

Load case	L [mm]	B [mm]	t [mm]	E [$\frac{N}{mm^2}$]	ν [-]
Axial tension	280	140	0.14	1	0.499
Bi-axial tension	500	500	0.025	3500	0.31
Shear	380	128	0.025	3500	0.31

Table 5.1: Benchmark Cases Model Dimensions

Axial tension case The axial tension case is performed by clamping the structure on the left edge, while applying tension on the right edge, in the axial direction. This loading induces symmetrical deformation over the transverse axis. Furthermore, Fu et al. [27] found that symmetrical and anti-symmetrical buckling modes arise in the axial tension case at the same eigenvalue, and therefore they

are equally likely to appear once the critical wrinkling threshold is reached. Therefore symmetrical or anti-symmetrical boundary conditions can be applied on the longitudinal axis.

Symmetrical boundary conditions are modelled by allowing zero slopes at the symmetry axis, combined with a constrain on displacements perpendicular to the axis. Anti-symmetry is modelled by allowing rotations at the anti-symmetry axis while constraining displacements in line with the axis and perpendicular to the axis. In this case, symmetrical boundary conditions are enforced at the left edge and anti-symmetrical boundary conditions are applied at the bottom edge. This is done by restricting x-displacements and z-rotations on the left edge and constraining y-displacements and z-displacements on the bottom edge. This way, only one-fourth of the geometry is modelled to save computational costs.

Bi-axial load case The bi-axial load case consists of a square sheet being pulled on one corner, while all other corners are clamped. On the lower right side, the edge is clamped. On the upper right side, a bi-axial tension load is applied. On the lower left, and upper right sides also a bi-axial tension load is applied. The absolute load on the upper left edge is four times higher than the absolute load on the other diagonal axis. This type of asymmetrical loading is applied, as it has shown to produce large global wrinkles [93], which is convenient for the analysis.

Shear analysis The shear analysis is carried out by clamping a rectangular membrane on the bottom side while the top edge is displaced laterally. The left and right edges can move freely.

For further validation of the results and the sensitivities of input parameters, the shear case will be investigated in detail in section 5.4, comparing the results with the experimental data from Wong and Pellegrino [95].

The axial and bi-axial tension cases are demonstrated in the coming section. The axial case has been validated in detail by Lavaerts [41]. In this study, it was found that the wrinkling behaviour is highly dependent on the initial deformation which is used. Analysis of negative principal stresses was proposed as an alternative method for predicting the wrinkling behaviour for this case, as this type of analysis does not rely on user-defined inputs.

The bi-axial load case is presented and compared qualitatively, but a quantitative comparison is not possible with results from literature [93, 95], since it is not clear what exact boundary conditions have been used.

5.2 Wrinkling Analysis Approach

This section considers the steps which have to be taken to perform wrinkling analyses in ANSYS FEA software, using principal stress analysis and post-buckling analysis.

5.2.1 Principal Stress Analysis

Principal stress analysis studies principal stresses, to inspect the presence of wrinkling and the region and direction of potential wrinkles. Principal stresses are normal stresses at an angle θ_p , where the shear stress θ_{xy} is zero. The first principal stress is the stress in line with the first principal axis, and the second principal stress is orthogonal to the first principal stress. If the second principal stress is negative, we know that there is local compression. When local compression occurs in flexible membranes, wrinkling can occur. Furthermore, the direction of wrinkles can be observed from the orientation of negative principal stresses; as wrinkles form orthogonal to compression vectors.

Principal stresses are obtained by performing a static or dynamic structural analysis. Depending on

the size of strains and material type, a linear or nonlinear structural analysis should be selected.

The principal stress analyses are performed in general as follows.

1. Perform a (nonlinear) structural analysis using a force or displacement control
2. Post process principal stress results

In this thesis, the membrane structure can be modelled in 2D if wrinkling deformations are not considered. Then these steps are specified as follows.

1. Perform a 2D nonlinear static structural analysis using a force or displacement control
2. Post process principal stress results

5.2.2 Post-Buckling Analysis

Post-buckling analysis is more computationally extensive than principal stress analysis, since first, a perturbation has to be applied before the nonlinear 3D analysis is performed. This analysis requires more input parameters which can influence the convergence of the analysis and the accuracy of the result.

The post-buckling analyses are performed in general as follows.

1. Perturb the geometry
2. Perform nonlinear static analysis on the perturbed geometry, using force or displacement control. Use stabilization for numerical damping if the simulation does not converge to a solution.
3. Post process wrinkling results

In this investigation, buckling modes are used as a perturbation for the post-buckling analysis. This requires a linear static analysis of the structure in combination with a buckling analysis, to find the buckling shapes. Then the steps are specified as follows.

1. Perform a linear static analysis with load or displacement control while calculating prestress effects
2. Execute a linear buckling analysis, which solves the linear eigenvalue problem to find the buckling modes
3. Perturb the geometry
4. Selection of relevant buckling modes
5. Impose combination of buckling modes for the initial displacement
6. Perform nonlinear static analysis on the perturbed geometry, using force or displacement control. Use stabilization for numerical damping if the simulation does not converge to a solution.
7. Post process wrinkling results

The procedure comprises several complexities. First of all, finding buckling modes in step 2 can be challenging, as it is unclear what the critical buckling load is. Secondly, it is important to select the right modes in step 3, as the selection of modes can influence the convergence behaviour. Furthermore, it is not trivial what modes should be applied to obtain the correct deformed geometry, according to simulations. Due to the inherent instabilities of the simulation, the solution can be very different when a different set of modes is applied as bifurcation. Three reasons can be identified for this numerically singular behaviour:

- Eigenmodes corresponding to low eigenvalues can resemble local deformation modes of the membrane [95], which will not result in global wrinkling
- Instabilities can be very close to each other [95], which means that the wrinkled shape forms due to a series of buckling events
- Another issue can be, that some load cases such as axial tension [27, 69], involve high strains, making it hard to obtain the right buckling modes using linear buckling analysis.

Furthermore, in load conditions where many wrinkles are generated, such as shear; or load cases which include very high steepness in the wrinkle, such as bi-axial tension; convergence can rarely be achieved, without the use of numerical stabilization. Stabilization adds numerical viscous damping to affected nodes of the structure. This is thoroughly explained in the article by Cities and Meeting [18]. The method dissipates energy from the model, to aid convergence for highly nonlinear activity. This helps, for example in the shear case when the geometry 'jumps' to an increased number of wrinkles. Both aspects and their influence on the result are further examined in section 5.4.

5.3 Results Principal Stress and Post-Buckling

The cases are solved using principal stress analysis firstly, after which full post-buckling analysis is performed. In table 5.2, the third principal stresses are plotted in the second column. In the red contours are regions of zero negative principal stress, while the other colour contours indicate negative principal stress regions. In the third column, the vector diagrams are shown. These indicate the direction of the negative principal stresses. From the vector directions, the local compression axes can be observed [68]. Hence, the wrinkles will form orthogonal to these vectors. From these two results combined, both the region and the direction of wrinkles can be estimated.

In table 5.2, the wrinkled geometry computed by post-buckling analysis is displayed in the fourth column. The contours indicate the out-of-plane displacements, i.e. wrinkles. Comparing these results to the principal stress analysis, it can be concluded that principal stress analysis well predicts the region and direction of wrinkles, but it gives no information about the number of wrinkling or the amplitude size.

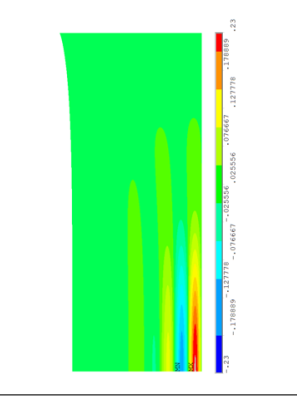
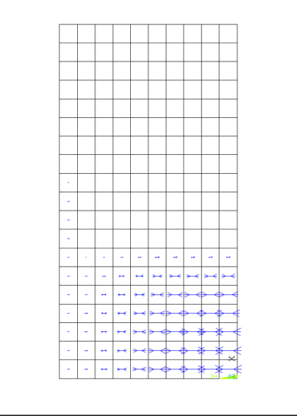
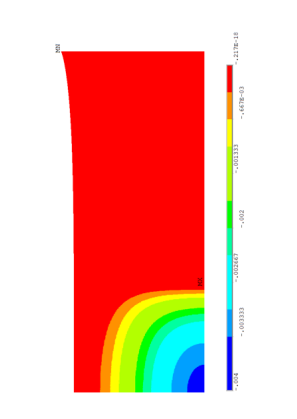
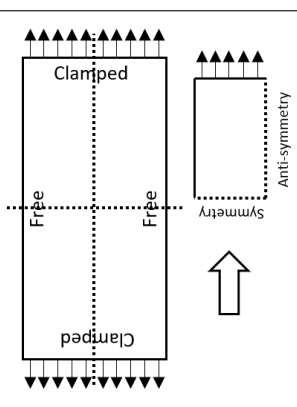
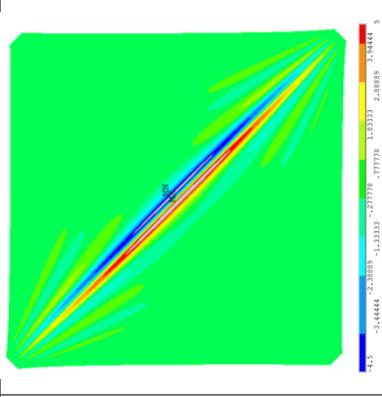
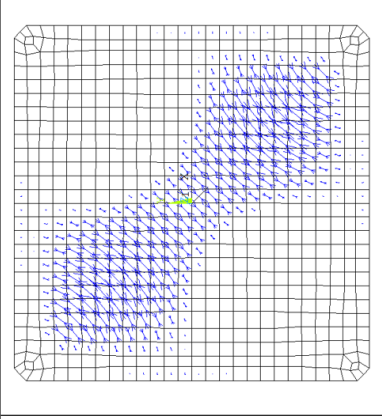
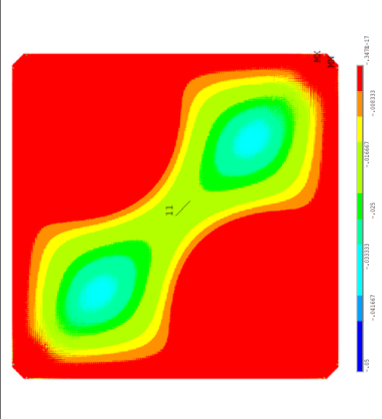
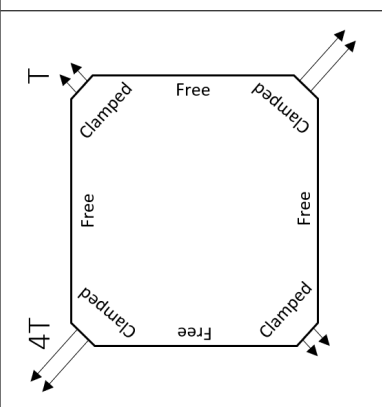
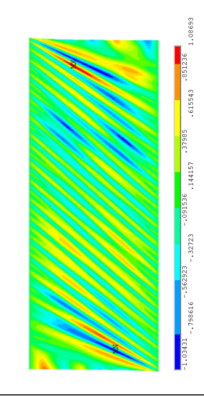
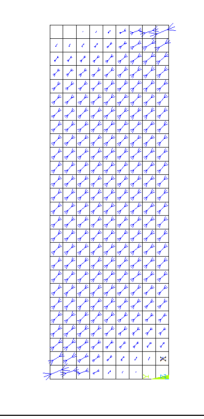
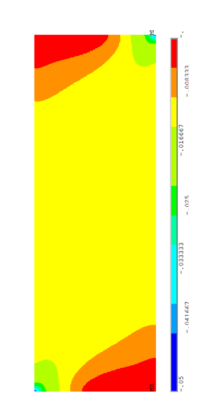
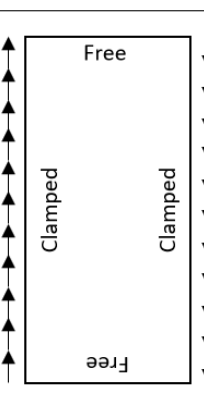
Load Case Sketch	Negative Principal Stress Contours	Negative Principal Stress Vectors	Wrinkled Geometry
 <p>Diagram showing a rectangular plate with boundary conditions: Clamped (top and bottom), Free (left and right). A vertical dashed line indicates symmetry. Applied loads are shown as arrows along the top and bottom edges. A smaller diagram shows the anti-symmetry condition with a horizontal dashed line and an upward arrow.</p>	 <p>Contour plot of negative principal stress. The color scale ranges from 0.000 to -0.00133. The plot shows stress concentration at the corners and along the bottom edge.</p>	 <p>Vector plot of negative principal stress. The plot shows a grid of blue arrows representing the direction and magnitude of the stress vectors across the plate.</p>	 <p>Contour plot of the wrinkled geometry. The color scale ranges from 0.000 to 0.00023. The plot shows the deformation of the plate, with wrinkles appearing along the bottom edge.</p>
 <p>Diagram showing a hexagonal plate with boundary conditions: Clamped (left and right), Free (top and bottom). Applied loads are shown as arrows along the top and bottom edges.</p>	 <p>Contour plot of negative principal stress. The color scale ranges from 0.000 to -0.00133. The plot shows stress concentration at the corners and along the bottom edge.</p>	 <p>Vector plot of negative principal stress. The plot shows a grid of blue arrows representing the direction and magnitude of the stress vectors across the hexagonal plate.</p>	 <p>Contour plot of the wrinkled geometry. The color scale ranges from 0.000 to 0.00023. The plot shows the deformation of the hexagonal plate, with wrinkles appearing along the bottom edge.</p>
 <p>Diagram showing a rectangular plate with boundary conditions: Clamped (left and right), Free (top and bottom). Applied loads are shown as arrows along the top and bottom edges.</p>	 <p>Contour plot of negative principal stress. The color scale ranges from 0.000 to -0.00133. The plot shows stress concentration at the corners and along the bottom edge.</p>	 <p>Vector plot of negative principal stress. The plot shows a grid of blue arrows representing the direction and magnitude of the stress vectors across the plate.</p>	 <p>Contour plot of the wrinkled geometry. The color scale ranges from 0.000 to 0.00023. The plot shows the deformation of the plate, with wrinkles appearing along the bottom edge.</p>

Table 5.2: Boundary Conditions and Results of the Wrinkling Analyses of Three Benchmark Cases

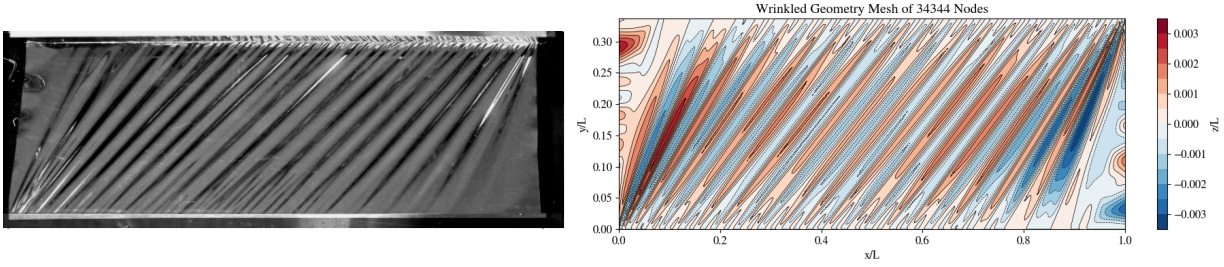


Figure 5.1: Wrinkled Shape in Experiment by Wong and Pellegrino [95] and Numerical Result

5.4 Numerical Parameter Sensitivities

When running the numerical procedure for post-buckling, described in section 5.2.2, several parameters are set. Firstly, buckling modes are applied to perturb the geometry before the nonlinear analysis is performed, to facilitate out-of-plane deformation. Here, a selection is made as to which modes are used to create initial displacements. Secondly, numerical stabilization might be required to allow convergence of the simulation. This method has the disadvantage, however, that it adds artificial damping to the analysis, which reduces the accuracy of the solution. Thirdly, grid size can also influence the wrinkled shape since larger elements will not be able to capture short-wavelength wrinkles. Therefore, the sensitivities of these three parameters are investigated.

The sensitivities of these parameters are investigated by solving the post-buckling analysis while varying the mode range, stabilization factor and grid size independently. The cross-sectional wrinkling results are compared to the experimental solution provided by Wong and Pellegrino [95], as a means of validation. The experimental wrinkled shape and the numerical wrinkled shape are illustrated in Figure 5.1. The number of wrinkles and maximum amplitude are also compared to the numerical results of Wong and Pellegrino [95] and Taylor, Bertoldi, and Steigmann [80].

To quantify the sensitivity of the result to the modal input, the spread in amplitudes is calculated. Firstly the mean amplitude is calculated per wrinkling result i , for each parameter separately.

$$\mu_{a,i} = \frac{\sum a_i}{n_a} \quad (5.1)$$

Whereby a_i is the amplitude size of one peak and n_a is the total number of peaks in the wrinkled state of result i . Then the standard deviation of the mean amplitudes of all results for each parameter are taken.

$$\sigma_a = \sqrt{\frac{\sum (\mu_{a,i} - \bar{\mu}_a)^2}{n_a}} \quad (5.2)$$

Whereby $\bar{\mu}_a$ is the average of all mean amplitudes of each result, per parameter. Hereby the numerical results of Wong and Pellegrino [95] are included. In the following sections, the sensitivity of each parameter is expressed by the standard deviation normalised by the average of the mean per parameter, this measure is also known as co-variance.

$$COV = \frac{\sigma_a}{\bar{\mu}_a} \cdot 100\% \quad (5.3)$$

Note that the computed co-variances are only the diagonal terms of the covariance matrix, i.e. the cross-correlation sensitivities between parameters are not taken into account in this analysis. Furthermore, the sensitivities computed here are based on three input parameters, which are assumed to be

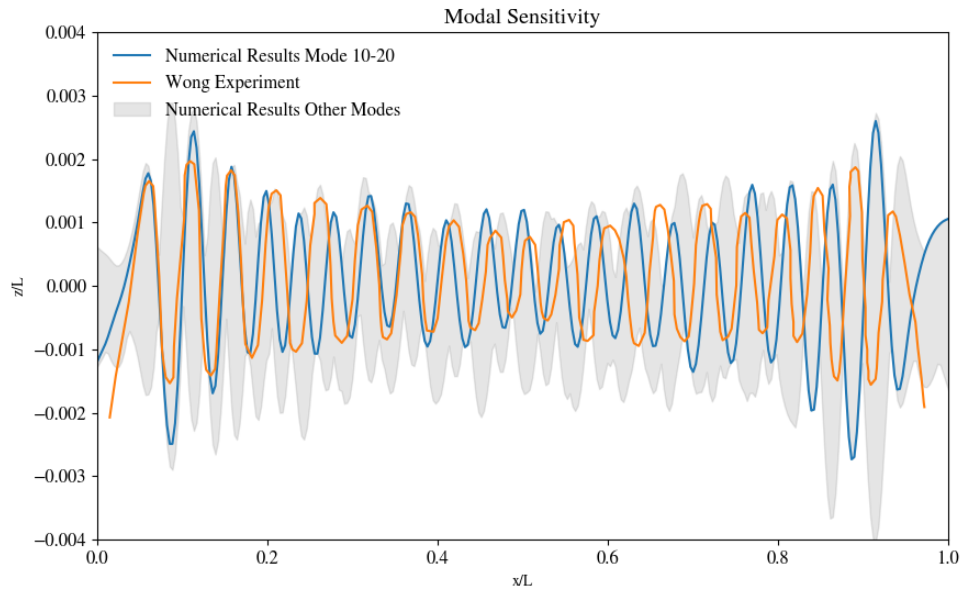


Figure 5.2: Cross-sectional Wrinkling Result for Varying Modes. The numerical results of mode 10-20 are plotted together with the experimental results by Wong and Pellegrino [94]. The shaded region highlights the variance in results which can be obtained by using different sets of modes as a bifurcation.

of high influence on the result. The actual sensitivities are dependent on a broad selection of other input variables as well, e.g. global dimensions, initial imperfection size, convergence tolerances, which are not investigated here. Therefore, the following computation does not serve as an exact quantification of the sensitivity of the results given the parameters, but functions as an indicator of the volatility of the results provided some main parameters. The actual sensitivity of the parameters could be obtained by varying all parameters independently, which is a very costly analysis.

5.4.1 Modes

To demonstrate the sensitivity of the analysis to the applied set of buckling modes, the shear case is performed six times using different ranges of modes as initial displacements:

- Mode 1-10
- Mode 10-20
- Mode 20-30
- Mode 30-40
- Mode 40-50
- Mode 1-50

In Figure 5.2, the modal sensitivity is illustrated by plotting the cross-section of wrinkled geometries for the different results. The result of the analysis with mode 10-20 lies closest to the benchmark of Wong's experiment [95], based on the number of wrinkles and the amplitude sizes as discussed in upcoming section 5.4.4. The other results are indicated by a bandwidth. From these results, it can be observed qualitatively, that the sensitivity of the wrinkled geometry to the selection of perturbation modes is high.

From the mean amplitudes of all results, the co-variance is taken to compute the spread in amplitudes.

$$COV_{modes} = 18.7\% \quad (5.4)$$

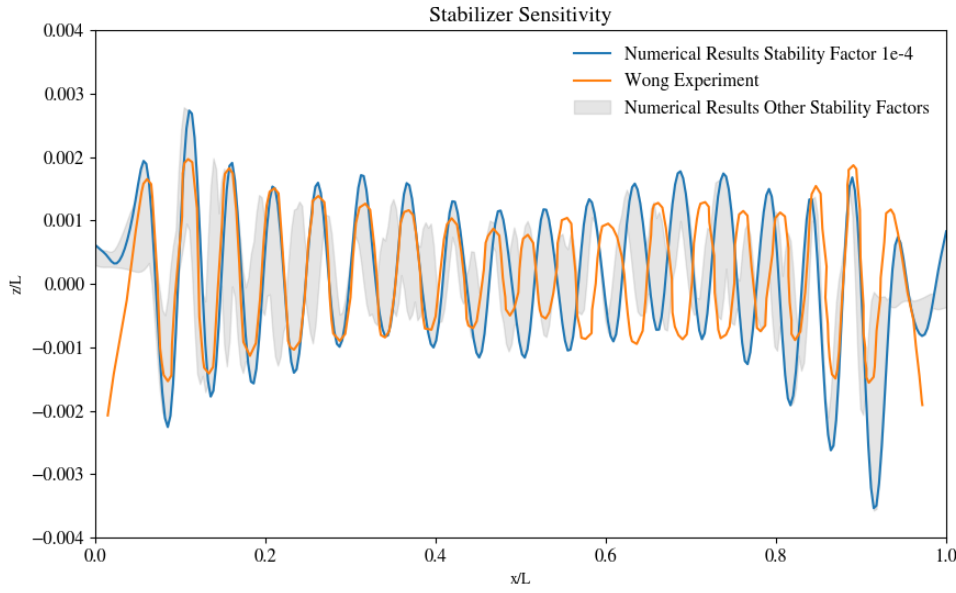


Figure 5.3: Cross-sectional Wrinkling result for varying stabilization factors. The numerical results of stability factor $1e^{-4}$ are plotted together with the experimental results by Wong and Pellegrino [94]. The shaded region highlights the variance in results which can be obtained by using different stabilization factor.

5.4.2 Stabilization

The sensitivity of the stabilization is investigated by performing three analyses of the shear case, with the same parameters but with different stabilization values.

- constant stabilization factor of 10^{-4}
- constant stabilization factor of 10^{-3}
- constant stabilization factor of 10^{-2}

In Figure 5.3, the wrinkled geometries for different stability factors are plotted. The stability factor of 10^{-4} is plotted since this is the most accurate, based on the number of wrinkles discussed in forthcoming section 5.4.4. Higher stability factors of 10^{-3} and 10^{-2} are located in the grey range. From the figure, it can be observed that the numerical stabilization dampens the size of amplitudes and also influences the locations.

From the mean amplitudes of all results, the co-variance is taken to compute the spread in amplitudes.

$$COV_{stabilization} = 29.5\% \quad (5.5)$$

5.4.3 Grid size

The grid size sensitivity is studied by varying the element size. Four meshes of 2.2k, 8.8k, 25.4k and 34.3k nodes are used for comparison. In Figure 5.4 the different results are shown, together with the experimental values. The two rougher grids of 2.2k and 8.8k nodes respectively result in a lower number of wrinkles and higher amplitudes. From the mesh of 25.4k nodes to the most refined mesh of 34.3k nodes, the number of wrinkles is converged and the amplitudes are in the same range as well.

From the mean amplitudes of all results, the normalised spread taken by computing the co-variance in amplitudes.

$$COV_{grid} = 44.8\% \quad (5.6)$$

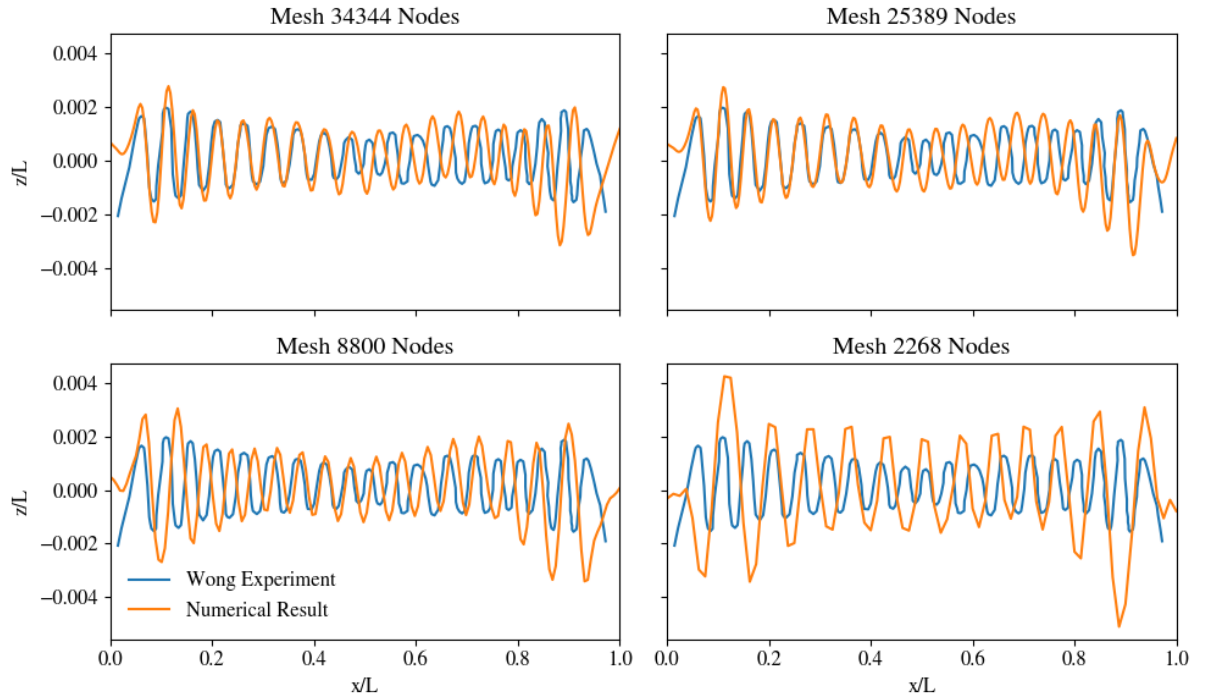


Figure 5.4: Cross-sectional wrinkling results for different grid sizes. The rougher meshes show a large deviation from the results of Wong and Pellegrino [95], both in number of wrinkles as in amplitude

5.4.4 Sensitivities Wrinkles and Amplitudes

Combining the sensitivities of all three parameters, the influence on the number of wrinkles and amplitude is substantiated. In Figure 5.5, the influence of the three parameters on the number of wrinkles is illustrated in a bar chart. The orange bar indicates the run which is the same in all three variations. Here it can be seen, that using different mode ranges, a number of wrinkles between 18 and 20 can be obtained, while the experiment showed 19 wrinkles. The stabilization increases the number of wrinkles, by adding artificial stiffness. Furthermore rougher meshes cannot capture the fine wrinkling features of highly wrinkled sheets and hence will result in a lower number of wrinkles.

In Figure 5.6, the sensitivity of different parameters on the amplitude is indicated. The amplitude indicator is taken by integration of the squared amplitude values:

$$\text{Amplitude indicator} = \int_x z(x)^2 dx$$

For different mode ranges, different amplitude results are obtained. All analyses resulted in over-predicted amplitudes. The stability factor influences the amplitude size as depicted in the chart. For a stability factor of 10^{-2} , the amplitudes decrease and the number of wrinkles increased. The grid size shows to have a large sensitivity as well; rougher grids result in a lower number of wrinkles which often means higher amplitudes since the total sheet length remains constant.

5.4.5 Sensitivities Conclusion

In the above section, the sensitivities of the input parameters are listed, expressed by the co-variance in mean amplitude height. Grid size has the largest sensitivity, but the other two parameters have also been shown to be of significant influence. Grid convergence is very important for the accuracy of the result, for too rough meshes, the small wrinkling wavelengths can not be captured which will result in inaccurate results. Next to that, the stabilization factor also has a significant sensitivity, therefore the of

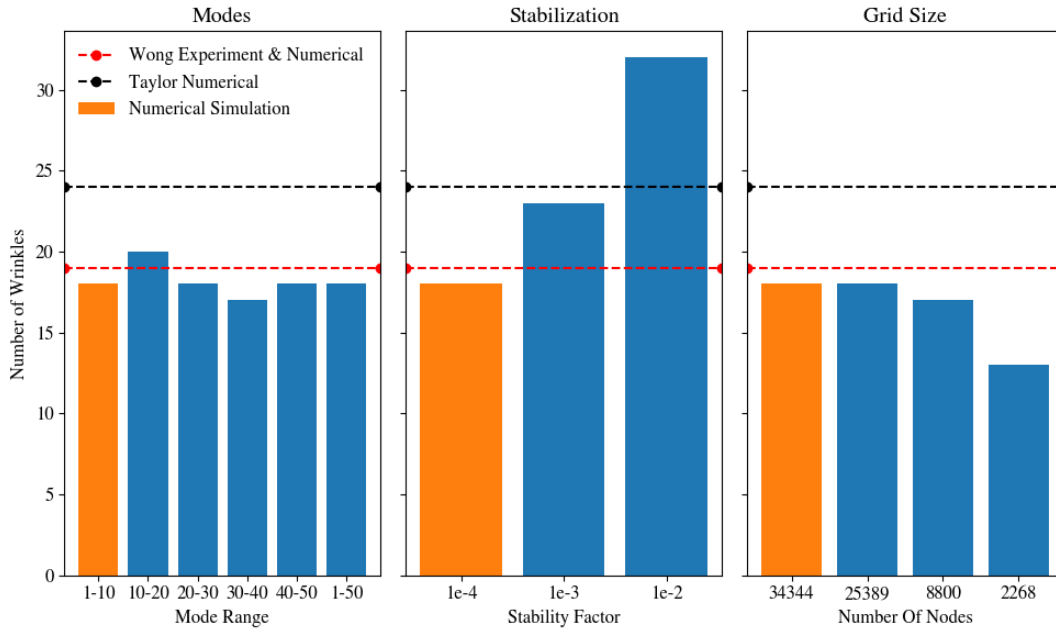


Figure 5.5: Number of wrinkles for varying input parameters. The orange bar indicates one result, while all blue bars are different results. The experimental and numerical result by Wong and Pellegrino [94, 95], as well as the numerical results by Taylor, Bertoldi, and Steigmann [80] are depicted for reference.

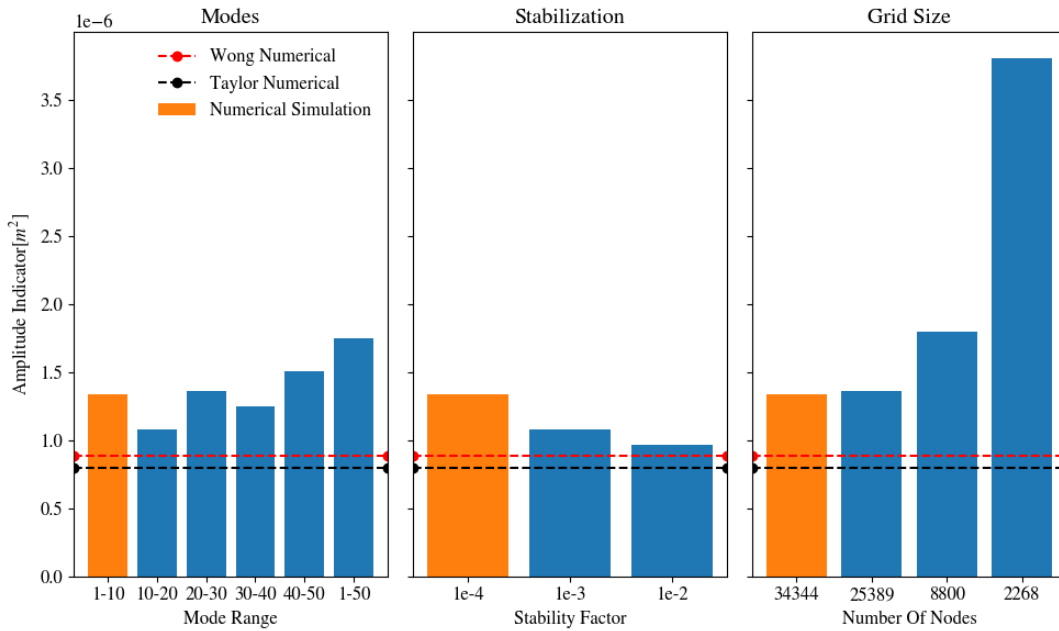


Figure 5.6: Maximum amplitudes for varying input parameters. The orange bar indicates one result, while all blue bars are different results. The experimental and numerical result by Wong and Pellegrino [94, 95], as well as the numerical results by Taylor, Bertoldi, and Steigmann [80] are depicted for reference.

it use should be minimised. For the selection of the stabilization factor, there is a fine balance between accuracy and convergence. Moreover, the type of modes that are applied as bifurcation affects the outcome of the analyses. This influence can not be neglected. Even though these numbers are not a complete quantification of the uncertainty of the result, the numbers indicate the volatility of the results, given the used parameters. It provides more insight into the sensitivity of certain parameters. Comparing the bandwidth of results in the shaded areas in Figure 5.2, Figure 5.3 and Figure 5.4, it seems that the applied modes have to highest sensitivity for the result. However, this effect is caused by the shifting of wrinkle peaks because different modes are triggered, which has the least significant effect on amplitude sizes and the number of wrinkles.

5.5 Conclusion

The previous chapter discusses analyses of the influence of numerical tools on the wrinkling behaviour of OFFSSs. This has led to the following conclusions, answering the research sub-question 1.c.

- The results of **principal stress analysis and post-buckling analysis** for the benchmark cases axial tension, bi-axial tension and shear, are presented and compared. It has been shown that using the contours and vectors of second principal stress, the region and orientation of potential wrinkling can be predicted well.
- For the shear load case, the sensitivity of the numerical parameters modes, stabilization and grid size are investigated. The results demonstrated that **the selection of modes as a perturbation; the stabilization factor and the grid size of the mesh all have significant on the wrinkling result**; both the number of wrinkles as well as the amplitudes. This indicates the volatility of wrinkling results given the used parameters, in commercial FEA software.

6

Wrinkling of Offshore Flexible Floating Solar Structures

In this chapter, the wrinkling behaviour of OFFSSs will be analyzed. This will answer the following sub-questions:

1. d) *What is the wrinkling behaviour of Offshore Flexible Floating Solar Structures?*
1. e) *How can wrinkling resistant design methods be utilized to reduce wrinkling in Offshore Flexible Floating Solar Structures?*
1. f) *How can the properties of auxetic materials be incorporated in Offshore Flexible Floating Solar Structures to create wrinkling resistance?*

The second research question will be answered in section 6.1, by first analyzing the wrinkling behaviour of platforms without solar panels with hydrostatic stiffness, and then by analyzing the behaviour of OFFSSs with both rigid and flexible solar panels.

The third research question will be resolved in section 6.2. Firstly, a shear compliant zone, inspired by work from Leifer et al. [42], will be added to the OFFSS structure to investigate the influence on the wrinkling behaviour. Then, a novel solar panel layup method will be introduced inspired by auxetic structures, and the effect on the wrinkling behaviour will be examined.

6.1 Wrinkling affecting parameters

In this section, the effect of hydrostatic stiffness on wrinkling behaviour of three relevant load cases is researched. Thereafter, wrinkling analyses are performed including solar panels in the OFFSSs. The wrinkling behaviour for OFFSSs with rigid and flexible solar panels is compared. The wrinkling behaviour is considered on static loads, dynamic environmental loads are not considered in this research. The boundary conditions, used for the upcoming wrinkling analyses are outlined in section 5.1 and illustrated in Table 5.2. The main parameters used for the analyses are summarized in Table 6.1, these are described in detail in chapter 4 and forthcoming subsection 6.1.2.

Table 6.1: Wrinkling Analyses Parameters

Section	L [m]	B [m]	t [m]	E [MPa]	ν [-]
Membrane	25.00, 50.00, 75.00	8.42, 16.84, 25.25	0.10	15	0.31
Rigid solar panel	1.60	1.60	0.05	50e3	0.22
Thin film flexible solar panel	1.00	1.00	3.50e-07	100e3	0.22

6.1.1 Hydrostatic Stiffness

As the research focuses on solar platforms in offshore environments, the hydrostatic pressure induced by the water comes into play in the deformation behaviour. In the work of Pocivavsek et al. [71], the effect of an elastic foundation on the wrinkling behaviour of membranes under compressive loading was highlighted. They proved that, for these cases, the wrinkled geometry is obtained by minimisation of bending and potential energy. The hydrostatic stiffness introduces the potential energy of the water into this balance for OFFSSs. Therefore, it penalizes larger wavelengths, as these require more energy for the water to be displaced. Since buckling modes exhibiting smaller wrinkle wavelengths are triggered at higher strain rates than high wavelength buckling modes, the onset of wrinkling will be delayed during the hydrostatic stiffness as well.

In this section, the effect of the hydrostatic stiffness is studied, on the wrinkling behaviour of typical load conditions of the OFFSSs. The material and thickness, selected in chapter 4, are used in these simulations.

The influence of the hydrostatic stiffness is investigated for load conditions axial tension, bi-axial tension and shear, recall Figure 2.1. As described in chapter 2, these cases have been shown to exhibit wrinkling behaviour. Furthermore, recall from chapter 4 that these cases are closely related to the actual loading conditions of OFFSSs. In light of this, the boundary conditions of these cases are used to analyse the influence of hydrostatic stiffness on the wrinkling behaviour of OFFSSs. The boundary conditions are described in section 5.1 and illustrated in Table 5.2.

The wrinkling behaviour of platforms with and without hydrostatic stiffness, i.e. hydroelastic wrinkling and non-hydroelastic wrinkling, is compared for three different platform sizes. The dimensions of $L = 25\text{m}$, 50m and 75m are selected, as this is the largest feasible range to be analysed by the numerical software, due to memory limitations. For larger sizes, the absolute wrinkle wavelengths reduce such that an extremely fine mesh would be required for the simulation to run.

In Figure 6.1, on the left side, the maximum wrinkle amplitude z , normalised by the initial bifurcation z_0 , is shown per load case. The plot on the right side of Figure 6.1 shows the hydroelastic wrinkling results independently to observe the amplitude growths in more detail.

The amplitude growth of wrinkles with applied strain is non-linear, due to geometric non-linearity and material non-linearity (depending on the strain rates), as described in chapter 3. Therefore, non-linear growth of amplitude with strain is expected for the cases where wrinkling occurs. Furthermore, if the maximum amplitude of wrinkles is in the same order of magnitude as the initial perturbation, wrinkling is considered to be insignificant.

Looking at the plots in Figure 6.1, it can be observed that axial tension does not result in wrinkling for the dimensions $L = 25$, 50 and 75 . The amplitude stays in the same order of magnitude as the initial displacement, which indicates wrinkling does not occur. This result implies that axial tension is not resulting in wrinkling for the chosen material EVA; of thickness 0.1m , in the analysed load conditions. As mentioned earlier, the hydrostatic stiffness is expected to delay the onset of wrinkling. Therefore, it could be that the geometrically nonlinear effects are too large for the actual wrinkling onset to occur. Accordingly, for other materials, geometrical parameters or strain intervals, this behaviour might differ.

In the bi-axial tension load cases, a large difference between the results with and without hydrostatic stiffness is noticed. For the cases without hydrostatic stiffness, the maximum amplitude grows non-linearly with the strain, two to three orders of magnitude larger, while for a platform with hydrostatic stiffness, this behaviour is absent. Thus, it is concluded that for the bi-axial case with hydrostatic stiffness, the effect of wrinkling is insignificant.

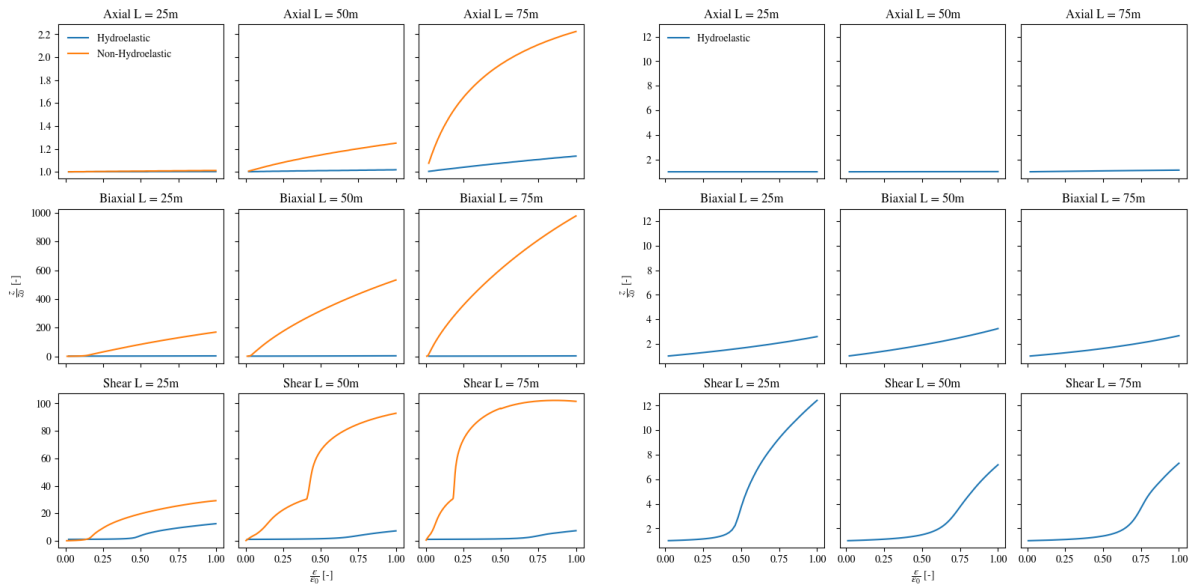


Figure 6.1: Hydrostatic stiffness influence on load cases: Axial Tension, Bi-axial tension and Shear, for 25m, 50m and 75m platform length. The x-axis shows normalised strain and the y-axis depicts the maximum wrinkle amplitude height, normalised by the initial bifurcation. The plot on the right side shows the hydroelastic wrinkling results in more detail

In the shear case, both results show non-linear amplitude growth at some point. The onset of wrinkling is delayed by hydrostatic stiffness, and the amplitude growth is dampened. This results in a lower maximum amplitude for wrinkling on hydrostatic stiffness. The discontinuities or 'bumps' in the graphs for shear are caused by the phenomenon of mode-jumping: when a new mode is triggered, the number of wrinkles can change abruptly which affects the absolute size of the amplitudes as well as the amplitude strain relation. This is specific for the shear case, as it has shown to trigger more modes within the strain interval than the axial or bi-axial load cases [95].

From the above observations, it is concluded that for an OFFSS of material type EVA located on water, wrinkling is only significant for shear load cases. For the axial load case, wrinkling will likely not occur at all. For the bi-axial load case, the hydrostatic stiffness removes the wrinkling behaviour.

Platform Size Effects

Figure 6.2 provides wrinkling amplitudes at a strain of $\epsilon = 0.006$. For the larger platforms (50m, 75m), smaller wrinkling amplitudes are observed compared to the size of the platform. This is caused by the penalization of large wrinkle wavelengths by the elastic foundation following the theory of Pocivavsek et al. [71]. Smaller wavelengths result in smaller amplitudes [15]. Nonetheless, the wrinkling effect can also be hazardous for larger solar platforms, as the absolute wrinkle wavelengths are similar to the smaller panels, namely between $\lambda = 4.0\text{m}$ and 4.5m (for platforms with hydrostatic stiffness), which is the same order of magnitude as $L_{panel} = 1.6\text{m}$ (see chapter 4).

The penalization effect can be well observed by comparing the contours of wrinkling deformation for the shear cases in Figure 6.2. In the wrinkled geometries of the cases with elastic foundation, the wavelengths are significantly smaller than for the wrinkles without hydrostatic stiffness. In addition, the amplitudes are significantly smaller in the cases with hydrostatic stiffness (close to a factor 4 for 75m platforms), which can be observed in the contours of the plots. This is in line with the observations of Pocivavsek et al. [71], who showed that an increase in amplitude requires an increase of energy in the system.

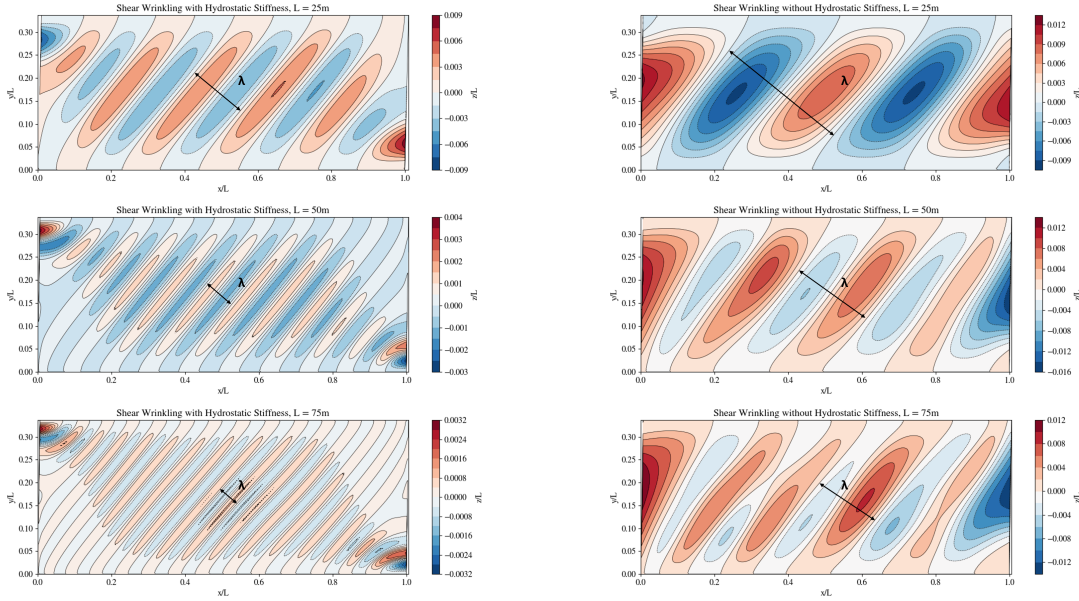


Figure 6.2: Shear Wrinkles with hydrostatic stiffness (left column), and Shear Wrinkles without hydrostatic stiffness (right column) for $L = 25\text{m}$, 50m and 75m . The wavelengths $\frac{\lambda}{L}$ are, from left to right, top-down: 0.16, 0.36, 0.08, 0.22, 0.06 and 0.18.

Table 6.2: Solar Panel Main Parameters

Solar Panel Type	$L_{panel} \times B_{panel} \times t_{panel}$ [m]	Material	E [MPa]	ν [-]	Reference
Conventional rigid	$1.60 \times 1.00 \times 0.05$	Glass	50e3	0.22	[23]
Thin film flexible	$1.60 \times 1.00 \times 350e-9$	a-Si:H	100e3	0.22	[57, 82]

6.1.2 Embedded Solar Panels

The effect of embedding solar panels in the wrinkling behaviour of OFFSSs is investigated. Conventional rigid solar panels are used for the wrinkling analyses firstly, and flexible thin film panels are investigated subsequently.

In Table 6.2, the main parameters of rigid and thin film flexible solar panels are provided. In Figure 6.3, the embedded solar panel structure is illustrated. The Figure shows only one corner of the platform including the main parameters of the panel structure.

Using the material properties of the solar panels listed in chapter 4, the model is created employing multilayered shell elements of element type SHELL181. With this element type, different material properties are assigned to different thickness sections. This way, the solar panels are embedded in the EVA platform.

In Figure 6.4, the principal stress results of the platform without solar panels are given. As indicated in the figure, a whole parallelogram shaped region on the centre of the platform is in compressive stress. This global compressive stress state results in wrinkling behaviour. This result is used throughout the following sections for comparison of the results with solar panels.

Rigid Solar Panels

The first model consists of a platform with rigid solar panels. The panels are modelled using glass properties with a thickness of $t = 0.05$ [m]. The same boundary conditions are applied as described in Chapter 5.

The principal stress results of the solar platform with rigid panels in the shear analysis are depicted in

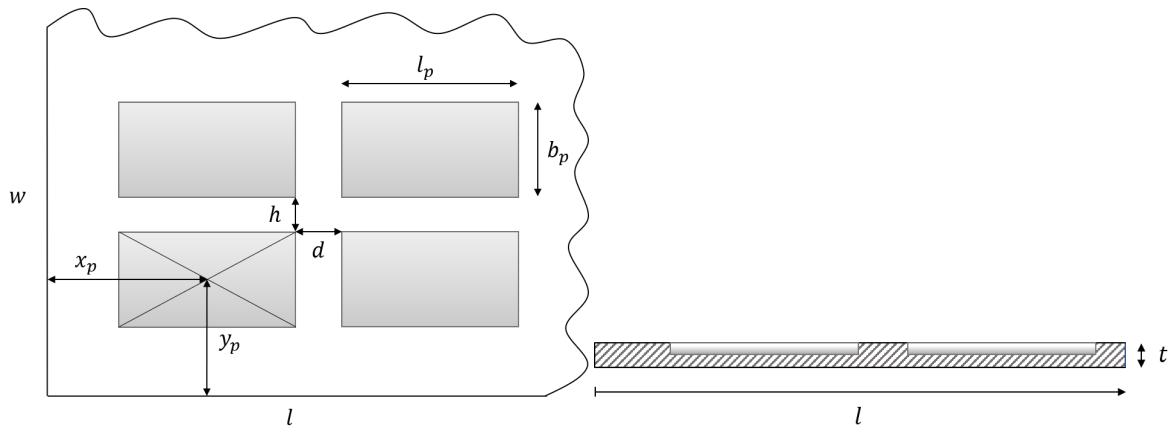


Figure 6.3: Schematic of the one corner of the solar platform with straight panels. The curled line indicates the sides where the platform continues. Left to Right: Top view of the platform and cross-section of the embedded solar panels. Dimensions indicated in the figure: $l = 25.00\text{m}$, $w = 8.42\text{m}$, $t = 0.1\text{m}$, $l_p = 1.6\text{m}$, $b_p = 1.0\text{m}$, $x_p = 1.6\text{m}$, $y_p = 1.3\text{m}$, $h = 2.18\text{m}$ and $d = 1.45\text{m}$

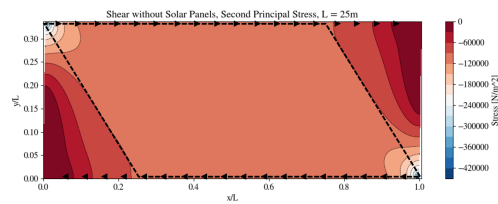


Figure 6.4: Second principal stress field for the platform without solar panels. The direction of shear is indicated by arrows. The parallelogram highlights the zone of compressive stresses.

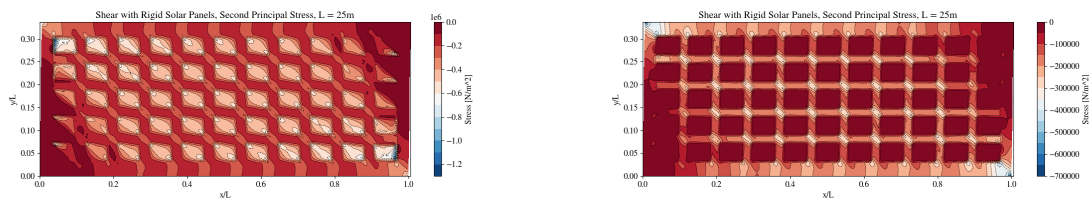


Figure 6.5: Second principal stress field for the platform with rigid solar panels embedded. Compressive stress zones are observed over the whole platform. Stress peaks in the solar panels are caused by the rigidity of the material. Left: platform front, right: platform aft

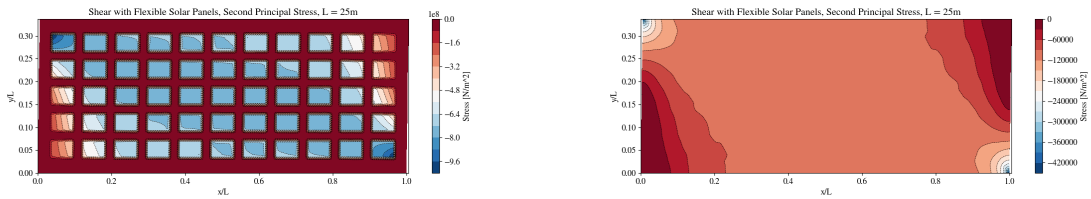


Figure 6.6: Second principal stress field for the platform with flexible thin film panels. The high axial stiffness of the flexible thin film panels results in high stress concentrations, indicated by the blue zones. The aft of the platform has a similar stress distribution as the platform without solar panels in Figure 6.4. Compressive stress zones over the whole platform suggest the risk of global wrinkling. Left: platform front, right: platform aft

Figure 6.5. Looking at the plots, the principal stresses concentrate at the corners of the solar panels on the front side. This is expected, as the shear strain induces compression to the second principal stress axis and the axial stiffness of the rigid panels is higher than the flexible membrane, hence allowing less strain and taking up more stress. In the plot of the platform aft, it is observed that compressive stresses below the solar panels are near zero since the membrane below the panels is connected to the panels and hence deformations are equally small as for the rigid material. In between the panels, compressive zones are observed throughout the whole platform. Since there are compressive zones over the whole platform, it is expected that there is a risk of global wrinkling in this configuration.

Since the principal stress analysis pinpoints the potential wrinkling behaviour of solar platforms with rigid solar panels, it is worthwhile to perform a post-buckling analysis on the case to see this behaviour in more detail. In Figure 6.7, the wrinkled geometry of the platform can be seen. Comparing these results to the wrinkling behaviour of the 25m long platform without solar panels and hydrostatic stiffness in Figure 6.2, slightly lower amplitudes can be observed on the platform with rigid solar panels, and higher wavelengths. The platform without solar panels exhibits two and a half wrinkle wavelengths, while the platform with rigid solar panels deforms into a shape of one and a half wavelength. This decrease in amplitude and number of wrinkles in rigid solar platform configuration is expected to be caused by the increased bending stiffness of the platform due to the embedded rigid panels.

Flexible Thin Film Solar panels

Flexible thin film solar panels are known for their flexibility as well as their low weight due to small thickness, making them fit for curved or odd-shaped surfaces or lightweight structures. Envisioned applications for thin film solar are: vehicles, infrastructure and buildings [83]. In the context of OFFSS applications, they might be considered as well, as their flexibility could be favourable in dynamic environmental loadings. To discover their potential for OFFSS design, their wrinkling behaviour is compared to that of rigid panels. In Figure 6.6 the second principal stress of the flexible solar panels platform is presented. The platform front shows high compressive stress peaks in the flexible thin film panels, which can be explained by the fact that, even though their bending stiffness is negligible, their axial stiffness is relatively high. On the aft side of the platform, a parallelogram of compressive stresses can be seen on the platform, analogous to that of the platform without panels in Figure 6.4. This indicates global wrinkling behaviour.

As the principal stress analysis of the flexible panel platform suggests global wrinkling, post-buckling analysis is required to see the wrinkling development of the structure. Reviewing the post-buckling geometry allows comparison between the effect of rigid versus flexible thin film panels on global wrinkling behaviour of the OFFSSs. The results of both rigid solar panel and flexible thin film solar panel platform wrinkles are given in Figure 6.7 and 6.8 respectively. Looking at Figure 6.8, it can be recognized that the flexible thin film solar platform deforms similarly to the platform without panels, but the amplitudes are slightly lower. The expected cause of this is the axial stiffness added by the thin film

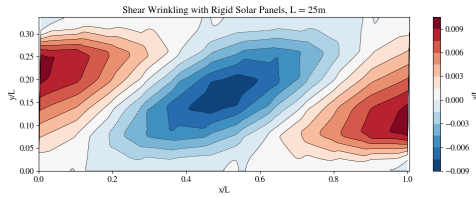


Figure 6.7: Wrinkled deformation of the solar platform with rigid solar panels. The increased bending stiffness of the platform with embedded rigid solar panels is expected to be the cause of the decreased number of wrinkles and amplitudes, compared to the same sized platform without solar panels and hydrostatic stiffness in Figure 6.2

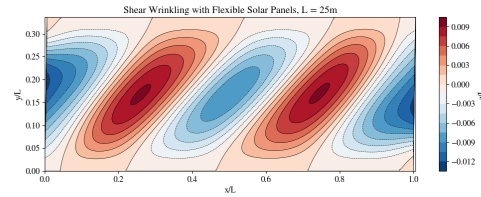


Figure 6.8: Wrinkled deformation of the solar platform with flexible thin film solar panels. The flexible has no influence on the wrinkling wave lengths, however the amplitudes are lower than for the same sized platform without solar panels and hydrostatic stiffness in Figure 6.2.

panels. Furthermore, the number of wrinkles is the same and the peaks lie in the same location. Comparing the rigid wrinkling results in Figure 6.7 to the flexible thin film wrinkling in Figure 6.8, it can be concluded that the increased bending stiffness of the rigid panels platform increases the wrinkling wavelengths, while the maximum amplitudes are in the same size range.

6.2 Wrinkling resistant design

After studying the wrinkling behaviour of solar platforms with two types of panels, structural design adaptations are created in the rigid solar panel platform model to see if it is possible to reduce the wrinkling behaviour. The desired second principal stress field would not exhibit compressive stresses over the whole domain, ideally no compressive stresses are present. Shifting compressive stresses from the middle of the structure to its edges is assumed to improve the wrinkling behaviour, as demonstrated by Bonfanti and Bhaskar [10].

The first wrinkling resistant design method is the addition of shear compliant zones. The second design aspect is inspired by auxetic materials, namely to place the rigid panels in an auxetic structure.

6.2.1 Shear Compliant Zone

The first design adaptation applied to the platform is the shear compliant zone. Shear compliant zones are zones in the structure that are permeable. Permeability has been shown to reduce wrinkling, as discussed in Chapter 2, by releasing compressive stresses after deformation.

For the designed shear compliant zone, inspiration is drawn from the investigation on the effect of shear compliant zones on shear wrinkling in membranes by Leifer et al. [42]. The shear compliant zones are applied on a solar platform with rigid solar panels.

In Figure 6.9, the outlines of the shear compliant zone model are illustrated. Note that the width of this model is slightly larger than the other platforms, to accommodate the shear compliant zone. The number of solar panels is equal to that of the platform with rigid solar panels in subsection 6.1.2. Two versions of the shear compliant zone are analysed: one with $d_h = 0.80\text{m}$ and one with $d_h = 0.40\text{m}$, i.e. twice as much holes. The two shear compliant zones are compared to the solar platform without a shear compliant zone. The principal stress results of the shear compliant zone analyses are granted in Figure 6.10.

From the Figures, the effect of the shear compliant zones can be seen. The half shear compliant zone reduces the number of compressive stresses in the middle of the platform. Local stress peaks are found around the corners of the holes. The full shear compliant zone reduces the compressive stresses in the midsection of the platform even further. Only local compression concentrations are spotted at the

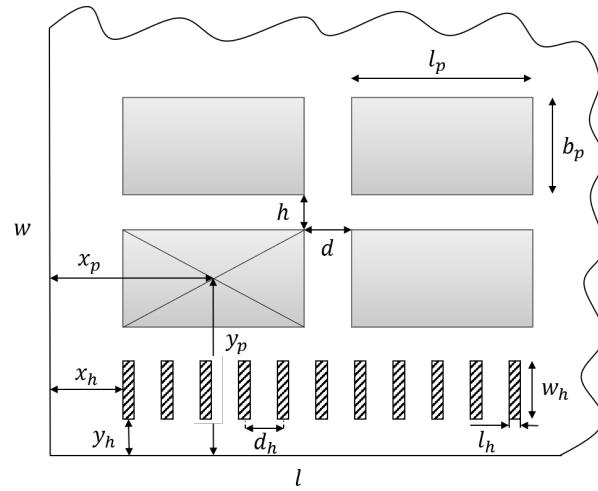


Figure 6.9: Schematic of the top view of one corner of the shear compliant zone platform. The curled line indicates the sides where the platform continues. The diagonal striped zones mark the holes in the platform. The dimensions in the figure are: $l = 30.00\text{m}$, $w = 8.42\text{m}$, $t = 0.10\text{m}$, $l_p = 1.60\text{m}$, $b_p = 1.00\text{m}$, $x_p = 1.60\text{m}$, $y_p = 2.14\text{m}$, $h = 2.18\text{m}$, $d = 1.45\text{m}$, $x_h = 0.80\text{m}$, $y_h = 0.42\text{m}$, $l_h = 0.20\text{m}$, $w_h = 0.84\text{m}$ and $d_h = 0.8\text{m}$ for a half shear compliant zone and $d_h = 0.4\text{m}$ for a full shear compliant zone.

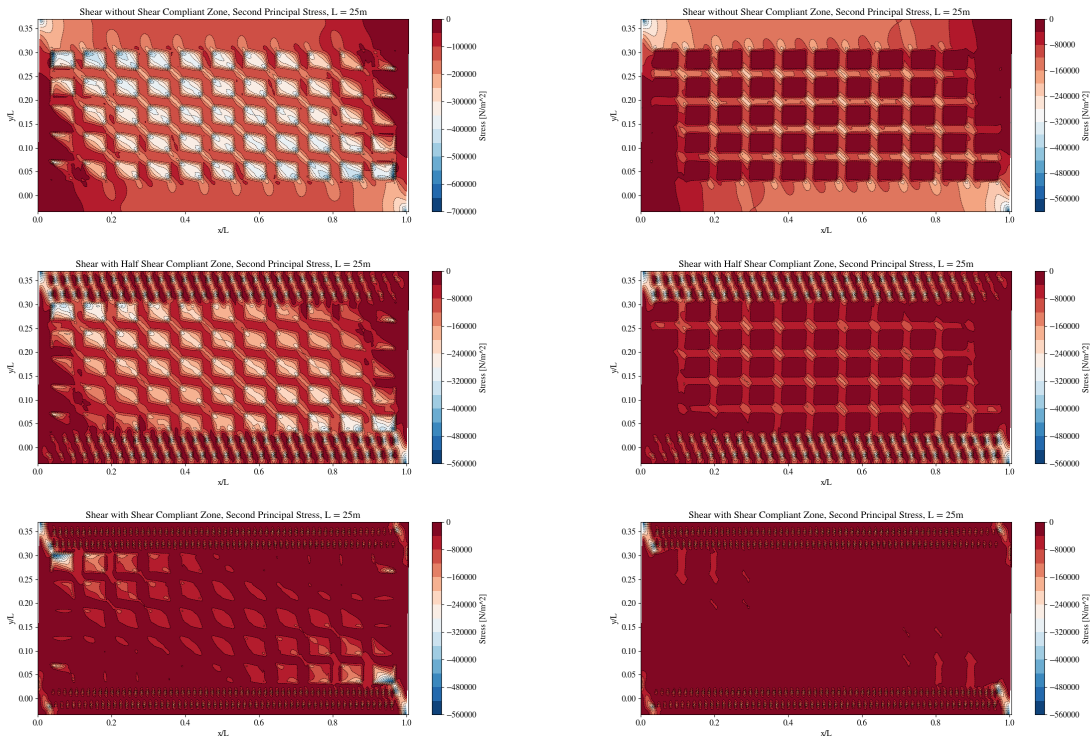


Figure 6.10: Second principal stress field of platforms with rigid solar panels and shear compliant zones. The results point out the positive effect of the shear compliant zones on the negative stress field; compressive stresses are reduced significantly throughout the whole platform by adding holes near the boundaries. From top to bottom: no shear compliant zone, half shear compliant zone and full shear compliant zone. From left to right: platform front and platform aft.

upper left corner and lower right corner of the platform, around the holes and on the edges of the solar panels. From these results, it can be concluded that the global wrinkling behaviour of OFFSSs can be reduced by applying shear compliant zones.

Further Considerations It is expected that permeability will be required throughout the whole platform, to release green water, which is pushed on the platforms due to waves, as well as air bubbles that are trapped below the platform, caused by wave dynamics. Holes in the platform will be required as green water could cause the platform to sink, and air bubbles below the platform could potentially induce harmful impact loads. In Appendix C, the wrinkling behaviour of some elementary platform designs with permeability over the whole platform is analysed.

Additionally, a risk of the above-analysed shear compliant zones with rectangular holes might be that stress concentrations might arise around the corners of the holes. Arcs generally allow more smooth distribution of stresses than sharp angles. Therefore some elementary shear zone designs with elliptical and circular holes are analysed for their wrinkling behaviour in Appendix C.

6.2.2 Auxetic Solar Panel Orientations

For the auxetic structure, inspiration is drawn from the work of Kolken and Zadpoor [40]. Appendix A provides an in-depth elaboration on the auxetic structure design and its working principle. This structure is build up from rigid rectangles, geometrically similar to solar panels. The rigid rectangles are connected on their corners, and when the structure is displaced in x-direction or y-direction, they rotate causing an auxetic effect. This auxetic effect has been shown to reduce wrinkling in membranes [10]. Since the solar platform requires solar panels anyway, why not use them in a way which aids wrinkling reduction. As the shape of rigid solar panels is similar to that of rigid rectangles in auxetic structure [40], it is assumed that an auxetic structure can be formed from solar panels. Therefore it is investigated if solar panels in an auxetic structure have the potential to reduce wrinkling.

Since the load case is shear, the principal stretch is not exclusively in x- or y-direction, but it is in bi-axial direction, even varying throughout the domain (see the vector plots in Table 5.2). For the auxetic structure to be effective in this case, it is rotated roughly in the direction of the principal stress inside parallelogram in the case without panels, ignoring the difference in principal stress direction near the left and right boundary. In this case, for the sake of modelling simplicity, the rotation is equal to the angle of the auxetic structure θ , as this aligns the lower solar panel with the boundary of the platform. For further research, this angle should be set more close to the direction of first principal stress, as this optimises the auxetic behaviour.

The general structure and main dimensions are illustrated by a sketch of one corner of the platform in Figure 6.11. Principal stress analysis is performed to analyze the effect of the auxetic structure on the wrinkling behaviour. The results are presented in Figure 6.12.

Looking at the plots in Figure 6.12, it can be noticed that the front of the auxetic platform shows high compressive stress peaks at the corners of the rigid panels. This is related to the rotation of the panels around their corners. On the aft side of the platform, the edges of the platform show compressive stress concentrations, but in the middle of the platform, these are absent. This indicates that the panel structure behaves auxetic, causing the compressive stresses to be released from the platform middle. Observing these results, similar behaviour is identified as in the wrinkling of an auxetic membrane, studied by Bonfanti and Bhaskar [10]. While the straight panel layup shows compressive stress zones over the whole platform, the auxetic platform only shows compressive stresses near the corners of the panels as well as on the edges of the platform. It is expected that this behaviour is more favourable for OFFSSs, as this does not indicate global wrinkling.

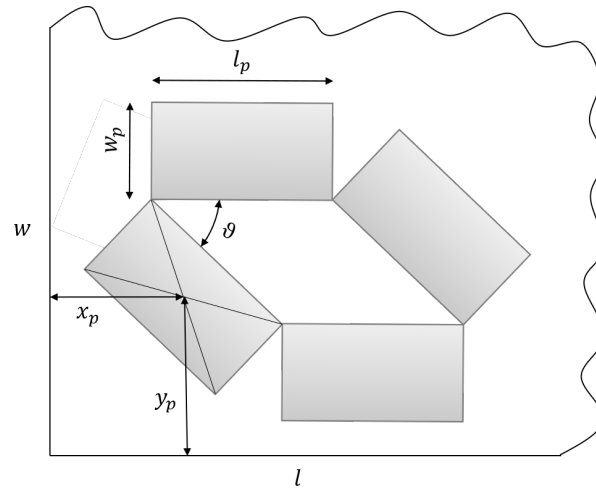


Figure 6.11: Schematic of the auxetic solar platform. Note that only one corner section of the platform is illustrated, the platform continues at the curled line. The indicated dimensions are: $l = 25\text{m}$, $w = 8.42\text{m}$, $l_p = 16.0\text{m}$, $w_p = 1.00\text{m}$, $x_p = 1.47\text{m}$, $y_p = 0.85\text{m}$ and $\theta = 0.2$

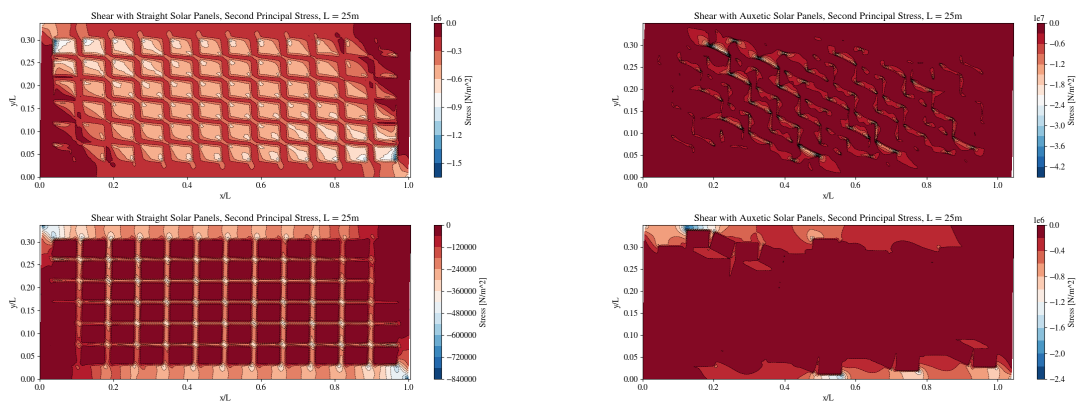


Figure 6.12: Straight Solar Panels Versus Auxetic Solar Panels. Left to right column: Straight Panels and Auxetic Panels Results. First to second row: Front and Back of Platform.

Further Considerations The auxetic structure as modelled in the above section is a preliminary design. The auxetic behaviour is caused by the rotating rigid structures, connected by hinges [40]. In the above analysis, these hinges are modelled as a single node, which allows rotations. In practice, structural hinges are required to allow this behaviour. Therefore, some effort is prescribed to engineer the system in detail.

Next to that, in OFSSs, loads may alternate in direction, causing the principal stress axis to be variable. For an auxetic structure to be effective in all cases which are significant for wrinkling, a study into the most effective layup orientation for varying load conditions, using rigid square solar panels, is required.

6.3 Conclusions

Analyses have been performed of the wrinkling behaviour with hydrostatic stiffness, with two types of solar panels and two types of structural adaptations concerning wrinkling reduction. This led to the following conclusions, answering sub-question 1.d.

- Analyzing the wrinkling behaviour of load cases axial tension, bi-axial tension and shear with **elastic foundation** in Figure 6.1, for the considered dimensions and material, it showed that only in the shear case wrinkling behaviour occurs when a hydrostatic stiffness is present.
- Comparing the wrinkling behaviour of a platform without solar panels, one with **rigid solar panels** (Figure 6.7) and one with **flexible thin film solar panels** (Figure 6.8), it appeared that the wrinkling amplitudes, as well as the number of wrinkles, is reduced by adding rigid solar panels, while flexible panels only change the amplitudes. It is expected that the influence of rigid panels is more favourable than flexible panels, as larger wrinkle wavelengths with the same amplitudes entail smaller rotations around the solar panels, which are assumed to be hazardous to the solar system.

From the wrinkling analyses with shear compliant zones and auxetic solar panels, conclusions can be drawn regarding sub-questions 1.e and 1.f.

- Results of simulations of solar platforms with shear compliant zones displayed that **shear compliant zones** have the potential to reduce wrinkling behaviour by minimising compressive stress.
- When applying rigid solar panels on the platform as an **auxetic structure**, compressive stresses localize at the boundaries of the structure but are removed from the middle of the platform. Therefore it is concluded that global wrinkling can be reduced by applying an auxetic solar panels structure when encountering shear.

7

Conclusions

After presenting wrinkling results for OFFSSs with and without wrinkling resistant design methods, it is now time to reflect on the research questions which were posed for this thesis. Firstly, the answers to the sub-question are summarized, which will lead up to the conclusion to the main research question.

1. a) *What load conditions adhere to wrinkling in offshore flexible floating solar structures?*

Load cases uni-axial tension, bi-axial tension and shear. In literature, it appeared that OFFSSs are susceptible to wrinkling. Wrinkling can be provoked by elementary loading conditions uni-axial tension, compression on an elastic substrate, bi-axial tension and shear. The phenomenon of wrinkling arises when in-plane forces are in balance with the bending resistance in the sheet. For OFFSSs, this induces structural risks, as wrinkling is assumed a potential limit state. As solar platforms are typically moored by tension, only load cases uni-axial tension, bi-axial tension and shear are relevant. Hydrostatic stiffness will be of influence at sea, and therefore it is incorporated in the wrinkling analyses.

1. b) *How can a base design for offshore flexible floating solar structures be developed, taking into account location and installation?*

Offshore wind farms are a sensible location for locating OFFSSs. Based on this, the global dimensions of the platform can be determined. For the thickness of the platform, the aspects of installation; material type and hydrostatics are considered. The platform can be transported coiled on reels, to enhance transport and installation efficiency. The material type EVA is chosen for the platform, for its buoyancy and weather resistance properties. Due to the low density of the material, buoyancy forms no constraint on the selection of a thickness. Based on minimal reel size and platform weight as well as solar panel protection considerations during transport; a thickness of 0.1 meters will be selected for the base design. The main dimensions of the base case are summarized in Table 4.3.

1. c) *What is the influence of numerical tools on wrinkling results of offshore flexible floating solar structures?*

The results of principal stress analyses and post-buckling analyses for three benchmark cases from literature, axial tension, bi-axial tension and shear, are presented and compared. It has been shown that using the contours and vectors of second principal stress, the region and orientation of potential wrinkling can be well predicted. For the shear load case, the sensitivity of the numerical parameters modes, stabilization and grid size are investigated. The results demonstrated that the selection of modes as a perturbation; the stabilization factor and the

grid size of the mesh all have significant on the wrinkling result; both the number of wrinkles as well as the amplitudes. This indicates the volatility of wrinkling results given the used parameters, in commercial FEA software.

1. d) *What is the wrinkling behaviour of Offshore Flexible Floating Solar Structures?*

Analyzing the wrinkling behaviour of load cases axial tension, bi-axial tension and shear with elastic foundation, it showed that only in the shear case wrinkling behaviour occurs when hydrostatic stiffness is present. Comparing the wrinkling behaviour of a platform without solar panels, one with rigid solar panels and one with flexible thin film solar panels, it appeared that the wrinkling amplitudes, as well as the number of wrinkles, is reduced by adding rigid solar panels, while flexible panels only change the amplitudes. It is expected that the influence of rigid panels is more favourable than flexible panels, as larger wrinkle wavelengths with the same amplitudes entail less steep wrinkles around the solar panels, which are assumed to be hazardous to the solar platform. Even though the flexibility of thin film solar panels can potentially reduce structural loads when encountering offshore dynamics, this risk should not be overlooked in the design of OFFSSs.

1. e) *How can wrinkling resistant design methods be utilized to reduce wrinkling in Offshore Flexible Floating Solar Structures?*

Results of simulations of solar platforms with shear compliant zones displayed that shear compliant zones reduce compressive principal stresses globally, moreover, compressive stresses are localized to the corners of the platform. This indicates that the wrinkling behaviour of structures with embedded rigid (solar) panels is reduced by adding shear compliant zones. The optimal geometry of shear compliant zones should be improved further for higher compressive stress reductions, but it has been shown that wrinkling resistance can be created for OFFSSs by adding shear compliant zones.

1. f) *How can the properties of auxetic materials be incorporated in Offshore Flexible Floating Solar Structures to create wrinkling resistance?*

When applying rigid solar panels on the platform as an auxetic structure, compressive stresses localize at the boundaries of the structure but are removed from the middle of the platform. Therefore it is concluded that global wrinkling can be reduced by applying an auxetic solar panels structure when encountering shear. Even though further research is required into the optimal auxetic structure for OFFSSs, the potential of incorporating auxetics in the design of OFFSSs is underlined in this work.

What is the wrinkling behaviour of Offshore Flexible Floating Solar Structures, and how can it be modelled and reduced?

The wrinkling behaviour of Offshore Flexible Floating Solar Structures is presented in this thesis for solar platforms with rigid solar panels and flexible solar panels.

- In combination with hydrostatic stiffness, wrinkling behaviour is only significant in the load case shear for the OFFSS of the considered geometry and material.
- Platforms with rigid solar panels show smaller wrinkle amplitudes and longer wavelengths than platforms with thin film flexible solar panels, or platforms without solar panels. The expected cause for this is the increased bending stiffness by the embedded rigid solar panels. Consequently, based exclusively on wrinkling behaviour, rigid solar panels seem more favourable for OFFSS application than flexible panels.

Numerical tools for wrinkling modelling are discussed in the thesis.

- Wrinkling can be modelled using principal stress analysis and post-buckling analysis. Principal stress analysis can provide the region and direction of potential wrinkles. If wrinkling will occur, can not be concluded from principal stress analysis.
- Post-buckling analysis requires numerical tools: selection of modes for perturbation, application of stabilization factors and grid refinement. The sensitivities of all these parameters, provided the specific benchmark boundary conditions, is 18.7% for mode selection, 24.5% for stabilization factors and 44.8% for grid refinement. The sensitivities of all parameters are significant, hence wrinkling results obtained by this method are volatile and should be interpreted with care.

Finally, reduction methods are proposed.

- Shear compliant zones can reduce wrinkling behaviour of OFFSSs, as predict principal stress results in Figure 6.10. Moreover, in general, it can be concluded that shear compliant zones reduce the wrinkling behaviour of sheets with embedded panels.
- Auxetic solar panels can potentially reduce wrinkling as well, indicated by the decrease of compressive stresses over the whole structure and especially in the middle, in Figure 6.12.

8

Future Work

During the wrinkling results analyses, some aspects were found that require further research to extend or improve the results of this study. Keeping in mind future engineering practices of OFFSSs, enhancements are recommended to increase the understanding of wrinkling modelling of OFFSSs and wrinkling resistant engineering for these structures. Recommendations are discussed on the facets wrinkling modelling method, wrinkling modelling in OFFSSs conditions, wrinkling resistant design, structural design with solar panels and mooring.

8.1 Wrinkling Modelling Method

As discussed in Chapter 5, wrinkling analysis for OFFSSs using post-buckling is very computationally expensive. Wrinkle wavelengths are very small compared to platform sizes and therefore require very fine meshes. Additionally, it has been shown that wrinkling results obtained by post-buckling analysis with commercial FEM software are sensitive to user-defined parameters, which are typically unknown. Due to the volatility of the results, given the input parameters, the wrinkling features must be interpreted with care. Thus, for engineering OFFSSs, there is a demand for computationally less intensive, and more reliable wrinkling analysis methods.

Principal stress field analysis and tension field analysis have the benefits of being computationally cheap, and not dependent on user-defined input parameters. Nonetheless, principal compressive stress zones can only function as an indicator for wrinkling, as these compressive zones will not always result in wrinkling. Therefore, a higher level of understanding of the interpretation of these principal stress results is required. Besides the presence of global compressive stress zones, it would be advantageous if more indicators can be obtained from principal stress results that give conclusive proof of wrinkling in general. For example, as seen in Table 5.2 in Chapter 5, principal stress field distributions which lead to wrinkling can be very different for various load cases. For the bi-axial case, compressive stresses are distributed in two (connected) zones, while the axial and shear load case show a single compressive stress zone. Therefore, the question arises if multiple local (not connected) stress zones can lead to global wrinkling. Further inspection of these items is suggested.

Next to that, the drawback of these methods is that they can not provide any information on quantitative wrinkling features, such as wavelengths and amplitudes. For the engineering of OFFSSs, these quantitative features are assumed to be relevant in their structural design, for example, to assess the potential failure of solar panels. Accordingly, there is a requirement for an approach that provides this information at low computational costs. In literature, analytical methods were identified which can provide additional information on quantitative wrinkling features when analysing wrinkling be-

behaviour using tension field theory [36, 38, 37]. It is recommended to investigate if such a method would also be applicable for the wrinkling analysis of OFFSSs.

For proper analysis of wrinkling behaviour of OFFSSs, hydrostatic stiffness should be incorporated in the model. Elastic foundations in numerical software do not yet allow accurate modelling of buoyancy and surface tension effects. Currently, the elastic foundation is modelled using the bonded contact method (described in Appendix B), which presumably overestimates the influence of surface tension at full scale and hence the wrinkling reduction effect of hydrostatic stiffness. It should be investigated, how these physics can be modelled more accurately in a numerical model. The next step would be to examine what the influence of this model would be on the wrinkling behaviour of OFFSSs, and if the wrinkling behaviour of the bi-axial tension case then can still be neglected. Besides, the elastic foundation is currently modelled by springs that apply stiffness normal to the platform surface, hence out of plane deformations are required in the computation. The effect of hydrostatic stiffness can only be modelled using post-buckling analysis, which induces high computational costs and sensitivity to user-defined input. Thus, future work is proposed to obtain a method for taking into account hydrostatic stiffness effects in wrinkling analysis, without inducing high computational costs.

8.2 Wrinkling Modelling of OFFSSs and Ocean Dynamics

In this thesis, ocean dynamics are not taken into account. However, waves will induce additional deformations and curvatures which might affect the wrinkling behaviour. It is therefore recommended to investigate how ocean dynamics relate to wrinkling behaviour. Moreover, in literature [88] it was noticed, that curvatures in membranes can have a significant effect on their wrinkling behaviour. In the recent study it has been proven that curvature can effectively tune the wrinkling localization and amplitude, and localized wrinkles can be remotely smoothed or even suppressed with the rise of curvature. Therefore, further investigation of this effect for OFFSSs is recommended especially.

8.3 Wrinkling Resistant Design

In Chapter 6, shear compliant zones and auxetic solar panel structures have been proposed as solutions for wrinkling behaviour reduction of OFFSSs. These design solutions have been shown to reduce wrinkling behaviour for a specific shear load condition. For the design of OFFSSs, wrinkling is to be avoided in design, for varying load conditions and directions. Therefore, further research is required to investigate how shear compliant zones and auxetic solar panel structures can be utilized, keeping in mind varying load conditions and load directions. In the first section of Appendix C, the wrinkling behaviour of several elementary permeable OFFSS designs was analysed. Here it was concluded, that a grid of holes spread around the platform will likely not remove wrinkling from the structure. However, additional benefits of these hole grids are identified for OFFSSs, such as the release of green water and trapped air bubbles. Therefore, it is recommended to investigate how these permeable grids can be incorporated in a wrinkling reduced OFFSS design.

In the principal stress results auxetic structures in Chapter 6, it was observed that auxetic behaviour in OFFSSs can induce local compressive stress concentrations. As stress concentrations can result in the structural risk of tears and fractures, it is recommended to investigate how these can be avoided while maintaining auxetic performance. Furthermore, auxetic behaviour has been shown to remove compressive stresses from the middle of the structures and creating local compressive stress peaks at the edges of the structure. Further investigation of the effect of these peaks on the structural behaviour of the platform is advised.

8.4 Structural Design with Solar Panels

In this thesis, the structural analysis of solar panels is not performed. As solar panels form an integral part of the OFFSS, it is recommended to explore their structural limit states. This could pose a constraint on the maximum allowable wrinkling behaviour of the solar platforms. Furthermore, the ratio of OFFSS area and embedded panel area presumably affects the global wrinkling behaviour, by changing the equivalent stiffness of the platform. It is recommended to research what the influence of this ratio is on the wrinkling behaviour of OFFSSs.

8.5 Mooring

In literature, described in Chapter 2, it was noted that for the design of Gossamer structures, wrinkling reduction methods have been applied such as tension cables along the circumference of these structures. For OFFSSs, a similar wrinkling reduction might be achieved when such a solution is adapted. Mooring is required definitely for OFFSSs, thus designing a mooring system that is similar to the tension cable structures could result in the synergy of the two systems. Consequently, it is suggested to examine the wrinkling reduction potential of mooring configurations inspired by wrinkling reduction methods for Gossamer structures.



Auxetic Structure Design

This appendix covers the creation of the auxetic solar panel structure based on an auxetic structure from literature.

A.1 Auxetic Solar Panels Design

The auxetic solar panels, discussed in chapter 6, are based on an auxetic structure consisting of rigid rotating rectangles by Kolken and Zadpoor [40]. In Figure A.1, the structure is shown, in rest and in tensile loading.

This has been modelled using rigid solar panels with dimensions $l_p \times w_p = 1.60\text{m} \times 1.00\text{m}$. Subsequently, the auxetic structure is tested in the axial tension case, equal to the loading in Figure A.1. To check whether the structure shows auxetic deformation, the case is running for a setup with straight solar panels and one with auxetic solar panels. In Figures A.2 and A.3 schematic illustrations of the geometries, together with their dimensions, are given for the auxetic and straight platform respectively. In Figure A.4, the geometries of both models, as well as the analysis boundary conditions, are depicted.

A.2 Auxetic behaviour

A stretch of 5% of the platform width w is applied in the y-direction to both structures. To analyse the auxetic behaviour, the x-displacement contours are viewed. From there, it can be observed whether the structure has expanded laterally (x-direction) as a consequence of the longitudinal (y-direction) displacement. Looking at the results in Figure A.5, it can be observed that the auxetic platform shows auxetic behaviour, as opposed to the straight panel platform which does not display auxetic behaviour.

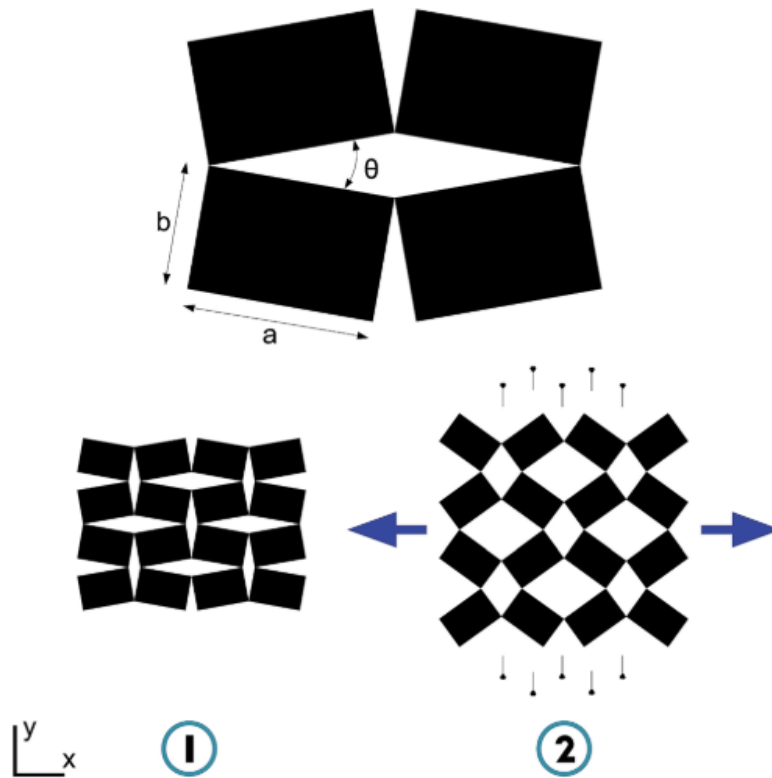


Figure A.1: Auxetic Rotating Rigid Rectangles Structure by Kolken and Zadpoor [40]. (1) Shows structure in rest, (2) tensile loading in x-direction.

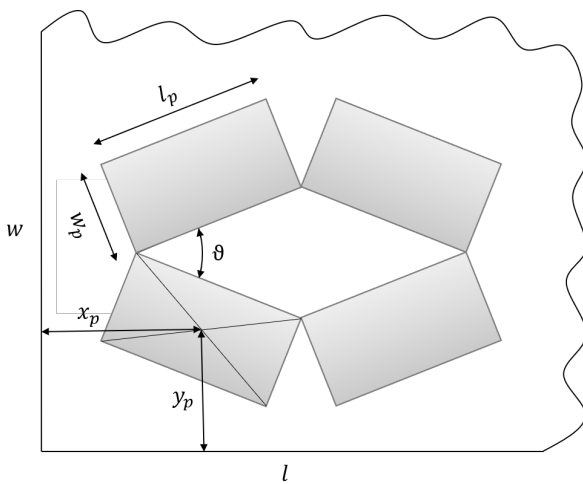


Figure A.2: Schematic of one corner of the auxetic platform. The indicated dimensions are: $l = 10.78\text{m}$, $w = 5.46\text{m}$, $l_p = 1.60\text{m}$, $w_p = 1.00\text{m}$, $x_p = 1.00\text{m}$, $y_p = 0.73\text{m}$, $\theta = 0.2$, platform thickness is $t = 0.10\text{m}$ and rigid panel thickness $t_p = 0.05\text{m}$.

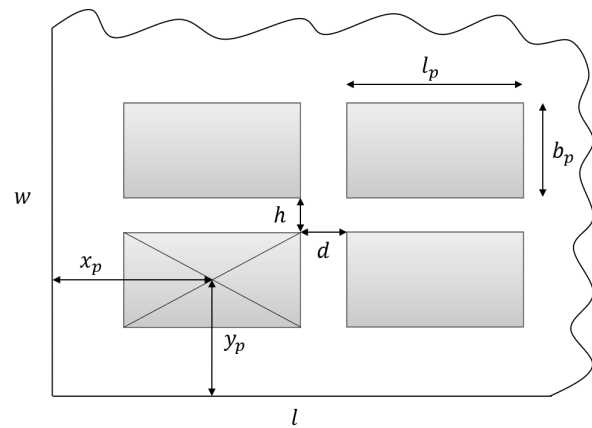


Figure A.3: Schematic of one corner of the auxetic platform. The indicated dimensions are: $l = 10.78\text{m}$, $w = 5.46\text{m}$, $l_p = 1.60\text{m}$, $w_p = 1.00\text{m}$, $x_p = 1.00\text{m}$, $y_p = 0.73\text{m}$, $h = 0.34\text{m}$, $d = 0.16\text{m}$, platform thickness is $t = 0.10\text{m}$ and rigid panel thickness $t_p = 0.05\text{m}$.

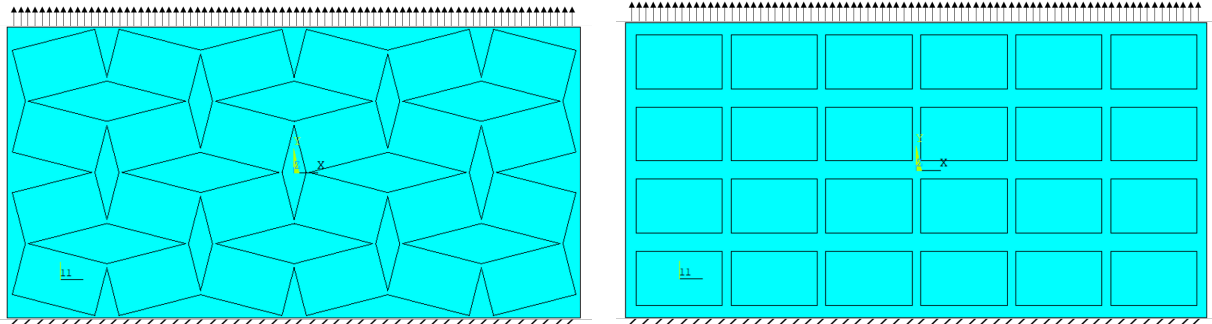


Figure A.4: Geometries of two test structures in axial tension. On the left, the auxetic structure. On the right, the straight panel platform. The lower edges of the structure is fully constrained and the top edges are pulled upwards with a displacement based load.

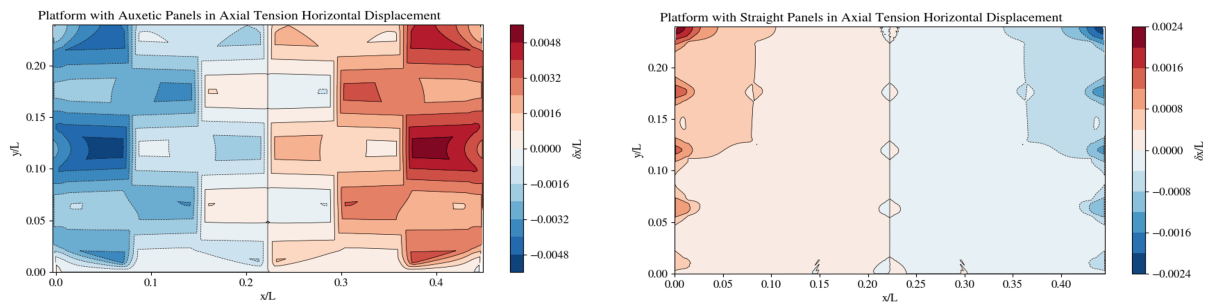


Figure A.5: Horizontal displacement contours as a result of longitudinal stretch. The auxetic structure on the left shows negative x -displacement on the left of the platform center and positive x -displacement on the right of the platform center, which indicates expansion, hence auxetic behaviour. The straight panel structure on the right shows positive x -displacement on the left of the platform center and negative x -displacement on the right of the platform center, which indicates contraction, thus non-auxetic behaviour.

B

Elastic Foundation Contact Type

As discussed in Chapter 3, there are several options for implementing hydrostatic stiffness into wrinkling analyses. In this investigation, an elastic foundation is used which applies hydrostatic stiffness normal to the face of the structure using springs. One of the decisions which have to be made with the selection of an elastic foundation is whether the springs should apply stiffness in both directions, i.e. bonded contact; or only when a wrinkle presses downward, i.e. unilateral contact. Here, the results of the two respective methods are compared.

B.1 Working Principles

Figure B.1 illustrates the working principle of the two methods under wrinkling deformation. In the bonded contact method, the hydrostatic stiffness is applied in both vertical directions, as if the water 'sticks' to the platform. At model scale, the same behaviour is recognized in the experiments of compressed membranes on the fluid by Pociavsek et al. [71], due to surface tension effects. However, at full scale, these effects are assumed to be negligible compared to inertia forces, as OFFSS size will be orders of magnitudes larger, while the surface tension of water is close to constant (depending on water type and temperature) [60]. Therefore the sticking behaviour is not expected at full scale. Unilateral contact only provides stiffness when the structure is pressed into the elastic foundation, the structure is free to move upwards. Hence, this method neglects the effect of surface tension, which might be more realistic based on the previous argument. Depending on the wrinkling results of both methods, a conclusion will be drawn.

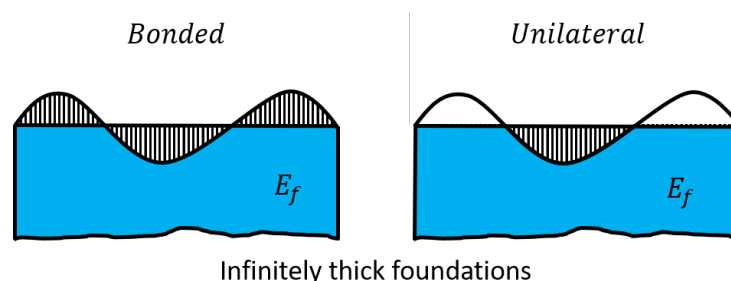


Figure B.1: Schematic of a wrinkled sheet on an infinitely thick elastic foundation (E_f). The striped areas indicate displaced elastic foundation volumes, the bonded contact applies stiffness to both upward as well as downward vertical displacements, while unilateral contact only offers stiffness to downward vertical displacements; the structure is free to move upwards with unilateral contact.

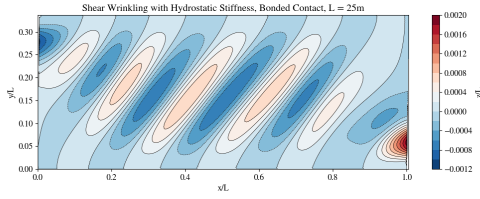


Figure B.2: Wrinkling Amplitudes of Sheet with Bonded Contact

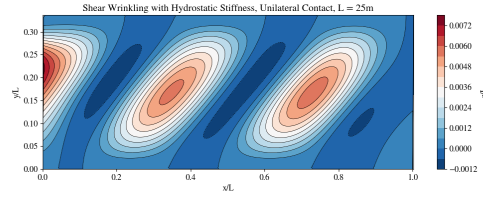


Figure B.3: Wrinkling Amplitudes of Sheet with Unilateral Contact

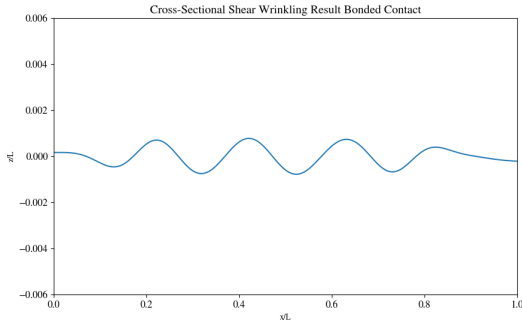


Figure B.4: Cross-sectional Wrinkling of Sheet with Bonded Contact

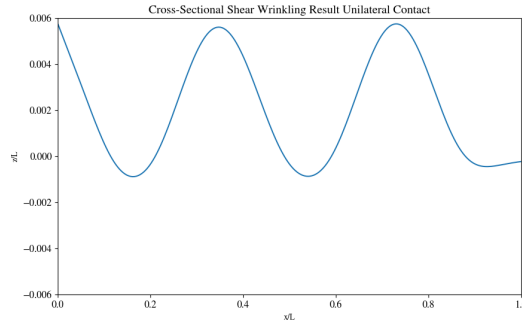


Figure B.5: Cross-sectional Wrinkling of Sheet with Unilateral Contact

B.2 Wrinkling Results

To compare the effect of the elastic foundations, the shear case with the same boundary conditions as in Section 6.1.1 is analysed, using the two different elastic foundation settings. The wrinkling amplitudes are presented in Figures B.2 and B.3. Note that the result in Figure B.2 is slightly different than the result for a platform of 25m in Section 6.1.1, as the analysis in the current comparison is performed for a smaller strain, as higher strains induced convergence issues for the unilateral model. From the wrinkling amplitude results, it can be observed that the wrinkle wavelengths are smaller for the bonded case than for the unilateral case. This can be explained, that in the bonded case, the elastic foundation offers a more significant contribution to the energy balance between bending, stretching and potential energies. As the potential energy penalizes long wavelengths, these are reduced with bonded contact.

For a more in detailed comparison between the bonded and unilateral elastic foundation effects, the cross-sectional wrinkling results are compared of the sheets, at half the width. See Figures B.4 and B.5 for the wrinkling cross-sections. Here, it can be seen that the bonded contact wrinkles are symmetrical around the $z = 0$ axis, while the unilateral contact is not symmetrical around the $z = 0$ axis, but has a mean which is located at a positive z -coordinate. This is caused by unilateral stiffness, applying pressure in the upward direction.

B.3 Conclusion

The behaviour as a result of the unilateral method is expected to be unrealistic, as the structure's mass has not been taken into account in this computation and it is assumed that the behaviour of the unilateral contact element underestimates the effect of gravity, pulling the sheet downward. The behaviour of the bonded contact foundation is assumed to overestimate the surface tension effect, however, it is assumed to model gravity more realistically than the unilateral contact method. Therefore in this research, the bonded contact method will be applied for the wrinkling analyses on an elastic founda-

tion.

For future research, there is a demand for a deeper understanding of the physics that play a role in the interaction between a large scale flexible platform exhibiting wrinkles on water, and how to model this accurately in an elastic foundation model. To improve the accuracy result with an unilateral model, it should be investigated whether applying mass to the structure results in a more realistic solution.



OFFSS Permeability Variations

In this appendix, additional examples of permeable OFFSS designs are presented with their wrinkling behaviour. Permeability is expected to be a very important design feature for OFFSSs, to reduce wrinkling behaviour as seen in Chapter 6 and in the work of Lavaerts [41], as well as a method to release green water on top of the structure due to waves, along with the removal of air trapped below the platform. In the following sections, some elementary permeability designs are tested for their wrinkling behaviour, using the rigid solar panel shear case described in Chapter 6.

Secondly, it is expected that rectangular holes in shear compliant zones (Section 6.2.1) are prone to have stress concentrations at the corners of the holes. Holes with smooth arcs instead of sharp corners might reduce this risk of stress concentrations. Therefore, in this appendix, it will be investigated if shear compliant zones with elliptical or circular shaped holes can reduce wrinkling.

In the first section, various elementary designs of solar platforms with a grid of holes over the whole platform are analysed for their wrinkling behaviour. In the second section, variations on the shear compliant zone with elliptical and circular holes are presented.

C.1 Grid of Holes Over the Whole Platform

As holes are expected to be required over the whole platform to release green water and trapped air below the platform, it would be beneficial if such a grid can also reduce wrinkling. In this section, four designs are presented and their wrinkling behaviour is analysed using principal stress results. The global geometry is the same as the rigid solar panel platform, in Subsection 6.1.2, and the main dimensions can be found in Figure 6.3.

C.1.1 Conclusion

Four elementary permeable solar platform designs are analysed and their wrinkling behavior is presented by principal stress field plots in Figures C.5, C.6, C.7 and C.8. From the results, it can be observed that most designs reduce compressive stresses throughout the platform. However, as compressive stress zones are still present, often spread over the middle of the platform, it can not be concluded that these methods remove global wrinkling. This indicates, that the elementary design of a grid of holes around the platform is likely not sufficient to remove global wrinkling behaviour, under the given load and boundary conditions.

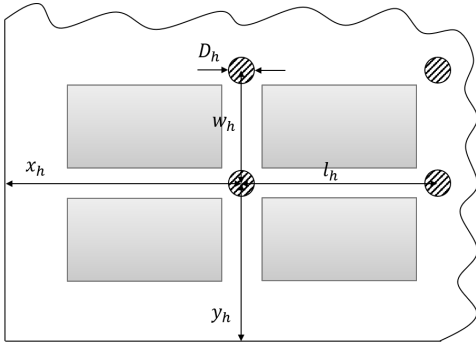


Figure C.1: Design A: Circular holes in between solar panels. The indicated dimensions are: $x_h = 2.69\text{m}$, $y_h = 2.02\text{m}$, $l_h = 2.18\text{m}$, $w_h = 1.45\text{m}$, $D_h = 0.40\text{m}$

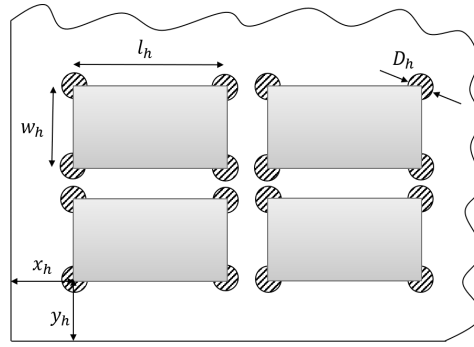


Figure C.2: Design B: Circular holes at corners of solar panels. The indicated dimensions are: $x_h = 0.80\text{m}$, $y_h = 0.80\text{m}$, $l_h = 1.60\text{m}$, $w_h = 1.00\text{m}$, $D_h = 0.40\text{m}$

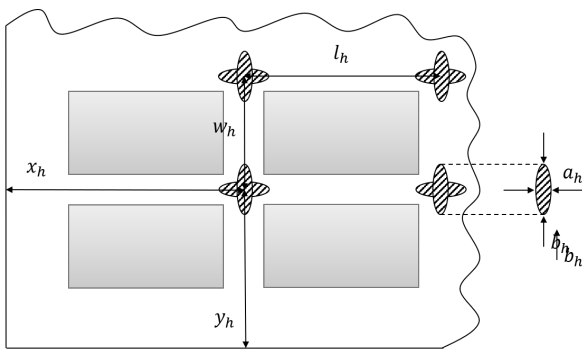


Figure C.3: Design C: Cross-shaped holes (two ellipses), located between the solar panels. The indicated dimensions are: $x_h = 2.69\text{m}$, $y_h = 2.02\text{m}$, $l_h = 1.60\text{m}$, $w_h = 1.00\text{m}$, $a_h = 0.20\text{m}$, $b_h = 1.00\text{m}$

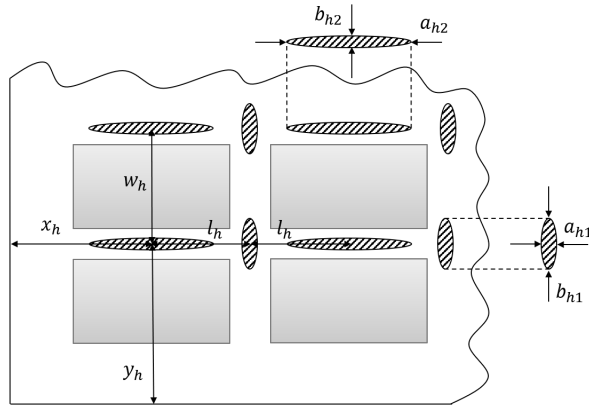


Figure C.4: Design D: Different sized elliptical holes in between solar panels. The indicated dimensions are: $x_h = 1.60\text{m}$, $y_h = 2.02\text{m}$, $l_h = 0.80\text{m}$, $w_h = 1.00\text{m}$, $a_{h1} = 0.20\text{m}$, $b_{h1} = 1.00\text{m}$, $a_{h2} = 1.60\text{m}$, $b_{h2} = 0.20\text{m}$

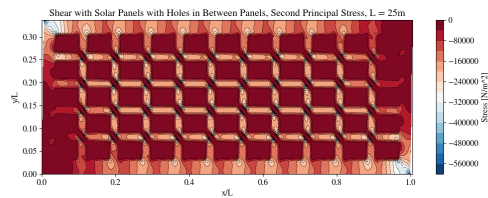
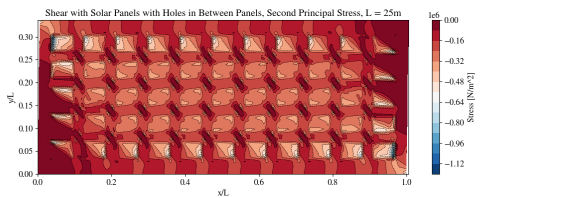


Figure C.5: Design A: Circular holes in between solar panels. The principal compressive stress field of this design shows a small reduction of compressive stresses in the middle of the platform compared to a solar platform with no holes, but still compressive stresses are observed throughout the whole platform.

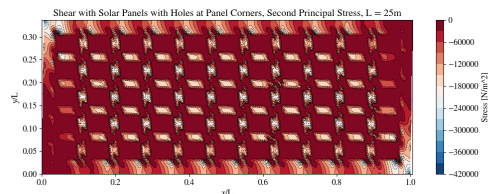
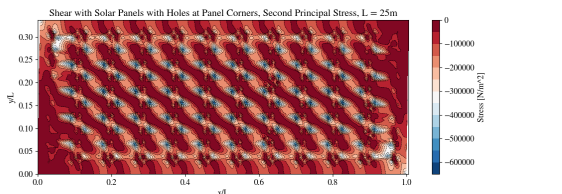


Figure C.6: Design B: Circular holes at corners of solar panels. In the principal compressive stress field of this design, larger reduction of compressive stresses is observed in the middle of the platform. The compressive stresses are significantly smaller than in Design A, however, compressive stresses are still present all over the platform. Moreover, the stress concentrations are located in the middle of the platform, which is expected to result in unfavorable wrinkling behavior.

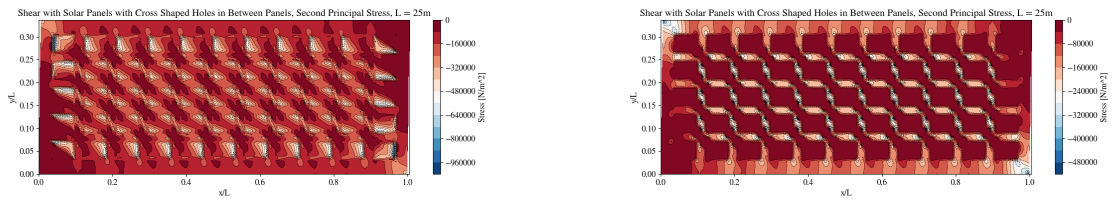


Figure C.7: Design C: Cross-shaped holes (two ellipses), located between the solar panels. The principal compressive stress contours indicate that some compressive stress are removed from the platform, however whether wrinkling is removed by this design can not be concluded.

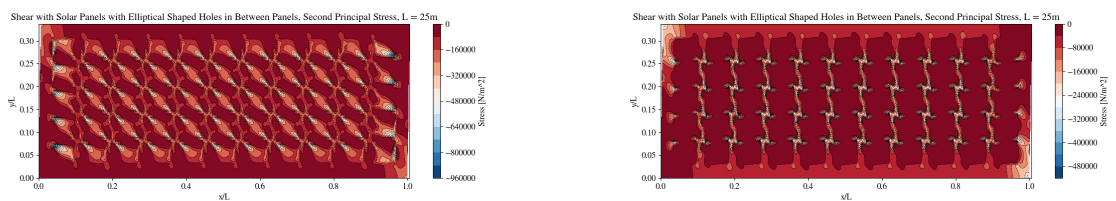


Figure C.8: Design D: Different sized elliptical holes in between solar panels. Principal stress results of this design show localization of compressive stress zones in multiple areas throughout the platform. Whether wrinkling behavior is reduced by addition of this permeability type can not be concluded, as compressive stresses are still present over the whole platform.

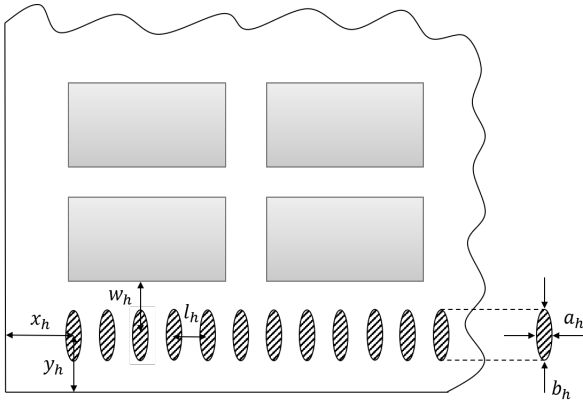


Figure C.9: Design E: Shear Compliant Zone with oval holes. The indicated dimensions are: $x_h = 0.80\text{m}$, $y_h = 0.84\text{m}$, $l_h = 0.40\text{m}$, $w_h = 0.84\text{m}$, $a_h = 0.20\text{m}$, $b_h = 1.00\text{m}$

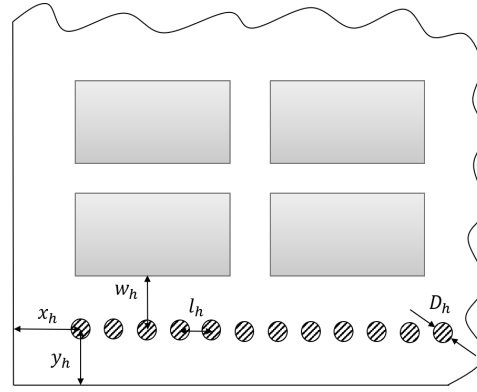


Figure C.10: Design F: Shear Compliant Zone with small circular holes. The indicated dimensions are: $x_h = 0.80\text{m}$, $y_h = 0.84\text{m}$, $l_h = 0.40\text{m}$, $w_h = 0.84\text{m}$, $D_h = 0.20\text{m}$. Note that D_h is the same size as a_h in Design E in Figure C.9.

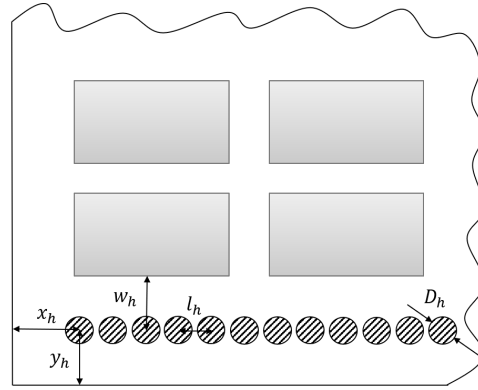


Figure C.11: Design G: Shear Compliant Zone with large circular holes. The indicated dimensions are: $x_h = 0.80\text{m}$, $y_h = 0.84\text{m}$, $l_h = 0.40\text{m}$, $w_h = 0.84\text{m}$, $D_h = 0.30\text{m}$.

C.2 Elliptical Hole Shear Compliant Zone

Due to the sharp corners of the rectangular holes on the shear compliant zones in Section 6.2.1, stress concentrations might arise which could lead to fracture of the platform. In this section, several elementary shear compliant zone designs are tested, using elliptical and circular holes instead of rectangles, to avoid stress concentrations. The effect of the different shaped holes on the wrinkling behaviour of the platforms is analysed. The main geometry of the platform used in the test cases is the same as depicted in Figure 6.9, which states the main dimensions. Note that in all three designs, the same number of holes is applied, which are located at the same positions. The shape of the wholes is the only variable in this analysis.

C.2.1 Conclusion

From the principal stress results of various elementary shear zone designs, displayed in Figures C.12, C.13 and C.14, it can be observed that shear compliant zones with elliptical holes result in the highest wrinkling reduction, by the decrease of compressive stresses over the whole platform. Furthermore, the decrease of compressive stresses in design G with large circular holes compared to design F with small circular holes indicates that larger circular holes result in higher compressive stress reductions when applied in a shear compliant zone.

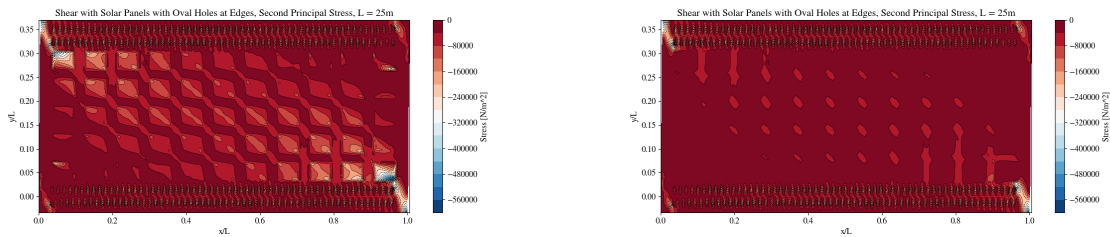


Figure C.12: Design E: Shear zone with elliptical holes. Principal stress results of this design show large reduction of compressive stresses throughout the whole platform, and specifically the middle. The reductions are similar to those of the full shear compliant zone with rectangular shaped holes in Figure 6.10. This indicates that ellipses can result in similar wrinkling reduction behavior for shear compliant zones as rectangular holes do.

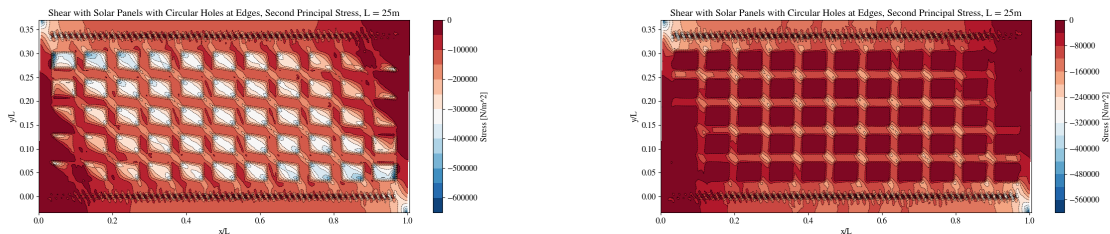


Figure C.13: Design F: Shear zone with small circular holes. Note that the diameter of the circular holes is the same as the width of the ellipses in Design E, see Figure C.9 and C.10. Principal stress results of this design show small reductions in compressive stresses throughout the whole platform. The reductions are similar to those of the platform without shear compliant zone Figure 6.10. This indicates that shear zones with small circular holes have negligible effect on the wrinkling behavior of solar platforms.

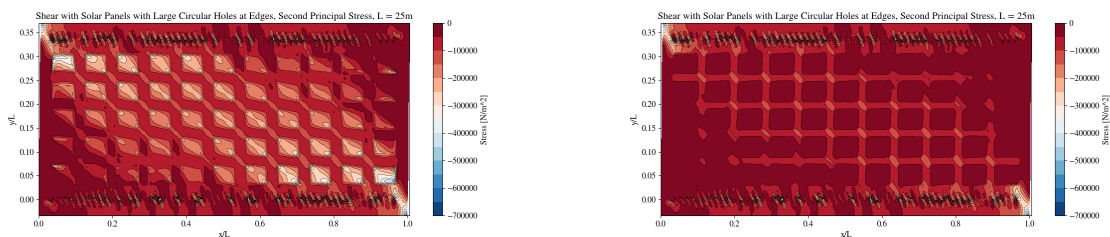


Figure C.14: Design G: Shear zone with large circular holes. Principal stress results of this design show larger reductions in compressive stresses throughout the whole platform compared to the small circular holes in design F. Yet, the compressive stress reductions are not as substantial as those caused by the elliptical holes in design E. Furthermore, as compressive stress zones are still observed around the platform, it is hard to conclude whether wrinkling is removed from the platform with this design.

Bibliography

- [1] International Energy Agency. “World Energy Outlook 2020”. In: (2020).
- [2] Vishal Agrawal and Sachin S. Gautam. “IGA: A Simplified Introduction and Implementation Details for Finite Element Users”. In: *Journal of The Institution of Engineers (India): Series C* 100.3 (2019), pp. 561–585. ISSN: 22500553. DOI: [10.1007/s40032-018-0462-6](https://doi.org/10.1007/s40032-018-0462-6). URL: <https://doi.org/10.1007/s40032-018-0462-6>.
- [3] A. R. Amelia et al. “Investigation of the effect temperature on photovoltaic (PV) panel output performance”. In: *International Journal on Advanced Science, Engineering and Information Technology* 6.5 (2016), pp. 682–688. ISSN: 24606952. DOI: [10.18517/ijaseit.6.5.938](https://doi.org/10.18517/ijaseit.6.5.938).
- [4] Department of Applied Mechanics. 2021. URL: https://www.mm.bme.hu/~gyebro/files/ans_help_v182/ans_cmd/Hlp_C_CmdTOC.html.
- [5] Aqua-Calc. 2021. URL: <https://www.aqua-calc.com/page/density-table/substance/rubber-coma-and-blank-neoprene>.
- [6] Mohamed Assidi and Jean-françois Ganghoffer. “Composites with auxetic inclusions showing both an auxetic behavior and enhancement of their mechanical properties”. In: *Composite Structures* 94 (2012). URL: <http://dx.doi.org/10.1016/j.compstruct.2012.02.026>.
- [7] I Beverte, Vladimir Yakushin, and Ugis Cabulis. “Mechanical properties of rigid polyurethane foams at room and cryogenic temperatures”. In: July (2011). DOI: [10.1177/0021955X11398381](https://doi.org/10.1177/0021955X11398381).
- [8] Grama R Bhashyam. “ANSYS Mechanical — A Powerful Nonlinear Simulation Tool”. In: September (2002).
- [9] Blauwwind. 2021. URL: <https://www.blauwwind.nl/>.
- [10] Alessandra Bonfanti and Atul Bhaskar. “Elastic stabilization of wrinkles in thin films by auxetic microstructure”. In: *Extreme Mechanics Letters* 33 (2019). URL: <https://doi.org/10.1016/j.eml.2019.100556>.
- [11] A. S. Bonin and K. A. Seffen. “De-wrinkling of pre-tensioned membranes”. In: *International Journal of Solids and Structures* 51.19-20 (2014), pp. 3303–3313. URL: <http://dx.doi.org/10.1016/j.ijsolstr.2014.05.001>.
- [12] R. Bouzidi and Y. Lecieux. “Experimental analysis on membrane wrinkling under biaxial load - Comparison with bifurcation analysis”. In: *International Journal of Solids and Structures* 47.18-19 (2010), pp. 2459–2475. ISSN: 00207683. DOI: [10.1016/j.ijsolstr.2010.05.005](https://doi.org/10.1016/j.ijsolstr.2010.05.005). URL: <http://dx.doi.org/10.1016/j.ijsolstr.2010.05.005>.
- [13] Gerard van Bussel. “Course Offshore Wind Farm Design”. In: (). URL: https://ocw.tudelft.nl/wp-content/uploads/Module_9_wind_farm_aspects.pdf.
- [14] R Cazzaniga et al. “Floating photovoltaic plants : Performance analysis and design solutions”. In: *Renewable and Sustainable Energy Reviews* 81.September 2016 (2018), pp. 1730–1741. URL: <https://doi.org/10.1016/j.rser.2017.05.269>.
- [15] E. Cerda and L. Mahadevan. “Geometry and Physics of Wrinkling”. In: *Physical Review Letters* (2003). ISSN: 10797114. DOI: [10.1103/PhysRevLett.90.074302](https://doi.org/10.1103/PhysRevLett.90.074302).
- [16] E. et al Cerda. “Wrinkling of an elastic sheet under tension”. In: *Nature* 419 (2002), pp. 579–580. URL: <http://www.nature.com/articles/419579b>.

- [17] A B Chmielewski. *Overview Of Gossamer Structures*. 2001, pp. 1–33. ISBN: 9781600866616.
- [18] Twin Cities and User Meeting. “Stabilization Damping for Nonlinear Convergence”. In: November (2019).
- [19] Molded Dimensions. 2021. URL: <https://moldeddimensions.com/mechanical-properties.php>.
- [20] Elissandro Monteiro Do Sacramento et al. “Scenarios for use of floating photovoltaic plants in Brazilian reservoirs”. In: *IET Renewable Power Generation* 9.8 (2015), pp. 1019–1024. ISSN: 17521424. DOI: [10.1049/iet-rpg.2015.0120](https://doi.org/10.1049/iet-rpg.2015.0120).
- [21] Swapnil Dubey, Jatin Narotam Sarvaiya, and Bharath Seshadri. “Temperature dependent photovoltaic (PV) efficiency and its effect on PV production in the world - A review”. In: *Energy Procedia* 33 (2013), pp. 311–321. ISSN: 18766102. DOI: [10.1016/j.egypro.2013.05.072](https://doi.org/10.1016/j.egypro.2013.05.072). URL: <http://dx.doi.org/10.1016/j.egypro.2013.05.072>.
- [22] Oceans of Energy. 2019. URL: <https://oceansofenergy.blue/2019/12/11/a-worlds-first-offshore-floating-solar-farm-installed-at-the-dutch-north-sea/>.
- [23] EnergySage. 2021. URL: <https://news.energysage.com/average-solar-panel-size-weight/>.
- [24] Huisman Equipment. 2021. URL: https://www.huismanequipment.com/en/products/references/674-107_160mt-Reel-lay-System.
- [25] Kenneth E. Evans and Andrew Alderson. “Auxetic materials: Functional materials and structures from lateral thinking!” In: *Advanced Materials* 12.9 (2000), pp. 617–628.
- [26] Evgueni T. Filipov et al. “Origami tubes assembled into stiff, yet reconfigurable structures and metamaterials”. In: *Proceedings of the National Academy of Sciences of the United States of America* 112.40 (2015), pp. 12321–12326.
- [27] C. Fu et al. “A modeling and resolution framework for wrinkling in hyperelastic sheets at finite membrane strain”. In: *Journal of the Mechanics and Physics of Solids* 124 (2019), pp. 446–470.
- [28] Shanshi Gao et al. “A new polymer-based mechanical metamaterial with tailorable large negative Poisson’s ratios”. In: *Polymers* 12 (2020), pp. 1–15.
- [29] Shiva Gorjian et al. “Recent technical advancements, economics and environmental impacts of floating photovoltaic solar energy conversion systems”. In: *Journal of Cleaner Production* 278 (2021). URL: <https://doi.org/10.1016/j.jclepro.2020.124285>.
- [30] Simutech Group. 2021. URL: <https://simutechgroup.com/a-normal-and-tangential-elastic-foundation-in-ansys-workbench-mechanical/>.
- [31] Longxin Gu et al. “Analysis of the mechanical properties of double arrowhead auxetic metamaterials under tension”. In: *Textile Research Journal* 90.21-22 (2020), pp. 2411–2427.
- [32] Rob Harris and Lars Johanning. “Mooring systems for wave energy converters : A review of design issues and choices”. In: (2006).
- [33] Timothy J. Healey, Qingdu Li, and Ron-Bin Cheng. “Wrinkling Behavior of Highly Stretched Rectangular Elastic Films via Parametric Global Bifurcation”. In: *Journal of Nonlinear Science* (2013), pp. 777–805. URL: <http://link.springer.com/10.1007/s00332-013-9168-3>.
- [34] Leonard R. Herrmann. “Elasticity equations for incompressible and nearly incompressible materials by a variational theorem”. In: *AIAA Journal* 3.10 (1965), pp. 1896–1900. ISSN: 00011452. DOI: [10.2514/3.3277](https://doi.org/10.2514/3.3277).
- [35] HSB International. “Seven Oceans”. In: (2007). URL: <https://www.royalihc.com/-/media/royalihc/image-carousel/products/product-images/offshore/pipelay-and-cable-lay/vessels/reel-lay-vessels/articleroyalihcsevenoceanshsb.pdf>.

- [36] Takashi Iwasa. "Approximate estimation of wrinkle wavelength and maximum amplitude using a tension-field solution". In: *International Journal of Solids and Structures* 121 (2017), pp. 201–211. ISSN: 00207683. DOI: [10.1016/j.ijsolstr.2017.05.029](https://doi.org/10.1016/j.ijsolstr.2017.05.029). URL: <http://dx.doi.org/10.1016/j.ijsolstr.2017.05.029>.
- [37] Takashi Iwasa. "Experimental verification on simplified estimation method for envelope curve of wrinkled membrane surface distortions". In: *Thin-Walled Structures* 122.June 2017 (2018), pp. 622–634. ISSN: 02638231. DOI: [10.1016/j.tws.2017.10.049](https://doi.org/10.1016/j.tws.2017.10.049). URL: <https://doi.org/10.1016/j.tws.2017.10.049>.
- [38] Takashi Iwasa. "Experimental verification on wrinkling behavior given by wrinkling analysis using the tension field theory". In: *International Journal of Solids and Structures* 136-137 (2018), pp. 1–12. ISSN: 00207683. DOI: [10.1016/j.ijsolstr.2017.11.028](https://doi.org/10.1016/j.ijsolstr.2017.11.028). URL: <https://doi.org/10.1016/j.ijsolstr.2017.11.028>.
- [39] Beomkeun Kim et al. "A comparison among Neo-Hookean model, Mooney-Rivlin model, and Ogden model for Chloroprene rubber". In: *International Journal of Precision Engineering and Manufacturing* 13.5 (2012), pp. 759–764. ISSN: 12298557. DOI: [10.1007/s12541-012-0099-y](https://doi.org/10.1007/s12541-012-0099-y).
- [40] H. M.A. Kolken and A. A. Zadpoor. "Auxetic mechanical metamaterials". In: *RSC Advances* 7 (2017), pp. 5111–5129.
- [41] E. Lavaerts. "Framework to research and design wrinkle free very large flexible offshore solar platforms by adding permeability". In: (2020).
- [42] J. Leifer et al. "Evaluation of shear compliant borders for wrinkle reduction in thin film membrane structures". In: *44th AIAA/ASME/ASCE/AHS/ASC Structures, Structural Dynamics, and Materials Conference* April (2003), pp. 1–7.
- [43] Jack Leifer. "Simplified computational models for shear-compliant borders in solar sails". In: *Journal of Spacecraft and Rockets* 44.3 (2007), pp. 571–581. DOI: [10.2514/1.20907](https://doi.org/10.2514/1.20907).
- [44] Lin Li et al. "Design optimization of mooring system : An application to a vessel-shaped offshore fish farm". In: *Engineering Structures* 197 (2019). URL: <https://doi.org/10.1016/j.engstruct.2019.109363>.
- [45] Ming Li et al. "Wrinkling and wrinkling-suppression in graphene membranes with frozen zone". In: *Thin Solid Films* 638 (2017), pp. 345–353. ISSN: 00406090. URL: <http://dx.doi.org/10.1016/j.tsf.2017.08.009>.
- [46] Peng Li. "A Theoretical and Experimental Study of Wave-induced Hydroelastic Response of a Circular Floating Collar A Theoretical and Experimental Study of Wave-induced Hydroelastic Response of a Circular Floating Collar". In: (2017).
- [47] Qingdu Li and Timothy J. Healey. "Stability boundaries for wrinkling in highly stretched elastic sheets". In: *Journal of the Mechanics and Physics of Solids* 97 (2016), pp. 260–274.
- [48] Haohui Liu, Abhishek Kumar, and Thomas Reindl. *The Dawn of Floating Solar—Technology, Benefits, and Challenges*. Vol. 41. Springer Singapore, 2020, pp. 373–383. URL: http://dx.doi.org/10.1007/978-981-13-8743-2%7B%5C_%7D21.
- [49] Luyao Liu and et al Wang. "Power Generation Efficiency and Prospects of Floating Photovoltaic Systems". In: *Energy Procedia* 105 (2017), pp. 1136–1142. URL: <http://dx.doi.org/10.1016/j.egypro.2017.03.483>.
- [50] Xiaodong Liu et al. "Tsunami-Induced Mooring Force on a Flexible Floating Structure". In: *International Offshore and Polar Engineering Conference* (2001).
- [51] Piero Ruol Luca Martinelli and Giampaolo Cortellazzo. "ON MOORING DESIGN OF WAVE ENERGY CONVERTERS: THE SEABREATH APPLICATION Luca Martinelli 1 , Piero Ruol 1 and Giampaolo Cortellazzo 1". In: (2011), pp. 1–12.

- [52] Yangjun Luo et al. "A multi-material topology optimization approach for wrinkle-free design of cable-suspended membrane structures". In: *Computational Mechanics* 59 (2017), pp. 967–980. ISSN: 01787675.
- [53] Yangjun Luo et al. "Wrinkle-free design of thin membrane structures using stress-based topology optimization". In: *Journal of the Mechanics and Physics of Solids* 102 (2017). ISSN: 00225096. URL: <http://dx.doi.org/10.1016/j.jmps.2017.02.003>.
- [54] PV-Magazine. 2020. URL: <https://www.pv-magazine.com/2020/02/22/the-weekend-read-dont-throw-caution-to-the-wind/>.
- [55] Renewable energy magazine. *DNV unveils its SUNdy floating solar field concept*. 2012. URL: https://www.renewableenergymagazine.com/pv_solar/dnv-unveils-its-sundy-floating-solar-field-20121029.
- [56] G. Marckmann and E. Verron. "Comparison of hyperelastic models for rubber-like materials". In: *Rubber Chemistry and Technology* 79.5 (2006), pp. 835–858. ISSN: 00359475. DOI: [10.5254/1.3547969](https://doi.org/10.5254/1.3547969).
- [57] "Mechanical properties of ZTO, ITO, and a-Si: H multilayer films for flexible thin film solar cells". In: *Materials* 10.3 (2017), pp. 1–11.
- [58] Candock Miami. URL: <https://candockmiami.com/floating-dock/>.
- [59] P. H. Mott, J. R. Dorgan, and C. M. Roland. "The bulk modulus and Poisson's ratio of "incompressible" materials". In: *Journal of Sound and Vibration* 312.4-5 (2008), pp. 572–575. ISSN: 0022460X. DOI: [10.1016/j.jsv.2008.01.026](https://doi.org/10.1016/j.jsv.2008.01.026). URL: <http://dx.doi.org/10.1016/j.jsv.2008.01.026>.
- [60] K G Nayar et al. "Surface Tension of Seawater Surface Tension of Seawater". In: 043103 (2014). DOI: [10.1063/1.4899037](https://doi.org/10.1063/1.4899037).
- [61] V. Nežerka et al. "A jigsaw puzzle metamaterial concept". In: *Composite Structures* 202.June (2018), pp. 1275–1279.
- [62] N. Nirmalkar, A. W. Patek, and M. Barigou. "Soft Matter Soft Matter". In: *Reviews of Modern Physics* 59.47 (2018), pp. 479–486. DOI: [10.1039/d0sm02209h](https://doi.org/10.1039/d0sm02209h).
- [63] Ocean Sun Norway. URL: <https://oceansun.no/>.
- [64] NOS. 2020. URL: <https://nos.nl/artikel/2344923-drijvend-zonnepark-nij-beets-loggeraakt-door-noodweer.html>.
- [65] SBM Offshore. "S3 Wave energy converter system". In: (2019).
- [66] Sara Oliveira-Pinto and Jasper Stokkermans. "Marine Floating Solar Plants: An overview of potential, challenges and feasibility". In: *Proceedings of the Institution of Civil Engineers - Maritime Engineering* (2020), pp. 1–39.
- [67] Omnexus. 2021. URL: <https://omnexus.specialchem.com/selection-guide/ethylene-vinyl-acetate/properties-of-eva>.
- [68] "On the applicability of tension field theory to a wrinkling instability problem". In: *Acta Mechanica* 190.1-4 (2007), pp. 57–72.
- [69] Andreea Panaitescu et al. "Birth and decay of tensional wrinkles in hyperelastic sheets". In: *Physical Review E* (2019).
- [70] Curbell Plastics. 2021. URL: <https://www.curbellplastics.com/Research-Solutions/Plastic-Material-Properties/EVA-Properties>.
- [71] Luka Pocivavsek et al. "Stress and fold localization in thin elastic membranes". In: *Science* (2008).

- [72] Yunan Prawoto. "Seeing auxetic materials from the mechanics point of view : A structural review on the negative Poisson ' s ratio". In: *Computational Materials Science* 58 (2012). DOI: [10.1016/j.commatsci.2012.02.012](https://doi.org/10.1016/j.commatsci.2012.02.012). URL: <http://dx.doi.org/10.1016/j.commatsci.2012.02.012>.
- [73] Chenhui Ren, Deqing Yang, and Haoxing Qin. "Mechanical performance of multidirectional Buckling-based Negative Stiffness metamaterials: An analytical and numerical study". In: *Materials* 11.7 (2018).
- [74] Marco Rivetti and Sébastien Neukirch. "Journal of the Mechanics and Physics of Solids The mode branching route to localization of the finite-length floating elastica". In: *Journal of the Mechanics and Physics of Solids* 69 (2014). ISSN: 0022-5096. DOI: [10.1016/j.jmps.2014.05.004](https://doi.org/10.1016/j.jmps.2014.05.004). URL: <http://dx.doi.org/10.1016/j.jmps.2014.05.004>.
- [75] Alok Sahu, Neha Yadav, and K. Sudhakar. "Floating photovoltaic power plant: A review". In: *Renewable and Sustainable Energy Reviews* 66 (2016).
- [76] Hiraku Sakamoto, K. C. Park, and Yasuyuki Miyazaki. "Dynamic wrinkle reduction strategies for cable-suspended membrane structures". In: *Journal of Spacecraft and Rockets* 42 (2005), pp. 850–858.
- [77] Hiraku Sakamoto, K. C. Park, and Yasuyuki Miyazaki. "Evaluation of membrane structure designs using boundary web cables for uniform tensioning". In: *Acta Astronautica* 60.10-11 (2007), pp. 846–857.
- [78] Krishna Kumar Saxena, Raj Das, and Emilio P. Calius. "Three Decades of Auxetics Research Materials with Negative Poisson's Ratio: A Review". In: *Advanced Engineering Materials* 18.11 (2016), pp. 1847–1870.
- [79] Ole Sigmund. "Tailoring materials with prescribed elastic properties". In: *Mechanics of Materials* 20 (1995), pp. 351–368.
- [80] Michael Taylor, Katia Bertoldi, and David J. Steigmann. "Spatial resolution of wrinkle patterns in thin elastic sheets at finite strain". In: *Journal of the Mechanics and Physics of Solids* 62 (2014). URL: <http://dx.doi.org/10.1016/j.jmps.2013.09.024>.
- [81] TE Tezduyar, Sunil Sathe, and Masayoshi Senga. "Finite element modeling of fluid–structure interactions with space–time and advanced mesh update techniques". In: *Fluid-Structure Interaction Lecture Notes in Computational Science and Engineering* 53 (2006), pp. 50–81. URL: http://www.tafsm.org/PUB_PRE/ipALL/ip117-NMCM05-FSI.pdf.
- [82] TNO. 2021. URL: <https://www.tno.nl/en/focus-areas/energy-transition/roadmaps/renewable-electricity/towards-ubiquitous-solar-energy/integration-solar-energy-environment/>.
- [83] TNO. 2021. URL: <https://www.tno.nl/en/focus-areas/energy-transition/roadmaps/renewable-electricity/solar-energy/solar-panel-efficiency/solliance/>.
- [84] Kim Trapani and Dean L Millar. "The thin flexible floating PV (T3F-PV) array : The concept and development of the prototype". In: *Progress in photovoltaics* (2014).
- [85] K. Venkatesh Raja and R. Malayalamurthi. "Assessment on assorted hyper-elastic material models applied for large deformation soft finger contact problems". In: *International Journal of Mechanics and Materials in Design* 7.4 (2011), pp. 299–305. ISSN: 15691713. DOI: [10.1007/s10999-011-9167-1](https://doi.org/10.1007/s10999-011-9167-1).
- [86] Wagner. *Flat sheet metal girders with very thin metal web*. 1929.
- [87] T. Wang et al. "On the wrinkling and restabilization of highly stretched sheets". In: *International Journal of Engineering Science* 136 (Mar. 2019), pp. 1–16. URL: <https://www.sciencedirect.com.tudelft.idm.oclc.org/science/article/pii/S0020722518323085>.

- [88] Ting Wang et al. “Curvature tunes wrinkling in shells”. In: *International Journal of Engineering Science* 164 (2021), p. 103490. ISSN: 00207225. DOI: [10.1016/j.ijengsci.2021.103490](https://doi.org/10.1016/j.ijengsci.2021.103490). URL: <https://doi.org/10.1016/j.ijengsci.2021.103490>.
- [89] Zhen Pei Wang et al. “Isogeometric shape optimization of smoothed petal auxetic structures via computational periodic homogenization”. In: *Computer Methods in Applied Mechanics and Engineering* 323 (Aug. 2017), pp. 250–271.
- [90] Wikipedia. 2021. URL: https://en.wikipedia.org/wiki/Triangular_number.
- [91] Wikipedia. 2021. URL: https://en.wikipedia.org/wiki/Ethylene-vinyl_acetate.
- [92] Wikipedia. 2021. URL: <https://en.wikipedia.org/wiki/Neoprene>.
- [93] Y Wong, Sergio Pellegrino, and K Park. “Prediction of wrinkle amplitudes in square solar sails”. In: *44th AIAA/ASME/ASCE/AHS/ASC Structures, Structural Dynamics, and Materials Conference*. 2003, p. 1982.
- [94] Y W Wong and Sergio Pellegrino. “Computation of wrinkle amplitudes in thin membrane”. In: *43rd AIAA/ASME/ASCE/AHS/ASC Structures, Structural Dynamics, and Materials Conference*. 2002, p. 1369.
- [95] Y. Wesley Wong and Sergio Pellegrino. “Wrinkled membranes part III: Numerical simulations”. In: *Journal of Mechanics of Materials and Structures* 1.1 (May 2006), pp. 63–95. ISSN: 15593959. DOI: [10.2140/jomms.2006.1.63](https://doi.org/10.2140/jomms.2006.1.63). URL: <http://msp.org/jomms/2006/1-1/p04.xhtml>.
- [96] Jian Xing et al. “Global shape optimization of fixtures to suppress wrinkles in large-displacement membrane structures”. In: *International Journal of Solids and Structures* 144-145 (2018), pp. 301–312. URL: <https://doi.org/10.1016/j.ijsolstr.2018.05.016>.
- [97] Sheng Xu, Shan Wang, and C Guedes Soares. “Review of mooring design for floating wave energy converters”. In: *Renewable and Sustainable Energy Reviews* 111.May (2019), pp. 595–621. URL: <https://doi.org/10.1016/j.rser.2019.05.027>.
- [98] Elly Yates-Roberts. 2018. URL: <https://www.cruiseandferry.net/More/advertise/viking-life-saving-equipments-lifecraft-passes-extreme-test-at-sea>.
- [99] Davood Younesian et al. “Elastic and viscoelastic foundations: a review on linear and nonlinear vibration modeling and applications”. In: *Nonlinear Dynamics* 97.1 (2019), pp. 853–895. ISSN: 1573269X. DOI: [10.1007/s11071-019-04977-9](https://doi.org/10.1007/s11071-019-04977-9). URL: <https://doi.org/10.1007/s11071-019-04977-9>.